学位論文（要約）

Structure-based agrochemical design of nitrification inhibitor targeting for hydroxylamine oxidoreductase in ammonia-oxidizing bacteria

（ヒドロキシルアミン酸化還元酵素を標的とした
硝化抑制剤の構造ベース創農薬）

平成 28 年 12 月博士（生命科学）申請

新領域創成科学研究科　先端生命科学専攻
応用生物資源学分野
学籍番号 47 - 127348

西ヶ谷　有輝

Structure-based agrochemical design of nitrification inhibitor targeting for
hydroxylamine oxidoreductase in ammonia-oxidizing bacteria

Nishigaya, Yuki

2016

Department of Integrated Bioscience,

Graduate School of Frontier Science,

The University of Tokyo

Abbreviations

Bacterium names

AOB: Ammonia-oxidizing bacterium

  βAOB: Beta-proteobacterial AOB

    NeAOB: *Nitrosomonas europaea* NBRC 14298   (βAOB)

    NmAOB: *Nitrosomonas multiformis* ATCC 25196 (βAOB)

  γAOB: Gamma-proteobacterial AOB

    NoAOB: *Nitrosococcus oceani* ATCC 19707   (γAOB)

Protein names

AMO: Ammonia monooxygenase

HAO: Hydroxylamine oxidoreductase

  NeHAO: HAO from NeAOB (βAOB)

  NmHAO: HAO from NmAOB (βAOB)

  NoHAO: HAO from NoAOB (γAOB)

Technical terms of drug discovery

BEI: Binding efficiency index {Inhibition activity (pIC_{50}) / molecular mass (kDa)}

IC_{50}:   The half maximal inhibitory concentration
           (The concentration of an inhibitor that is required for 50% inhibition)

  pIC_{50}: $-\log_{10}(IC_{50})$

HTS: High-throughput screening

SBDD: Structure-based drug design

FBDD: Fragment-based drug design

Abbreviations

RFU:	Relative fluorescence unit
S/B:	Signal background ratio
S/N:	Signal noise ratio
rmsd:	Root-mean-square deviation
SAR:	Structure activity relationship
	(Method for revealing effective chemical groups and chemical structures by determining IC_{50} value for target molecule and its analogs.)
MOE:	Molecular Operating Environment
	(Software package for drug discovery, Chemical Computing Group Inc.)

Contents

Contents

Figures

Abstract

Anthropogenic nitrogen input to global nitrogen cycle as a fertilizer affects the sustainability in agriculture and the health of the earth's environment. Ammonia-oxidizing bacteria (AOB), ubiquitous chemoautotrophic bacteria, cause nitrification of ammonium-fertilizers that is involved in nitrogen run-off and greenhouse gas nitrous oxide (N_2O) emission in agricultural land. Nitrification inhibitors, AOB specific bactericides, are widely used for prevention of nitrification. However, new nitrification inhibitors are desired because of toxicity and weak-effects of currently used inhibitors.

In this study, I have developed lead compounds of new nitrification inhibitor targeting to hydroxylamine oxidoreductase (HAO), a key enzyme of nitrification that catalyzes hydroxylamine to nitrite. Since a lot of uncultured AOB species have been discovered from soil by metagenomic analysis, the new nitrification inhibitor with wide-spectrum must be developed. For this purpose, I used two HAOs, NeHAO from *Nitrosomonas europaea* and NoHAO from *Nitrosococcus oceani*, which were phylogenetically distant from each other. My scheme utilizes combined use of X-ray crystal structure analysis, pharmacophore search, fluorescent HAO activity assay, cell-based nitrification assay, and structure-activity relationship (SAR) analysis.

I first solved the crystal structure of NoHAO, and then screened inhibitor seeds by soaking of substrate-mimicking hydroxylamine and hydrazine derivatives. An oxime compound and phenylhydrazine, a well-known HAO inhibitor, were bounded to the active center of HAO in the crystal structure. After setting HAO-inhibitor fragments of these compounds as pharmacophores, I performed pharmacophore search against a virtual library of 5 million commercial compounds (supplied by Namiki shoji) by using MOE software. The search provided approximately 100 hit-compounds.

In parallel, I developed a fluorescent HAO activity assay that can be applied to high-throughput screening on a 384-well plate. Using this assay, I analyzed inhibition activities of 77 out

General Introduction

Effect of human-induced nitrogen flow to global nitrogen cycle

In agriculture, nitrogen, phosphorus and potassium (N-P-K) are called 'the Big 3' primary nutrients that play fundamental roles in fertilizer for crop growing. However, available supplies of the three resources are different from one to another. Phosphorus and potassium are limited source which are supplied only by mining from rock resources. On the other hand, nitrogen can be supplied as industrial ammonium, which is synthesized using Haber-Bosh process from nitrogen molecule (N_2) in air. Therefore, nitrogen fertilizer is applied to farm-land excessively. Nitrogen fertilizer use has increased explosively since the 1950s due to appearance of the industrial inexpensive nitrogen fertilizer, and is substituted from rotation growth of food crop and forage legumes such as alfalfa, red clover, and sweet clover [1]. A large amount of the human applied nitrogen fertilizer affects nitrogen flows of the earth's biogeochemical cycles. Total nitrogen input was ~136.60 trillion grams (Tg) (= Mega ton) of nitrogen per year in the year 2000 [2]. Almost half of the nitrogen input was industrial fixed nitrogen fertilizer, such as anhydrous ammonium, ammonium sulfate, urea. 16 % of nitrogen input is from biofixation by microorganisms, such as rhizobium in root nodules of leguminous plants. Manure, recycled crop residues, and atmospheric deposition are contributed with each 8–13% of nitrogen input [2]. The large amount of human applied nitrogen has a significantly negative effect on the sustainability of agriculture, health of earth's environment, and human health [3].

Nitrification

Nitrogen is changing chemical forms in natural nitrogen cycle on soil **(Figure 1)** [3–5]. Under natural conditions, soil organic matters, which consists remains of living organisms, release ammonium (NH_4^+) by proteolysis and ammonification of soil microorganisms. The NH_4^+ is oxidized to nitrite (NO_2^-) by ammonium-oxidizing bacteria (AOB), and the nitrite (NO_2^-) is further oxidized to nitrate

(NO_3^-) by nitrite-oxidizing bacteria (NOB). The biological oxidation of NH_4^+ to NO_3^- is called "nitrification" [6]. The mineral nitrogen chemicals (NH_4^+ and NO_3^-) are immobilized (taken up and converted) to organic nitrogen, such as amino acid, by plants.
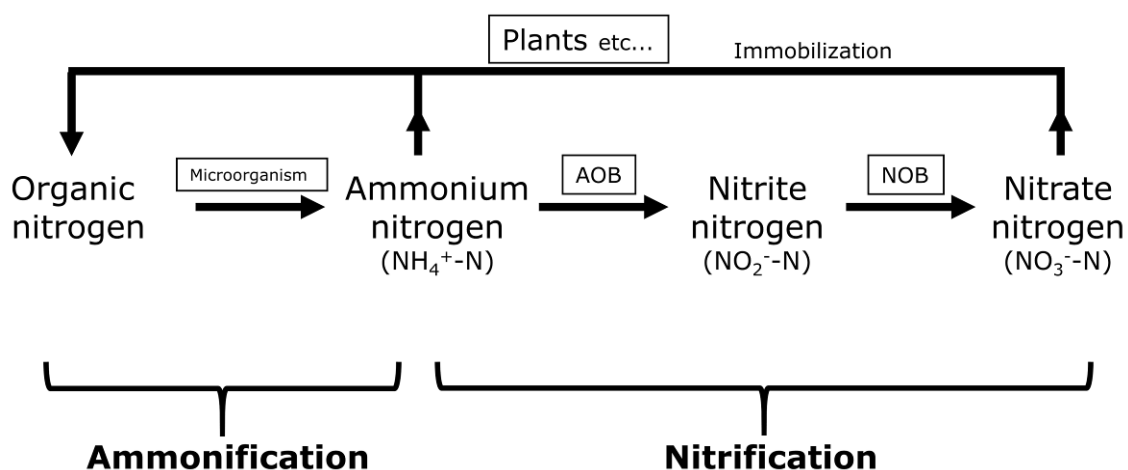
Figure 1. Major transformation of natural nitrogen cycle in soil.
Organic materials, such as plants, are decomposed by mainly heterotrophic microorganisms, and release ammonium (NH_4^+) (ammonification). The NH_4^+ is oxidized to nitrite (NO_2^-) by ammonium-oxidizing bacteria (AOB), and then the NO_2^- is oxidized to nitrate (NO_3^-) by nitrite-oxidizing bacteria (NOB) (nitrification). The NH_4^+ and NO_3^- are immobilized as organic nitrogen through assimilation by plants. (The figure is modified from Haynes *et al.* [4])

In farm-lands, excessive nitrogen fertilizers were applied and affected to nitrogen cycle (**Figure 2**). Nearly 90% of the applied nitrogen is in the NH_4^+ form [7]. Excessive application of the NH_4^+ leads to overgrowth of AOB and NOB. Then, the NH_4^+ is converted to NO_3^- by nitrification of AOB and NOB, mostly within four weeks after application [7]. The nitrification decreases nitrogen-use efficiency (NEU) by leaching of NO_3^- to surrounding waterbodies, such as underground water, river, lake, and sea. It has been estimated that a nearly 70% of applied nitrogen is lost from farm-land

[3]. The nitrogen leaching is caused by the difference in ionic mobility of NH_4^+ and NO_3^- in most soils. Because clay surface sand and soil organic matters are charged negatively, positively charged NH_4^+ can be binding to soil strongly by electrostatic forces. On the other hand, negatively charged NO_3^- makes very few interactions with the soil, and has high mobility (diffusion coefficient $\sim 10^{-6}$ cm^2 s^{-1}). It is suggested that the mobility of NO_3^- in soil is 50–500-fold higher than that of NH_4^+ [5]. Therefore, NO_3^- easily run off from farm-land during rains. Especially, in artificial drain system equipped farm-lands often on the middle to high-clay soil (e.g. in the upper Midwest Corn Belt of the United States), nitrogen leaching is very high [2]. The inversion of charge is caused by the nitrification of AOB. Therefore, control of nitrification rate is very important to decrease nitrogen runoff.
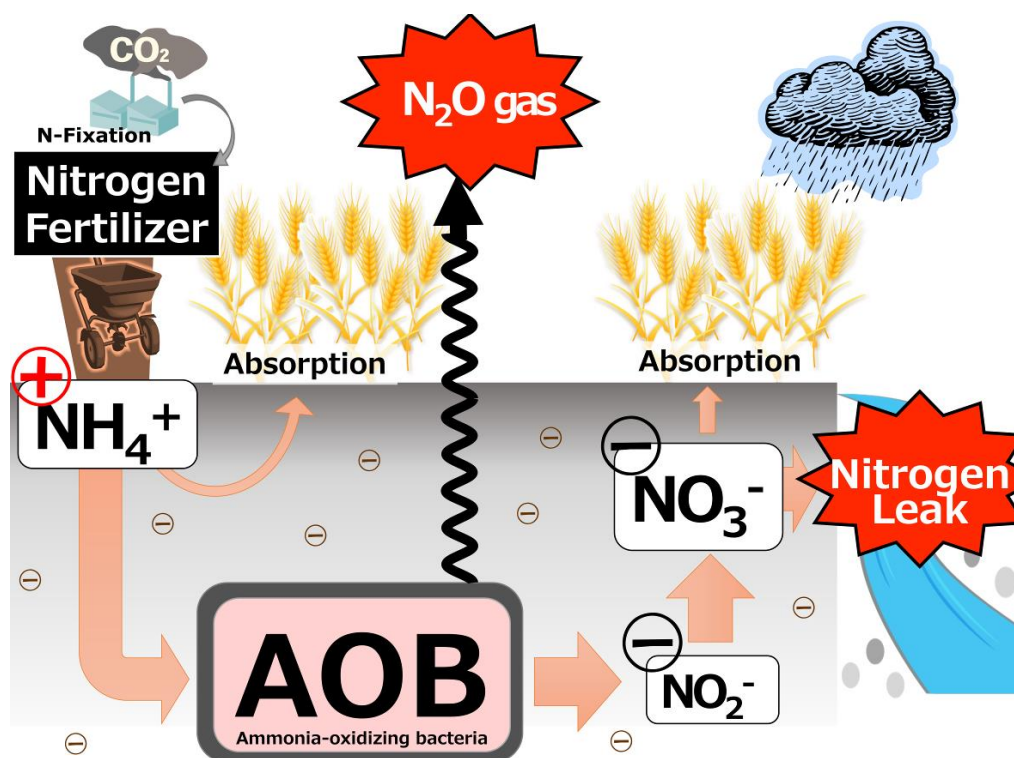
Figure 2. Nitrification of applied nitrogen fertilizer.

A large amount of ammonium (NH_4^+) synthesized by industrial nitrogen fixation was applied to farm-land as nitrogen fertilizer. A portion of the ammonium is uptaken directly by crops, however, most of the ammonium is metabolized to nitrite (NO_2^-) and byproduct of nitrous oxide (N_2O) gas (Greenhouse gas) by AOB. NO_2^- is subsequently metabolized to nitrate (NO_3^-) by nitrite oxidizing-bacteria (NOB, not

shown). NO_3^- accumulated to farm-land is uptaken slowly by crops. However, the NO_3^- is easily washed out from farm-land by rain fall. The charge of nitrogen compound is inverted from positive to negative by AOB metabolize. It is difficult for negatively charged soil to hold the negatively charged NO_3^-. The leaked NO_3^- cause eutrophication of water-bodies (river, lake, sea, under-ground water) and pollution of drinking water.

The unnatural nitrogen cycle caused by the large amount of human applied nitrogen leads to significantly negative effects to environment [3]. The three most important negative effects are eutrophication/pollution of water bodies, greenhouse gas emission, and energy loss associated with synthesizing of nitrogen fertilizer. Firstly, the eutrophication of water body is caused by leaching of NO_3^-, which promotes growth of cyanobacteria and phytoplankton. As a typical case, eutrophication and bottom-water hypoxia of northern Gulf of Mexico were caused by nitrogen leaching from fertilized corn fields around Mississippi river in U.S. [8]. Furthermore, pollution of NO_3^- to water-source of tap water leads to health risks that includes methemoglobinemia, which causes cyanosis, to human ("Blue Baby syndrome") [9] and live stocks [3]. Secondly, N_2O, a greenhouse gas 296 times stronger than CO_2, is proceeded during nitrification of AOB [3]. Furthermore, greenhouse gasses are also produced in the process of synthesizing nitrogen fertilizer. Thirdly, industrial nitrogen fixation process requires a large amount of energy (13,800 kcal kg^{-1} N fixed) [3] obtained by burning fossil fuels, and also leads to CO_2 emission. To decrease these negative effects, nitrification control technologies includes nitrification inhibitors are used.

Nitrification inhibitor

Nitrification inhibitor is a specific bactericide to AOB for controlling nitrification activity and is applied to farm-land with fertilizer. A number of nitrification inhibitors have been developed; 60

compounds including 20 commercially available nitrification inhibitors have been reported [3,10–18].

Typical studies have shown that commercial nitrification inhibitors decreased 63% of nitrogen

leaching [19] and 38% of N_2O emissions [18], and have a lot of other advantages both environmentally

and economically [3,18,20] (**Table 1A**). On the other hand, commercial nitrification inhibitors possess

particular problems such as toxicity and weak effects (**Table 1B**). Thus, next-generation nitrification

inhibitors are demanded. Since inhibition mechanisms of commercially available nitrification

inhibitors have not been determined, the rational modification of the inhibitors to improve inhibition

activity is difficult. Therefore, new methodology for nitrification inhibitor design is needed.

A. Advantages of using nitrification inhibitors

- Reduce applied nitrogen fertilizer.
- Reduction of labor by decreasing rate of fertilizer application.
- Increase crop production.
- Decrease N_2O gas emission (Greenhouse and ozone layer destruction gas).
- Decrease eutrophication of river, lake, and sea.

B. Disadvantages of conventional nitrification inhibitors

- Toxicity/Oncogenesity
- Volatilized at more than 20 °C (Nitrapyrin)
- Low nitrification inhibition effect

Table 1. Advantages (A) and disadvantages (B) of conventional nitrification inhibitors.

Nitrification inhibitor discovery innovated by using latest drug design techniques of medicine

For designing new and effective nitrification inhibitor in this study, I have tried to introduce latest drug

design techniques for medicinal chemistry, such as high-throughput inhibitor screening and evaluation

assay, structure-activity relationship (SAR) analysis, and structure-based drug design (SBDD) method

including fragment based drug design (FBDD) method and structure based *in-silico* screening [21].
Especially, SBDD is a prominent component of modern medicinal chemistry [22–24]. SBDD method
uses three-dimensional structural information of the drug target enzyme to visualize the shape of ligand
binding pocket for designing molecules fitting into the pocket. On the other hand, no agrochemicals
developed by SBDD have been launched so far, and have never applied to nitrification inhibitor design.
To perform SBDD, highly purified sample and experimentally determined structure information of
target protein are needed. I have selected for the target protein from key enzymes of nitrification
pathway in AOB.

Nitrification pathway; potential target of nitrification inhibitors

In AOB, ammonia monooxygenase (AMO) and hydroxylamine oxidoreductase (HAO) are key
enzymes of nitrification pathway, and catalyze ammonia (NH_3) to nitrate (NO_2^-) via hydroxylamine
(NH_2OH) by following chemical reactions [25]:

AMO: $NH_3 + 2H^+ + O_2 + 2e^- \rightarrow NH_2OH + H_2O$,

HAO: $NH_2OH + H_2O \rightarrow NO_2^- + 5H^+ + 4e^-$.
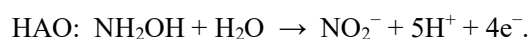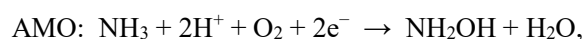
In this pathway, four electrons are generated by HAO; two electrons are transferred back to AMO as
the catalytic energy source, and the remaining two electrons are consumed as a growth energy through
generating NADPH and ATP [26] (**Figure 3**).
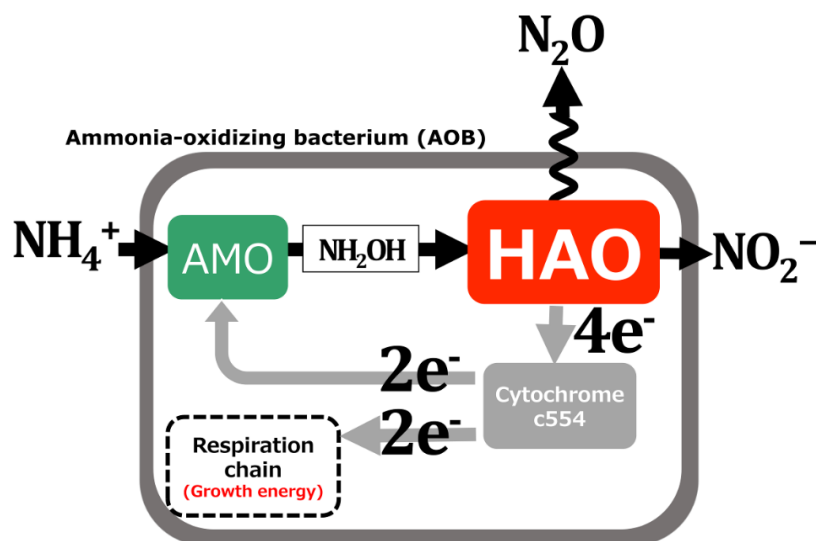
Figure 3. Nitrification pathway in AOB.

Ammonium (NH_4^+) is first oxidized to hydroxylamine (NH_2OH) by ammonia monooxigenase (AMO) using two electrons (e^-). The hydroxylamine oxidized to nitrite (NO_2^-) by hydroxylamine oxidoreductase (HAO), and four electrons are released by the reaction. The electrons are transferred to cytochrome c_{554}. Then, two electrons are returned back to AMO, and the remaining electrons are ultimately transferred to the terminal oxidases and used for the growth energy. The N_2O is possibly generated by HAO as a byproduct. The N_2O pathway has not been fully characterized and alternative routes are believed to exist [27].

Therefore, both of the enzymes, AMO and HAO, are potential targets of nitrification inhibitors. Actually, AMO is believed to be a molecular target of commercial nitrification inhibitors such as nitrapyrin [28]. However, rational design of AMO-targeting inhibitor is difficult. AMO is believed to be a membrane protein that assembled trimer-of-trimer structure including three subunits: AmoA, AmoB, AmoC (**Figure 4**). In general, analysis of membrane proteins forming a large complex is very difficult. Actually, purification of AMO has not been succeeded over more than 50 years. So, valuable *in vitro* assay methods and experimental three-dimension structure (e.g. crystal structure) information of AMO are not available yet.
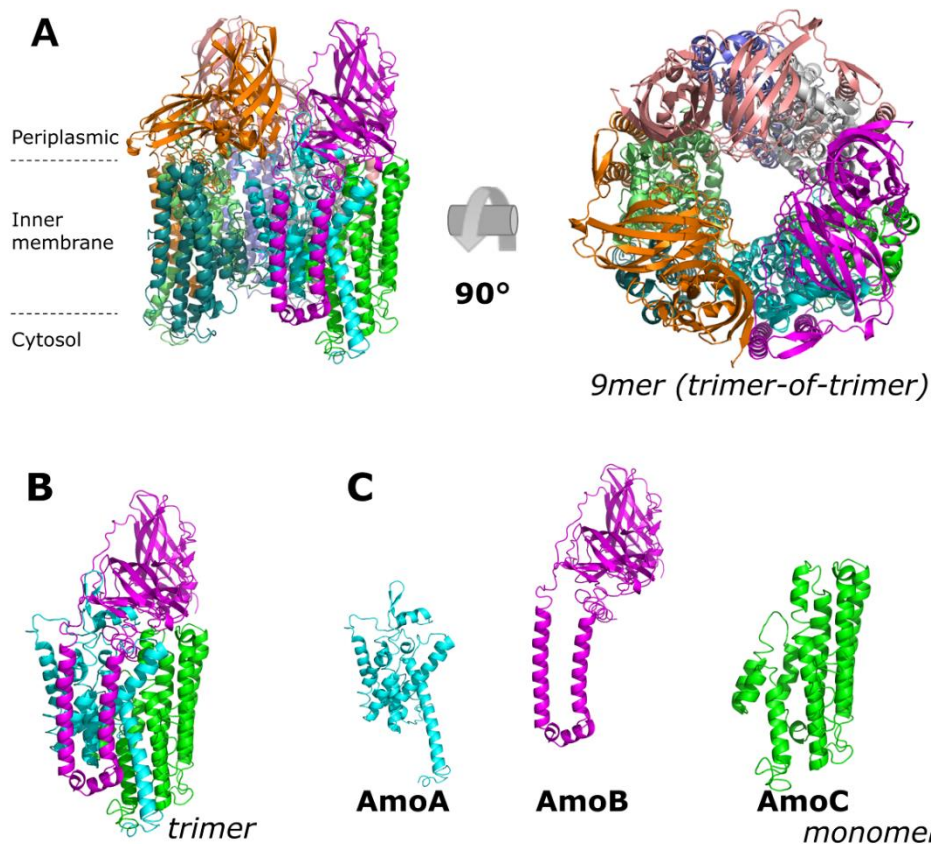
Figure 4. Ammonia monooxigenase (AMO) modeled structure.
(A) Whole structure of AMO that forms 9mer (trimer-of-trimer) structure includes each three AmoA, AmoB and AmoC subunits. (B) Trimer subunit structure of AMO. (C) monomer structure of AmoA, AmoB and AmoC subunits. The structures were modeled by I-tasser server [29] separately for each subunit that amino acid sequences are used with: AmoA (UniProt KB entry, AmoA1_NITEU), AmoB (AmoB1_NITEU), AmoC (AmoC2_NITEU). Assemble to 9-mer form was performed by PyMOL software using the methane monooxigenase structure (pMMO, PDB:1YEW) from *Methylococcus capsulatus* (methane oxidizing-bacteria) as a template.

HAO is a newly-emerging target of nitrification inhibitor. Recently, Wu *et al*. [30] have reported that the activity of soil nitrification was suppressed by organo-hydrazines that act as suicide inhibitors for HAO [31]. Crystal structures of naturally purified βAOB *Nitrosomonas europaea* HAO

(NeHAO) have been resolved [32–34], and they allow us to develop HAO inhibitors by structure-guided drug design. Therefore, I believed that HAO is more suitable as a nitrification-inhibitor target than AMO.

HAO is soluble trimer protein including total 21 heme-*c* and 3 heme P460 (**Figure 5**). The heme P460 is covalently connected to tyrosine that inserted from next subunit. So, each subunits of trimer were covalently connected. The active center was located on the heme P460 in the ligand binding pocket. If you could design to block the pocket, the hydroxylamine oxidoreductase reaction will be stop. This is the main reason why we have selected HAO as a target of inhibitor.
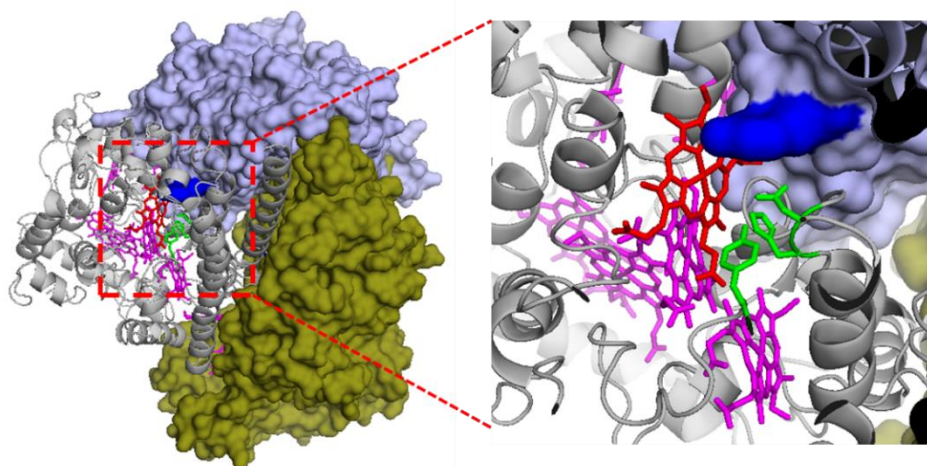
Figure 5. NeHAO structure.
Overall (left) and close up (right) view of trimer complex of NeHAO. Two subunits are represented in surface model (brown and light blue), one subunit is represented in cartoon model (grey) on left panel. Covalent bonded tyrosine side chain is shown in blue. Heme P460 and heme-*c* were colored red and pink, respectively. Conserved amino acid side chains in active center are shown in stick models colored in green. Structure representations were prepared by PyMOL.

Here, I show nitrification inhibitor discovery strategy adapted cutting edge medicinal drug discovery technologies and obtained effective lead compounds. My results will assist developing effective next-generation nitrification inhibitors, and will lead to promotion of sustainable agriculture.

Chapter 1
Establishment of the experimental technology for nitrification inhibitor development

Introduction

I first established fundamental methods that required for nitrification inhibitor development study; integrated preparation systems for HAO, high-resolution three-dimensional structural information for NeHAO and NoHAO, high-throughput inhibition assay systems for live AOB cell (colorimetric) and purified HAO (colorimetric and fluorescence).

Materials and methods

Culture media

The culture medium "NeMedium ver. 2014.12" modified for *Nitrosomonas europaea, Nitrosomonas* sp. JPCCT2, *Nitrosospira. multiformis,* and *Nitrosospira lacus* was prepared by slightly modifying NBRC Medium 829 [35] and the previous report [36]. The 1 L medium included 11.29 g HEPES (Sigma-Aldrich, St. Louis, MO, USA), 2.5 g ammonium sulfate, 40 mg Fe(III)-EDTA (Dojindo laboratories, Kumamoto, Japan), 0.5 g KH_2PO_4, 0.5 g $NaHCO_3$, 0.5 g $MgSO_4 \cdot 7H_2O$, 100 mg $CaCl_2 \cdot 2H_2O$, 0.001% (w/v) phenol red, 1 mL of 1000× trace-element mixture. Stock solution of the 1 L 1000× trace-element mixture included 30 mg H_3BO_3, 100 mg $MnCl_2 \cdot 4H_2O$, 190 mg $CoCl_2 \cdot 6H_2O$, 24 mg $NiCl_2 \cdot 6H_2O$, 2 mg $CuCl_2 \cdot 2H_2O$, 144 mg $ZnSO_4 \cdot 7H_2O$, 36 mg $Na_2MoO_4 \cdot 2H_2O$ and 8 mL of 12N HCl. The chemicals were dissolved in deionized water. The media was adjusted to pH 7.9 (25 °C)

with 10N NaOH. The 20 L media was autoclaved in the 20-L plastic carboy (Nalgene® Round Polycarbonate Clearboy® with Spigot, Thermo Fisher Scientific, Waltham, MA, USA).

The culture medium "NoMedium ver. 2014.12" for *Nitrosococcus oceani* was prepared according to previous reports [36,37] with slightly modification. The 1 L medium was prepared for 990-ml mother solution and 10 ml-metal solution, separately. The 990 mL mother solution included 10.46 g MOPS (Sigma-Aldrich), 2.5 g ammonium sulfate, 27.5 g NaCl, 15 mg KH_2PO_4, 0.2 g $NaHCO_3$, 6.78 g $MgSO_4 \cdot 7H_2O$, 5.38 g $MgCl_2 \cdot 6H_2O$, 0.72 g KCl, 0.001% (w/v) phenol red. The mother solution was adjusted to pH 7.9 (25 °C) with 10N NaOH. The 10-mL of metals solution included 100 mg $CaCl_2 \cdot 2H_2O$, 4 mg Fe(III)-EDTA, 1 mL of 1000× trace-element solution. For making 20-L medium, 19.8-L mother solution was autoclaved in the 20-L plastic carboy, and then the 200-mL metals solution was added to the mother solution, aseptically. Unless otherwise specified, highest grade available chemicals were purchased from Wako Pure Chemical Industries (Osaka, Japan) or Nacalai Tesque (Kyoto, Japan).

Cell lines and cell cultures

N. europaea strain NBRC 14298 (=ATCC 19718) (NeAOB) and *Nitrosomonas* sp. NBRC 108559 (=JPCCT2) were purchased from National Institute of Technology and Evaluation, Biological Resource Center (NBRC) (Chiba, Japan). *N. oceani* ATCC 19707 (NoAOB), *N. multiformis* ATCC 25196 (NmAOB) and *N. lacus* ATCC BAA2542 (=APG3) were purchased from ATCC (Manassas, Virginia, USA). Stocked culture stored at 4 °C was inoculated to 40 mL medium, and incubated for 1 week at 26 °C with gently shaking (~80 rpm). Then, the pre-culture was inoculated to the 20 L medium in a 20-L plastic carboy (Nalgene® Round Polycarbonate Clearboy® with Spigot, Thermo Fisher Scientific, Waltham, MA, USA), and was incubated for 2 weeks at room temperature (25 °C) with air ventilation (2.5 L/min) until phenol red turned to yellow (pH ~6.0). For the use of purification of HAO, the cells were harvested by centrifuge with 7000 × g, and were stored at −80 °C until purification. For

the use of live cell inhibitor assay, the culture is stored at 4 °C and used within 2 weeks. The yields of

the each AOB strain cells were approximately 1.5 g by 20-L cultures.

Nitrification activity assay for AOB cells

AOB cells transferred to same volume of fresh medium were divided into 100 μL to each wells of 384

deep well plate (BIO-BIK, Osaka, Japan). 0.5 μL DMSO solutions containing certain concentration

of phenylhydrazine were added to each wells. The plate was sealed with air-exchange film (AeraSeal™,

EXCEL Scientific, Victorville, CA, USA), and incubated for 18 hours at 25 °C. Then, 1 μL of the

media in each wells were transferred to 384-well non-binding clear microplate (Greiner) filled with

100 μL Greiss Reagent in each wells. After 20 min incubation at room temperature (25 °C), 545 nm

absorbance was measured by using Infinite® M1000 PRO microplate reader (Tecan). The Greiss

Reagent was optimized to be composed of same volumes of stock solution A {2% (w/w) sulfanilamide,

12% (v/v) phosphoric acid} and stock solution B {0.2% (w/w) N-(1-naphthyl)ethylenediamine}

according to Giustarini *et al*. [38] with slight modifications. The stock solutions A and B were stored

at 4 °C, and mixed just before measurements. The half-maximal inhibition concentration (IC$_{50}$) was

calculated by GraphPad Prism6 software (GraphPad Software, La Jolla, CA, USA).

Purification of HAO

Frozen cell pellet (~1.5 g) was suspended in 40 mL buffer A (pH 7.5, 50 mM Tris-HCl) and sonicated.

The suspension was then centrifuged at 40 000 × *g* for 40 min at 4 °C. The supernatant was applied to

an anion-exchange column system composed of three tandemly connected HiTrap™ Q HP 5 mL

columns (GE Healthcare, Buckinghamshire, England, UK), which were equilibrated with buffer A. A

linear gradient of NaCl was performed with 0–500 mM NaCl in 100 mL buffer A. Post-elution cleaning

was performed using 1 M NaCl. The eluted HAO fractions were subsequently applied to a HiLoad™

26/600 Superdex™ 200 pg gel-filtration column (GE Healthcare) equilibrated with buffer B (pH 7.5, 10 mM Tris–HCl, 150 mM NaCl). Then, the eluted HAO fractions were applied to hydroxyapatite column composed of 5 mL CHT™ Ceramic Hydroxyapatite media (Type 1, 20 μm particle size, Bio-Rad, Hercules, CA, USA) packed to 10 mm inner diameter column that was equilibrated with buffer C (pH 7.5, 20 mM potassium phosphate buffer). The elusion was performed by linear gradient of 20–500 mM potassium-phosphate buffer (pH 7.5). This hydroxyapatite chromatography step is not necessary for purification of NoHAO. Thereafter, the eluted HAO fractions were applied to a high-performance anion-exchange column Mono Q® 10/100 GL (GE Healthcare). The elution was performed using a linear gradient of NaCl in buffer A (0–500 mM, 100 mL). Post-elution cleaning was performed using 1 M NaCl. The eluted HAO fractions were then stored at 4 °C until further experiments.

All chromatography procedures were performed using the ÄKTA*explore* 100 system (GE Healthcare). All eluted fractions containing HAO were detected by two methods: 1) wavelength monitoring by ÄKTA*explore* (protein: 280 nm; *c*-type hemes in HAO: 409 nm) and 2) SDS-PAGE analysis with coomassie brilliant blue stain.

Characterizations of purified proteins

N-terminal sequences of the purified proteins were analyzed by Procice® 491HT Protein Sequencing System (Applied Biosystems, Foster, CA, USA). Crystallization of NeHAO was performed as described by Maalcke *et al*. [34]. Protein concentration was determined by Qubit® protein assay kit (Thermo Fisher Scientific) with Quick Start® Bovine Serum Albumin Standard Set (Bio-Rad, Hercules, CA, USA). The UV–vis spectra were measured from 220 to 800 nm with 0.2 nm bandwidth and 0.1 nm s^{-1} scan rate at 25 °C using a Cary 400 Bio spectrophotometer (Varian, Zug, Switzerland). The measurement buffer was 20 mM Tris-HCl with or without 50 mM dithionite. The dithionite was

prepared as a 1 M solution, and was added to the protein solution immediately before measurement.

Tris-Glycine-SDS-PAGE was performed on 5–20% gradient polyacrylamide precast-gel (e-PAGEL®

E-R520L, ATTO, Tokyo, Japan) with EzRunC+ electrophoresis buffer (ATTO). To detect low

molecular mass proteins, Tris-Tricine-SDS-PAGE was performed on 15% polyacrylamide precast-gel

(e-PAGEL® E-R15S, ATTO) with the electrophoresis buffer containing 100 mM Tris, 50 mM Tricine,

and 0.1% (w/v) SDS. The samples were boiled at 100 °C for 3 min with same volume of the Laemmli

sample buffer composed of 125 mM Tris-HCl, 0.004% (w/v) bromophenol blue, 4% (w/v) SDS, 20%

(w/v) glycerol, 10 mg/mL dithiothreitol (DTT), pH 6.8. The sample buffer was stocked in a −20 °C

freezer in single-use volumes because air oxidization of DTT leads to diffusion of the HAO bands.

The boiled samples in 10 µL were applied to the gel. BenchMark™ Protein Ladder (Thermo Fisher

Scientific) was used as a protein marker. The gel was stained by coomassie brilliant blue solution

EzStain AQua (ATTO).

Optimization for HAO colorimetric activity assay using cytochrome-*c*

HAO activity assay was performed based on the procedure reported by Logan *et al*, which was a

method detecting HAO activity by increase of 550 nm absorbance of reduced cytochrome-*c* coupled

with hydroxylamine oxidation by HAO [39]. 100 µL reaction mixture for one assay contained 50 µM

hydroxylamine, 50 µM horse-heart cytochrome–*c* (Nacalai Tesque), several buffer types, pH, NaCl

concentration, and additives. The reaction was started by addition of hydroxylamine. The absorbance

was measured by using Infinite® M1000 PRO microplate reader (Tecan) on a 384-well non-binding

clear microplate (Greiner bio-one, Kremsmünster, Austria). The reactions were performed at room

temperature (25 °C). The relative activity was calculated by defining highest absorbance after

incubation as 100% and initial absorbance as 0%. Optimization for pH and buffer was performed for

using following conditions; 20 mM citric acid buffer (pH 2.57, 2.27, 3.00, 3.16, 3.37, 3.60, 3.80, 4.06,

Wako), 20 mM citrate-phosphate buffer (pH 3.16, 3.38, 3.57, 3.67, 3.78, 4.02, 4.25, 4.66, 4.76, 4.91, 5.16, 5.35, 5.59 ,5.80, 5.90 ,6.00, 6.18, 6.35, 6.65, 6.66, 6.77, 6.85, 7.02 ,7.19, 7.33 ,7.48, 7.53, Wako), potassium-phosphate buffer (pH 5.55, 5.77, 5.94, 5.99, 6.08, 6.24, 6.39, 6.53, 6.65, 6.72, 6.81, 6.96, 7.09, 7.22, 7.37, 7.46, 7.52, 7.69, 7.83, 7.94, 8.05, 8.08, 8.11, 8.12, Wako), HEPES-NaOH buffer (pH 6.55, 6.75, 6.95, 7.12, 7.22, 7.31, 7.53, 7.75, 7.88, 8.07, Sigma-Aldrich), 20 mM Tris-HCl buffer (pH 6.78, 6.96, 7.34, 7.51, 7.57, 7.66, 7.84, 7.89, 8.14, 8.25, 8.35, 8.39, 8.47, 8.57, 8.65, Nacalai Tesque), CAPSO buffer (pH 8.98, 9.26, 9.47, 9.63, 9.82; Hampton research), CAPS buffer (pH 10.11, 10.21, 10.32, 10.55, 10.75, 10.83; Hampton research), n = 4, total 384 assays. Optimization for salt concentration was performed by NaCl varied with 0, 12.5, 25, 50, 100, 200, and 400 mM in 50 mM HEPES-NaOH (pH 7.0) buffer. HAO assay validation and inhibition assays were performed with 100 µL solution containing 50 mM HEPES-NaOH (pH7.0), 50 mM NaCl, 50 µM hydroxylamine, 50 µM horse heart cytochrome-c, 0.01% Triton X-100, and 0.5 µL DMSO in which certain concentration of phenylhydrazine was dissolved.

Crystallization for NeHAO

NeHAO was crystallized as described by Cedervall et al. [33,40] and Maalcke et al. [34]. In brief, stocked HAO solution was dialyzed with buffer C (pH 7.5, 25 mM HEPES-KOH, 25 mM KCl), and was concentrated to 5 mg/mL using VIVASPIN® concentrator (0.5 mL, 10,000 MWCO PES, Vivascience, Hannover, Germany). Under oil batch crystallization was performed on oval plates (Nunc® MiniTrays with Nunclon® Delta surface, 60-well, Thermo Fisher Scientific) using 2 µL of protein solution and 2 µL mother solution containing 42 % (v/v) PEG400 (Hampton Research, Aliso Viejo, CA, USA), 50 mM KNO$_3$ (Wako), MES (Wako) /NaOH buffer (pH 7.5) under thin layer of 10 µL Al's oil (Hampton Research). The crystals grew to more than 0.4 mm within 2 weeks.

Chapter 1
Establishment of the experimental technology for nitrification inhibitor development

Crystallization for NoHAO

Preliminary screening of crystallization conditions for NoHAO was performed by the sitting-drop vapor-diffusion method at 20 °C using Crystal Screen HT, Crystal Screen Cryo HT (Hampton Research) and Wizard JCSG+ (Emerald BioSystems). Drops containing 0.3 μL protein solution in 20 mM Tris-HCl buffer, pH 7.5, and 0.3 μL mother liquor were equilibrated against 50 μL reservoir solution. Tiny crystals of NoHAO were observed under several conditions with 2.4–2.8 M ammonium sulfate within a week. Further optimization of ammonium sulfate concentration, pH and buffer solution was carried out by the hanging-drop vapor-diffusion method with 8 μL protein solution with a concentration of 5 mg ml^{-1}, 8 μL mother liquor and 500 μL reservoir solution. Finally, diffraction quality crystals of NoHAO were obtained at 20 °C from solution containing 8 μL of the as-isolated protein at 7.9 mg ml^{-1} in 20 mM Tris-HCl buffer, pH 7.5, and in a reservoir solution containing 2.6 M ammonium sulfate and 100 mM Na/K phosphate buffer (NaH$_2$PO$_4$/K$_2$HPO$_4$), pH 6.6. The crystals appeared within two days and grew to the size of $0.2 \times 0.2 \times 0.2$ mm in 10 days.

Data collection and structure analysis for NeHAO and NoHAO

X-ray diffraction data were collected from a single crystal at the beamline AR-NW12A [41] of the Photon Factory (PF), High Energy Accelerator Research Organization, Tsukuba, Japan. A cryo-protectant solution containing 30% trehalose, 2.6 M ammonium sulfate and 100 mM Na/K phosphate buffer pH 6.6 was gently added to the crystallization drop. The crystal was scooped up in a nylon CryoLoop™ (Hampton Research) and flash-cooled in a nitrogen-gas stream at 100 K. No additional dehydration and/or annealing were performed. Diffraction data were collected with 1 s exposures for 180° with 0.5° step oscillations over a total of 360 data points at a wavelength of 1.0 Å using Quantum 210 CCD detector (Area Detector Systems Corp., Poway, CA, USA). Data were integrated and scaled using the program *DENZO*® and *SCALEPACK* from the *HKL*-2000® program suite [42]. The as-isolated (apo) NoHAO crystals belonged to the space group $I2_13$ and one molecule existed in the

asymmetric unit with the solvent content of 81.88%.

The structures of the as-isolated NeHAO and NoHAO in the apo-enzyme form were solved by the molecular replacement method using the previously reported NeHAO structure (Protein Data Bank ID code 4n4n) as a reference model by the program MOLREP [43]. Manual model building and molecular refinement were performed by using Coot [44] and Refmac5 within the CCP4 program suite [45–47]. The stereochemistry of the models was analyzed with the program Rampage [48]. Figures of the proteins were generated by PyMOL version 1.7.0.1, UCSF chimera package version 1.10.2 [49], Molecular Operating Environment (MOE) version 2015.1001 [50] and POV-Ray version 3.7.0 [51].

Results and discussion

Mass culture systems for AOB strains.

A large amount of AOB cell was required for inhibitor screening against live AOB and purification of HAO. Mass culture systems for AOB strains were reported only for *Nitrosomonas europaea* (NeAOB) and *Nitrosococcus oceani* (NoAOB). I have obtained six species of AOB strains that were deposited in public bioresource centers, and established mass culture systems for all the strains using modified culture medium and 20-L plastic carboy with air ventilation. The culture medium were modified by previously reported [35,37,52]. The yields of the wet cell pellets are about 1.5 g for each 20-L culture.

High-throughput nitrification assay using live AOB cell

Evaluation of activity of nitrification inhibitor candidates is important not only for *in vitro* enzyme assay level, but also for AOB live cell assay level. Many nitrification inhibitor assays have been performed for nitrification activity of AOB [13], but none of them could not be used for high-throughput screening and evaluation as they are. The most commonly used assay method for the nitrification activity of AOB determines NO_2^- concentration by a colorimetric assay using Griess

reagent, for which the absorbance is measured at 545 nm [38]. I optimized this method for high-throughput screening and evaluation of nitrification inhibitors. In particular, the assay method was optimized for the 384-well microplate by re-profiling composition of the Griess reagent by referring to Giustarini et al. 2008 [38]. The detail conditions and procedures are described in Materials and Methods section. This method allows me to perform more than 3,000 assays within two days by manually.

To assess my assay method quantitatively, I estimated a statistical parameter termed Z'-factor that determines the suitability of an assay for high-throughput screening based on the signal dynamic range and the data variability [53]. A score of $1 > Z' \geq 0.5$ indicates an excellent assay, $Z' = 1$ an ideal assay, $Z' < 0$ essentially impossible for screening. Calculated Z'-factors were 0.73 for the NeAOB assays, respectively, indicating that my method is suitable for high-throughput screening and inhibitor evaluation. Other validation statistics were summarized in **Table 2**. This method is considered to be suitable for screening to ~10,000 compounds class libraries and IC_{50} determination as a second screening to ~100 compounds.

Table 2. Validation statistics of nitrification inhibition assay for NeAOB on a 384-well microplate.

Benchmark	Formula	NeAOB
Coefficient value (**CV %**)[a]	$= SD_{100\%}/Av_{100\%}{}^{b} \times 100$	3.8
Signal Background ratio (**S/B**)	$= Av_{100\%}/Av_{0\%}{}^{c}$	2.0
Z'-factor[d]	$= 1 - \dfrac{3 \times SD_{100\%} + 3 \times SD_{0\%}}{Av_{100\%} - Av_{0\%}}$	0.73

[a]n = 4.

[b]545 nm absorbance measured at 30 min (without inhibitors).

[c]545 nm absorbance measured at 0 min (without inhibitors).

[d]Referred to *Zhang* et al. [53].

Purification of NeHAO and NoHAO by newly developed simplified methods

I report new integrated purification methods for NeHAO and NoHAO. my methods only employ a

series of chromatography purification steps instead of cumbersome steps such as ammonium-precipitation, buffer exchange, dilution and concentration used in the previously reported conventional methods [34,37,40,54,55]. Purification procedures and results for NeHAO and NoHAO are shown in **Figure 6** and **Figure 7**, respectively. Purity of the HAOs eluted from gel-filtration column may be enough for enzymatic assay; hydroxyapatite and MonoQ column chromatography steps are optional to remove minor contaminations (**Figure 6B** and **Figure 7B**). The hydroxyapatite column step is not necessary for NoHAO. The purified proteins were identified as NeHAO and NoHAO using a protein sequencer (determined sequences are shown in **Figure 27**). Yields were 0.8 mg for NeHAO and 0.6 mg for NoHAO from approximately 1.5 g of wet cell pellets.

Quality of the purified HAOs was analyzed by absorbance measurement (**Figure 6D** and **Figure 7D**). Judging from the 409/280 nm absorbance ratios of 3.39 and 3.94 respectively for the oxidized NeHAO and NoHAO, my purified proteins possess comparable or even higher purity than the corresponding proteins prepared by the conventional purification methods [22].
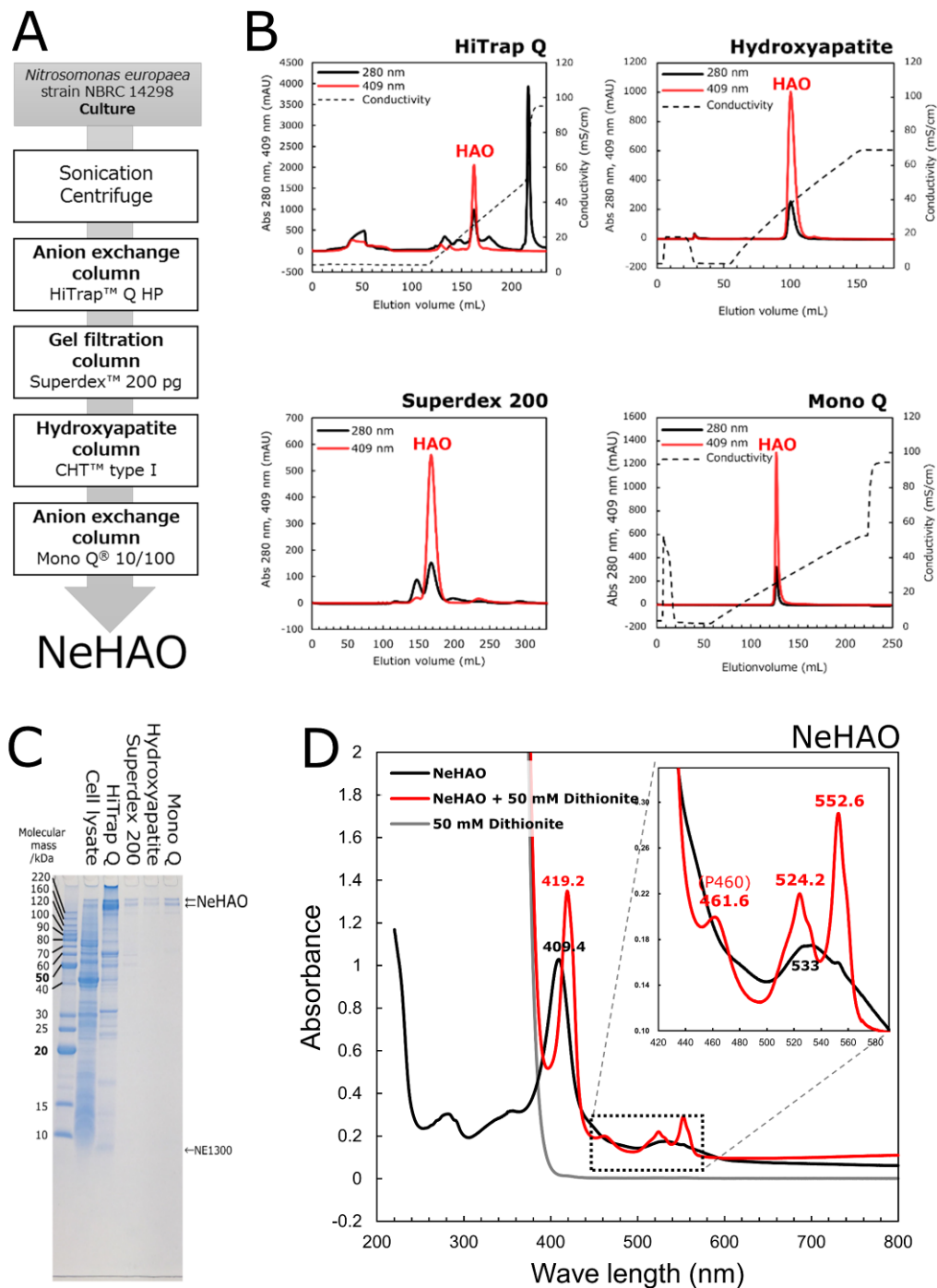
Figure 6. Integrated purification method for NeHAO.

(A) Purification scheme of NeHAO. (B) Elusion profiles of HiTrap Q ion-exchange, Superdex 200pg gel-filtration, CHT ceramic hydroxyapatite, and MonoQ ion-exchange chromatography of NeHAO. (C) SDS-PAGE analysis of HAO containing fractions at each chromatography steps of NeHAO. (D) UV-vis spectra for air-oxidized and dithionite reduced NeHAO.
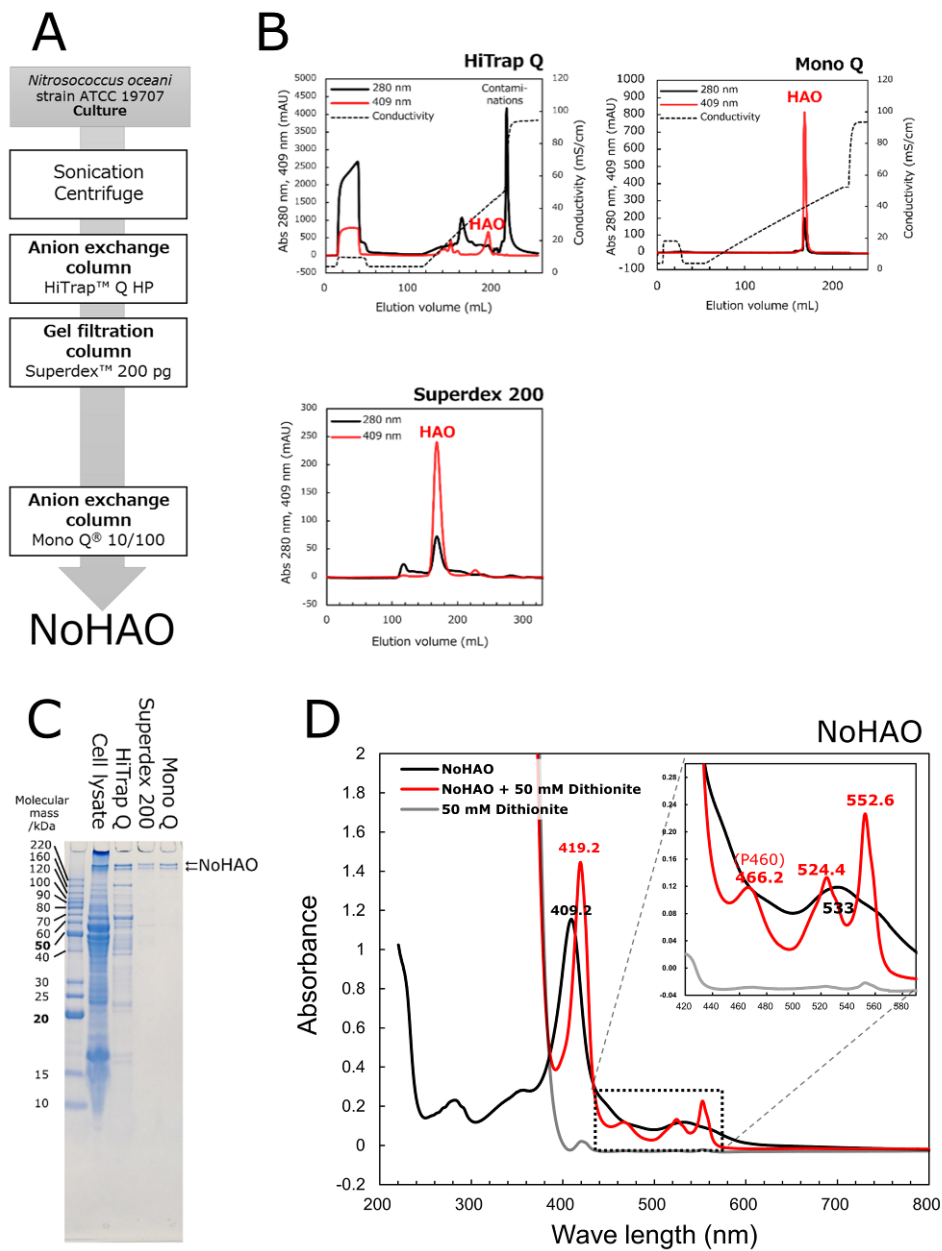
Figure 7. Integrated purification method for NoHAO.

(A) Purification scheme of NoHAO. (B) Elusion profiles of HiTrap Q ion-exchange, Superdex 200pg gel-filtration, and MonoQ ion-exchange chromatography of NeHAO. (C) SDS-PAGE analysis of HAO containing fractions at each chromatography steps of NoHAO. (D) UV–vis spectra for air-oxidized and dithionite reduced NoHAO.

Optimization of middle-throughput HAO "COLORIMETRIC" assay

Many activity assays and inhibitor assays have been performed for HAO [31,39,55], but none of them

could not be used for screening and evaluation against a few hundred of compounds as they are. The

most commonly used assay method is that the HAO activity is determined by monitoring the

absorbance change at 550 nm due to the reduction of an electron acceptor cytochrome-*c* coupled with

hydroxylamine oxidation by HAO [55]. I optimized this method for HAO inhibitor screening and

evaluation. In particular, the assay method was optimized for the 384-well microplate assay by re-

profiling conditions of the buffer, pH, salt and additives. **Figure 8A and B** show that NeHAO and

NoHAO displayed almost same pH-dependent activity profiles although the optimum pH values were

slightly different, pH 9.4 for NeHAO and 10.0 for NoHAO. As an optimized buffer condition, I

selected a pH 7.0, HEPES-NaOH buffer based upon the following reasons. (1) Since nitrous oxide

produced during the hydroxylamine oxidation by HAO decreases pH of the assay solution, the HAO

activity measured at an initial pH above 7.5 is too sensitive against pH decrease accompanied by

hydroxylamine oxidation. (2) The activities at pH 7.0, 15% for both HAOs, are large enough for the

inhibitor screening and evaluation. (3) The HAO activities measured at pH 7.0 in four different buffers

were essentially the same. In addition, I used HEPES-NaOH buffer as the *N. europaea* culture medium.

As an optimized salt concentration, I selected a 50 mM NaCl with which NeHAO and NoHAO

displayed highest activities (**Figure 8C and D**). Furthermore, I confirmed that no significant changes

in the NeHAO and NoHAO activities by addition of 0.5 % DMSO and 0.01% Triton X-100 (**Figure

8E**). DMSO is frequently used as a solvent to dissolve chemicals in screening libraries, and Triton X-

100 is a detergent to prevent chemical aggregation of compounds and non-specific binding of enzymes

to plastic wares [56]. Finally, measurements of the NeHAO and NoHAO reaction time courses under

the optimized conditions allowed us to employ the activity value at 30 min for evaluating inhibitory

response (**Figure 8F**). Calculated Z'-factors were 0.73 and 0.88 for the NeHAO and NoHAO assays,

respectively, indicating that the HAO colorimetric assay method is suitable for high-throughput screening and inhibitor evaluation. Other validation statistics were summarized in **Table 3**. This method is considered to be suitable for middle-throughput screening to ~1,000 compounds class libraries and IC_{50} determination as a second screening to ~100 compounds. On the other hand, the disadvantage of this assay method is using expensive horse cytochrome-*c* as a colorimetric probe (¥5,000/plate) and low sensitivity (S/B ~2).
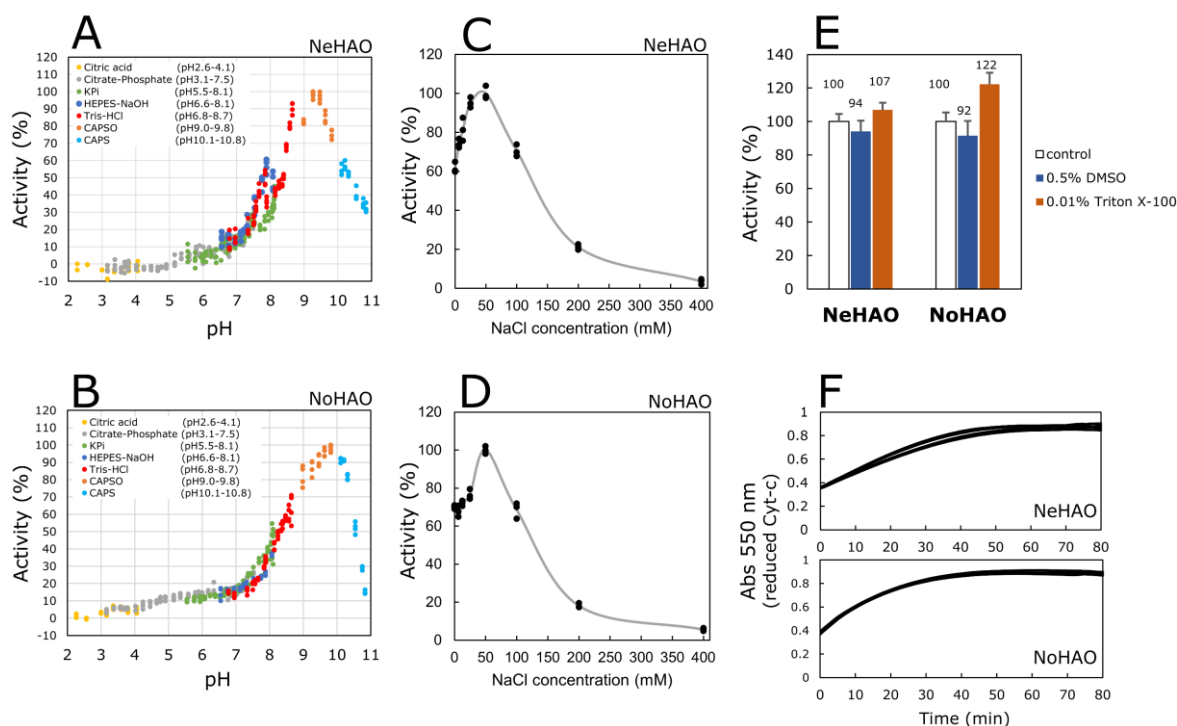
Figure 8. Optimization of HAO "COLORIMETRIC" assay using cytochrome-*c*.

Effect of pH and buffer types for activity of NeHAO (A) and NoHAO (B). Effect of salt concentration for activity of NeHAO (C) and NoHAO (D). (E) Effect of additives (0.5 % DMSO and 0.01% Triton X-100) for activity of NeHAO and NoHAO. (F) Time courses of activity measurements for NeHAO and NoHAO.

Table 3. Validation statistics for HAO "COLORIMETRIC" assay using cytochrome-*c* on a 384-well microplate.

Benchmark	Formula	NeHAO	NoHAO
100% Average (**Av$_{100\%}$**)[a,b]	-	0.72	0.82
100% Standard deviation (**SD$_{100\%}$**) [a,b]	-	0.0275	0.0084
Background Average (**Av$_{0\%}$**)[a,c]	-	0.36	0.38
Background Standard deviation (**SD$_{0\%}$**) [a,c]	-	0.0057	0.0092
Coefficient value (**CV %**)	$=SD_{100\%}/Av_{100\%} \times 100$	3.79	1.02
Signal Background ratio (**S/B**)	$=Av_{100\%}/Av_{0\%}$	2.01	2.17
Z'-factor[d]	$= 1 - \dfrac{3\times SD_{100\%}+3\times SD_{0\%}}{Av_{100\%}-Av_{0\%}}$	0.73	0.88

[a]n = 4.

[b]550 nm absorbance measured at 30 min (without inhibitors).

[c]550 nm absorbance measured at 0 min (without inhibitors).

[d]Referred to *Zhang* et al. [53].

Newly developed HAO "FLUORESCENCE" assay method

The optimized HAO "COLORIMETRIC" assay enabled middle-throughput assay (~1000 assay/day), and is, however, high cost and low sensitivity method. So, I have newly developed high-throughput, high-sensitive, and low cost HAO fluorescence assay (resazurin method) applied to inhibitor screening and evaluation. All conventional HAO assays employ colorimetric probes (cytochrome-*c*, cytochrome *c*$_{554}$, potassium ferricyanide, MTS {3-(4,5-dimethylthiazol-2-yl)-5-(3-carboxymethoxyphenyl)-2-(4-sulfophenyl)-2H-tetrazolium}, etc.) whose absorbance was changed by accepting electron [31,39,55]. In contrast, the assay that I have developed uses fluorescence probe, resazurin, as an electron acceptor. The resazurin is changed to resorufin, strong fluorescence material, by accepting an electron (**Figure 9**). The optimal wavelength of emission and excitation for resorufin was determined by 3D excitation-emission map (**Figure 10**), and selected 562 nm for excitation wavelength and 592 nm for emission wavelength. I optimized this method for high-throughput and robust assay. In particular, the assay method was optimized for the 384-well microplate by profiling conditions of the incubation time,

buffer pH, and additives tolerance.

Firstly, I optimized incubation time and buffer pH condition. The resorufin is changed to hydro-resorufin, fluorescence less material, by accepting one more electron (**Figure 9**). Controlling timing is critical to measure the fluorescence correctly. By profiling buffer conditions, fluorescence intensities of this method strongly dependent on the pH and buffer conditions (**Figure 11A**). This profile is different from HAO colorimetric assay which uses cytochrome-*c* as a probe (**Figure 8A and B**), and resorufin fluorescence itself (**Figure 11B**). The pH dependent fluorescence intensity change was caused by change of turn-over speed of resazurin reduced rate by HAO (**Figure 11C**). Fluorescence intensity was rapidly decreased by using optimum pH and buffer (e.g., pH5.5, Citrate-phosphate buffer). Therefore, I selected pH 7.7, Tris-HCl buffer which provided a stable fluorescence signals for a long time (1~2 hours) (**Figure 11C**).

Secondary, I optimized concentration of hydroxylamine (substrate). Fluorescence signal increased as raising the ratio of hydroxylamine/resazurin (**Figure 12**). In the ratio of 10, signal background ratio (S/B) is leaches 20, a very good value for screening. Theoretically, concentration of the hydroxylamine is enough as one fourth as resazurin, because HAO generates four electrons from one hydroxylamine (**Figure 3**). HAO may transfer a greater part of the generated electrons to the oxygen dissolved in the solution. Therefore, I selected the condition of 500 μM hydroxylamine and 50 μM resazurin (**Figure 13**).

Thirdly, I checked tolerance of the assay against addition of 0.1% BSA, 0.03% Triton X-100 (**Figure 14**), and several concentrations of DMSO (**Figure 15**). No significant signal change is detected by addition of the 0.1%BSA and 0.03%Triton-X. However, DMSO decreased the fluorescence signal of this assay significantly in a concentration dependent manner. Despite of 0.5% DMSO condition shows almost half S/B values (S/B = 10) compared with 0% DMSO condition (S/B = 23), the S/B value of 0.5% DMSO condition is enough for screening assay.

Calculated Z'-factor of this assay was 0.946 for NeHAO, indicating that the HAO fluorescence assay method is almost ideal for high-throughput screening and inhibitor evaluation. Other validation statistics were summarized in **Table 4**.

Advantages of this HAO fluorescence assay method are summarized as follows : very low cost (＜¥400/plate), high sensitivity (S/B ratio 5–23), good precision (CV value 0.8–2%), homogenous assay[1], hydroxylamine (substrate) and resazurin solutions can be stored in a freezer, effective pH range is wide as pH 5–7.3 (optimal pH value: pH5.8–6.0), whereas DMSO can be used concentration with less than 2%. This method is considered to be suitable for screening to ~200,000 compound class libraries and IC_{50} determination to ~1,000 compound class libraries.
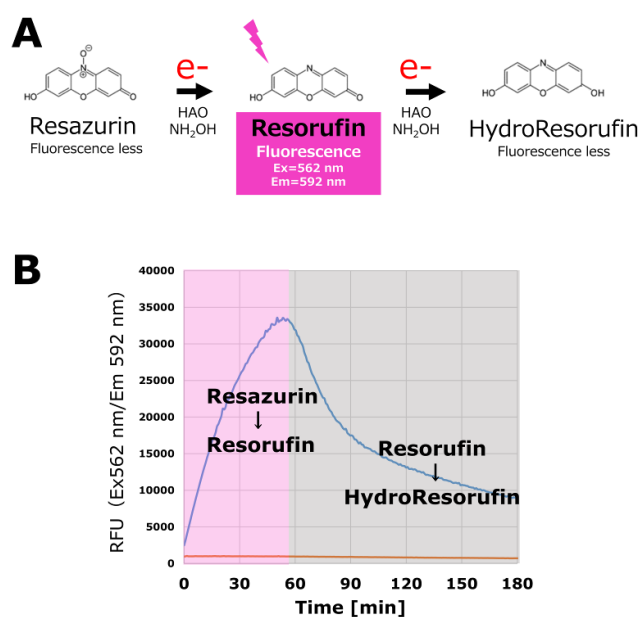
Figure 9. Measurement principle of HAO fluorescence assay.
(A) Fluorescence change of electronic states. (B) Time dependent fluorescence intensity change during HAO fluorescence assay.

---

[1] Homogeneous assay: An assay formatted by a simple add, mix and read procedure without separation or washing steps [77].
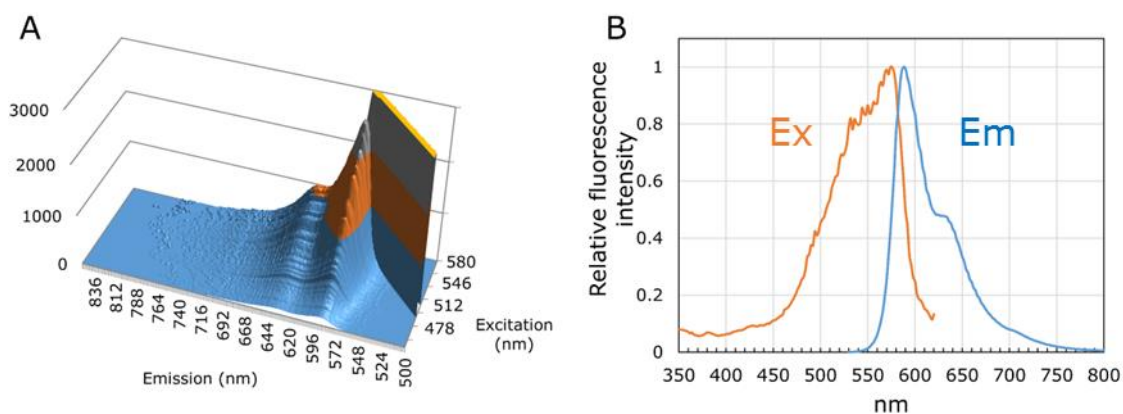
Figure 10. Excitation-emission profile for HAO fluorescence assay.

3D excitation-emission graph (A) and normalized sliced graph (B). The assay was performed by following conditions: 5 nM NeHAO, 1 mM NH_2OH, 100 μM Resazurin, pH 7.5, 50 mM KPi buffer, 300 mM NaCl, assay volume 100 μL, incubate at ambient temperature (26 °C) for 2h, half bandwidth = 5 nm.
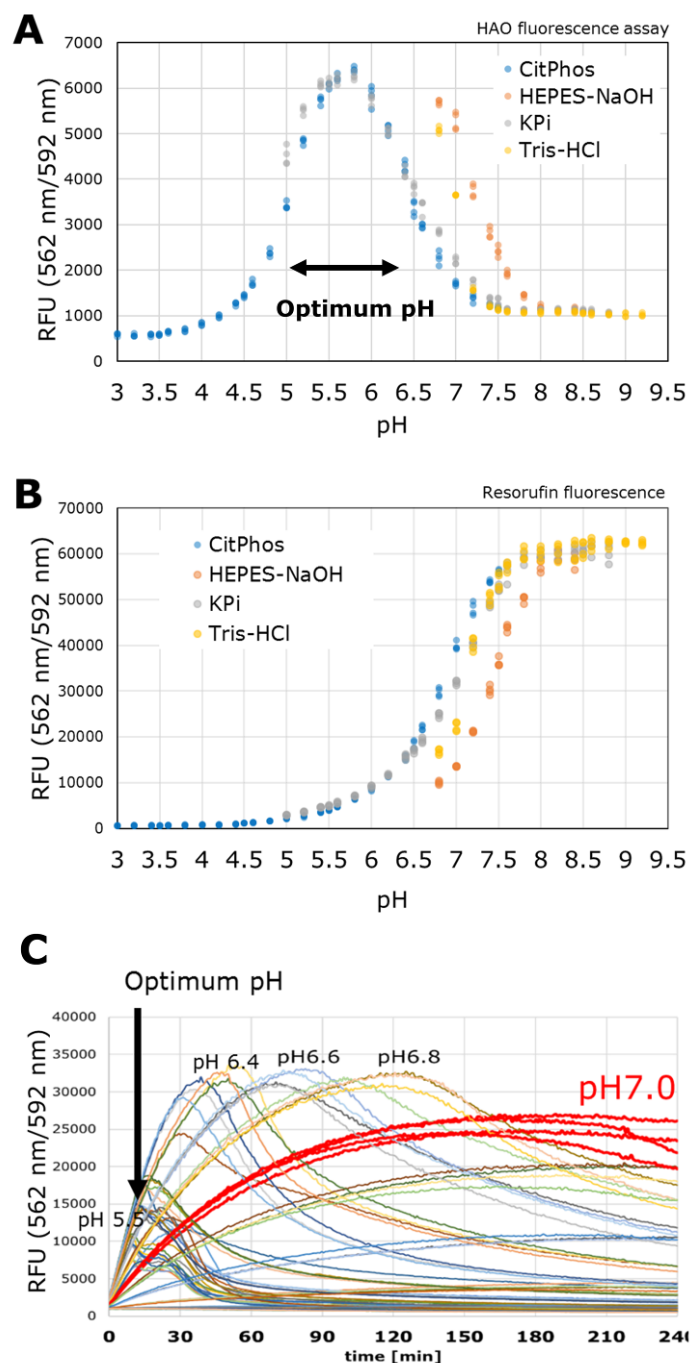
Figure 11. pH dependent fluorescent intensity difference for HAO fluorescence assay and resorufin.

(A) HAO fluorescence assay. The assay condition is following: 150 mM NaCl, 0.03 % Triton X-100, assay volume 100 μL, nonbinding 384-well black flat-bottom plate, incubation at ambient temperature (26 °C) for 1h. (B) Commercially available resorufin, a reduced form of resazurin. (C) Time course of the HAO fluorescence assay.
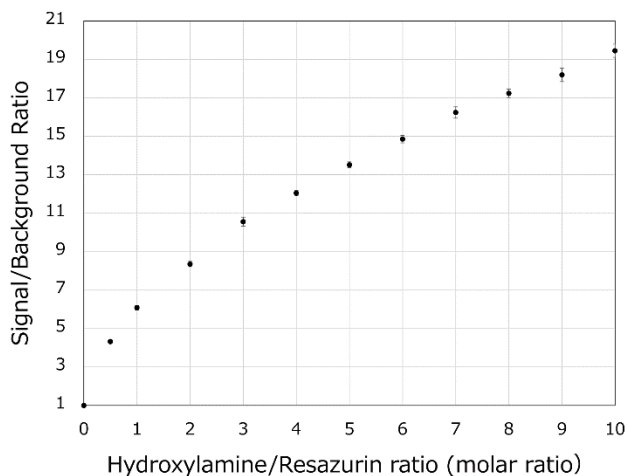
Figure 12. Ratio of hydroxyalamine and resazurin affects signal background ratio on HAO fluorescence assay.

Error bars represent standard deviations (n=3).
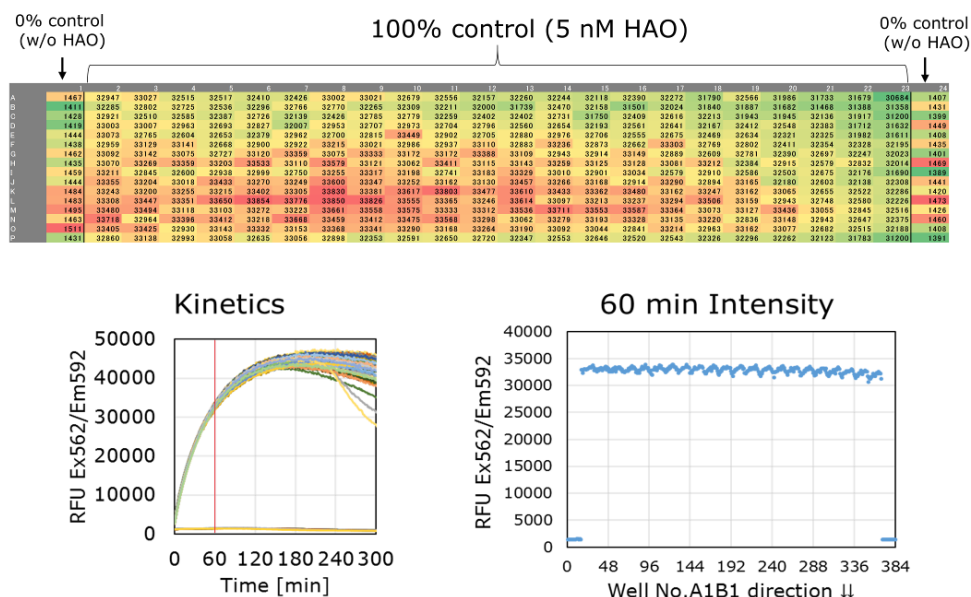
Figure 13. Validation for HAO fluorescence assay.

(A) Heat map of the validation assay that control assays performed for all wells on a 384-well plate. (B) Kinetics measurements for all the 384-well assays with 30 sec intervals. (C) Intensity validations at 60 min values, which aligned A1 to B1 directions of 384-well plate. Validation statistics of this assay are shown in **Table 4**.
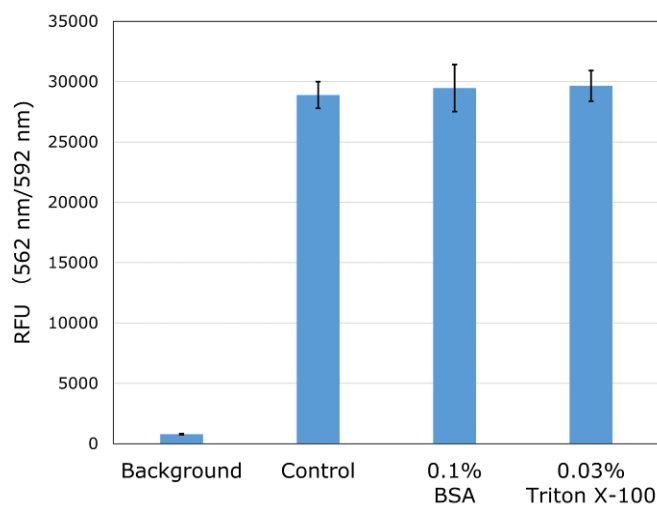
Figure 14. Additives check on HAO fluorescence assay.

NeHAO 5 nM, pH 7.0, 50 mM KPi buffer, 150 mM KCl, ambient temperature (26 °C), 60 min, hydroxylamine 1 mM, resazurin 50 µM BSA, 0.03% Triton X-100.
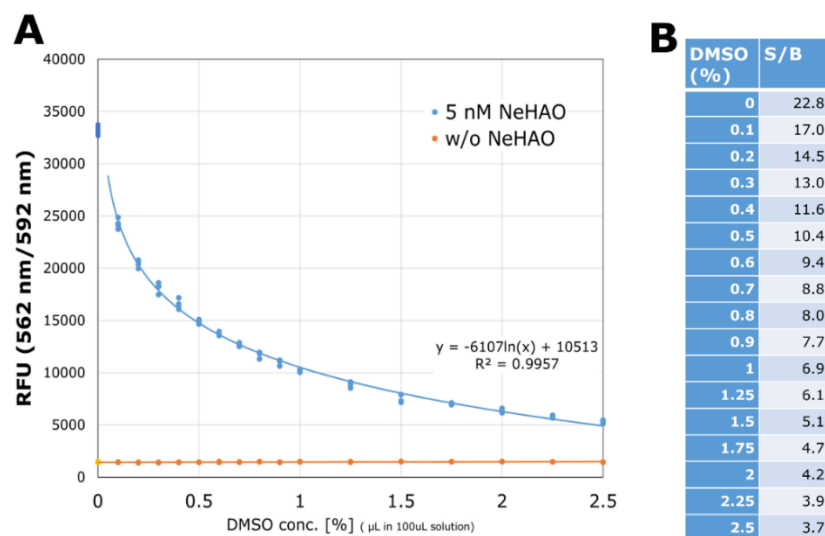
Figure 15. DMSO dependent activity of NeHAO fluorescence assay.

(A) Signal intensities of NeHAO fluorescence assay on several DMSO concentrations. (B) Signal background ratio on several DMSO concentration. 5 nM NeHAO, 1 mM NH_2OH, 100 µM resazurin, pH 7.0, 50 mM KPi buffer, 150 mM NaCl, 0.03 % Triton X-100, incubate 60 min, ambient temperature (26 °C), total 100 µL volume, n=4, (0% ctrl: n=32), (1% DMSO = 141 mM)

Table 4. Validation statistics for HAO fluorescence assay using cytochrome-*c* on a 384-well microplate.

Benchmark	Formula	NeHAO
100% Average ($Av_{100\%}$)[a,b]	-	32838
100% Standard deviation ($SD_{100\%}$)[a,b]	-	534
Background Average ($Av_{0\%}$)[c,d]	-	1440
Background Standard deviation ($SD_{0\%}$)[c,d]	-	31
Coefficient value (CV %)	$=SD_{100\%}/Av_{100\%}\times100$	2.16
Signal Background ratio (S/B)	$=Av_{100\%}/Av_{0\%}$	22.8
Signal Noise ratio (S/N)	$=(Av_{100\%}-Av_{0\%})/SD_{100\%}$	1010
Z'-factor[e]	$=1-\dfrac{3\times SD_{100\%}+3\times SD_{0\%}}{Av_{100\%}-Av_{0\%}}$	0.946

[a]$n = 352$.

[b]RFU measured at 60 min (100% control wells).

[c]$n = 32$.

[d]RFU measured at 60 min (0% control wells).

[e]Referred to *Zhang* et al. [53].

Structure analysis for NeHAO and NoHAO

I solved crystal structures of the as-isolated (apo) NoHAO (**Figure 16**, new structure) and NeHAO (replication of previous report [32,33,57]) at 2.6 Å and 2.2 Å resolutions, respectively. For the structure of NoHAO, I could continuously trace the electron density of 508 residues of the polypeptide starting at Asp30 which is consistent with my N-terminal sequence analysis for NoHAO (N-terminal sequence of NoHAO detected by protein sequencer was underlined in **Figure 27**).

The γAOB NoHAO maintains structural features previously reported for the βAOB NeHAO [32,33,57]. The structure of NoHAO is described as a garlic-like shape composed of a homotrimer in which identical monomers are related by a crystallographic 3-fold axis (**Figure 17** right). The subunits of NoHAO were linked by two covalent bonds between Tyr500 (Tyr491 in NeHAO) of one subunit and the active site heme P460 of an adjacent subunit as in NeHAO [33,34].
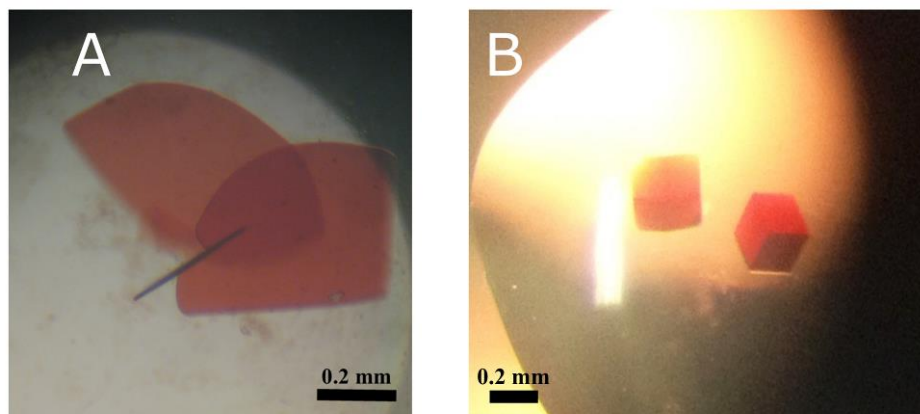
Figure 16. Crystals of NeHAO and NoHAO.

Thin layered crystals of NeHAO (A) and cubic shaped crystals of NoHAO (B). The crystals of the HAOs showed red colored due to hemes which is cofactor of the HAOs.
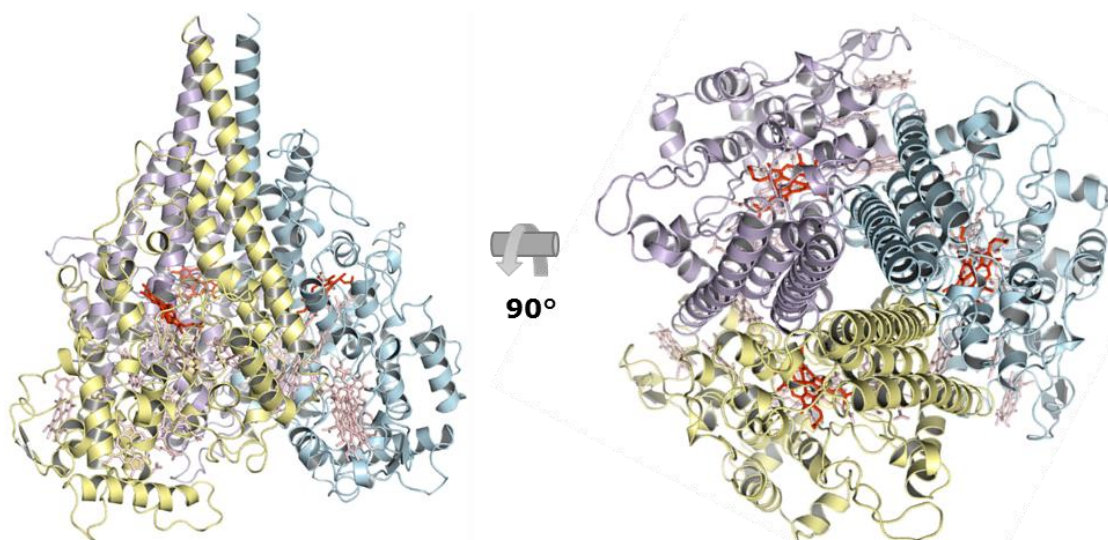
Figure 17. X-ray crystal structure of *Nitrosococcus oceani* HAO (NoHAO).

Two views of the NoHAO trimer perpendicular view (left panel) and the 3-fold symmetry axis view (right panel). The three monomers are shown in different colors. The three heme P460 and 21 heme-*c* groups are shown as stick models in red and pink, respectively.
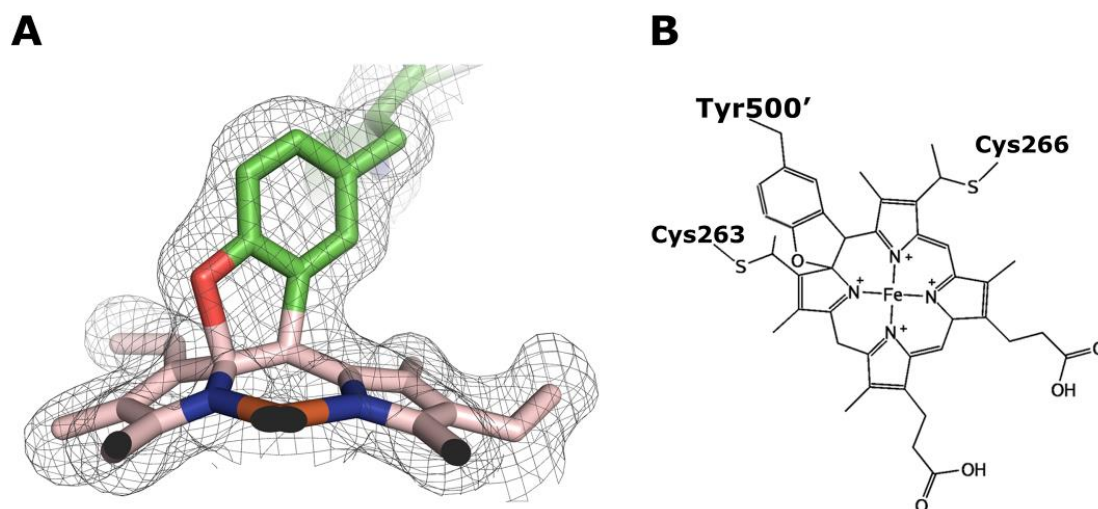
Figure 18. Heme P460 in NoHAO was linked to the Tyrosine.
(A) Close up view of the heme P460-Tyr500 two covalent bonds of the apo NoHAO. The mesh represents 2*Fo-Fc* electron density map contoured 1.0σ. (B) Chemical representation of the heme P460. Figures were prepared by PyMOL 1.7 (A) and MOE 2015.1001 (B).

Conclusion

I first established fundamental methods that required for nitrification inhibitor development study; integrated preparation systems for HAO, high-resolution three-dimensional structural information for NeHAO and NoHAO, high-throughput inhibition assay systems for live AOB cell (colorimetric) and purified HAO (colorimetric and fluorescence).

Established sample preparation systems for HAOs are summarized in **Table 5**. AOB mass culture systems (~20 L) were successfully established for six deposited AOB strains. Five HAOs (except for *N. lacus*) including three new HAOs were successfully purified by my new purification systems. The crystal structures of two HAOs (*N. europaea* and *N. oceani*) were resolved successfully the crystal structures. Another two HAOs (*N. sp* JPCCT2 and *N. multiformis*) provided crystals but their crystallization conditions need to be optimized. Remaining one HAO (*N. cryotolerans*) is now under crystallization trial.

Species	Strain	Isolated from	HAO purification	HAO Crystallization Structure analysis
Nitrosomonas europaea	NBRC14298	Europa, soil	Success by Simplified method	Crystal structure ＊resolution up
Nitrosomonas sp. JPCCT2	NBRC108559	Thermal power plant, shikoku, Japan, slurry	Success (Anaerobic enzyme)	Crystallization
Nitrosomonas cryotolerans	ATCC49181	Alaska Kasitsna bay, sea surface	Success (Anaerobic enzyme)	*Under preparation*
Nitrosococcus oceani	ATCC19707	North pacific, sea	Success by Simplified method	Crystal structure
Nitrosospira lacus APG3	ATCC BAA2542	North Amerika, lake, sediment soil	Undetected	--
Nitrosospira multiformis	ATCC 25196	Surinam, South America, soil	Success (Anaerobic enzyme)	Crystallization

Table 5. Summary for sample preparation of HAOs.

Description texts colored in red shows new results in this study.

Chapter 2
Re-profiling for known nitrification inhibitors

Introduction

In this chapter, I have performed for re-profiling of known nitrification inhibitors. It has two reasons for performing re-profiling; 1) Revealing reference values of inhibition activity for newly developed nitrification inhibitor, 2) Search for the seed compounds for structure optimization for new nitrification inhibitor.

In drug discovery project, it is required for designing new inhibitors that activity is stronger than the known inhibitors. As far as I know, 61 compounds, including 20 commercially available nitrification inhibitors, have been reported as nitrification inhibitors. Since inhibitory-activity of these nitrification inhibitors were examined by many different assay systems, such as field test and live AOB cell assay, etc., it is difficult to compare the reported activities directly. To overcome this difficulty and to determine the target value of inhibitory-activity for the newly developed nitrification inhibitors, I have purchased in-stock 38 compounds of known nitrification inhibitor (including 19 commercially available nitrification inhibitors registered in Japan and other countries) and performed re-profiling of theses known nitrification inhibitors using the standardized nitrification activity assay against live AOB cell (described in **Chapter 1**). This re-profiling results will be useful not only for determining target inhibitory-activity but also for discovery of seed compounds for nitrification inhibitor design [58,59].

Materials and methods

Nitrification activity assay

NeAOB live cell culture was used for nitrification activity assay (illustrated in **Figure 20**).

Nitrification activity assay including calculation of IC_{50} was performed by the method described in

Chapter 1.

Compounds

38 compounds of known nitrification inhibitors listed in **Figure 20** were purchased from several

chemical suppliers through the import company of Namiki Shoji (Tokyo, Japan).

Results and discussion

In this chapter, I have performed re-profiling of known nitrification inhibitors that were commercially

available and reported in papers. I have collected 38 compounds, including 19 commercial nitrification

inhibitors, that could be purchased from chemical suppliers. The compounds were analyzed for the

inhibition activity (IC_{50}) by using my optimized nitrification activity assay method against live AOB

cells (described in **Chapter 1**). The compounds were assayed against NeAOB, which is the model

species of AOB. The assay procedure was illustrated in **Figure 19**. The chemical list and the results

are shown in **Figure 20**, and sorted graph was shown in **Figure 21**.
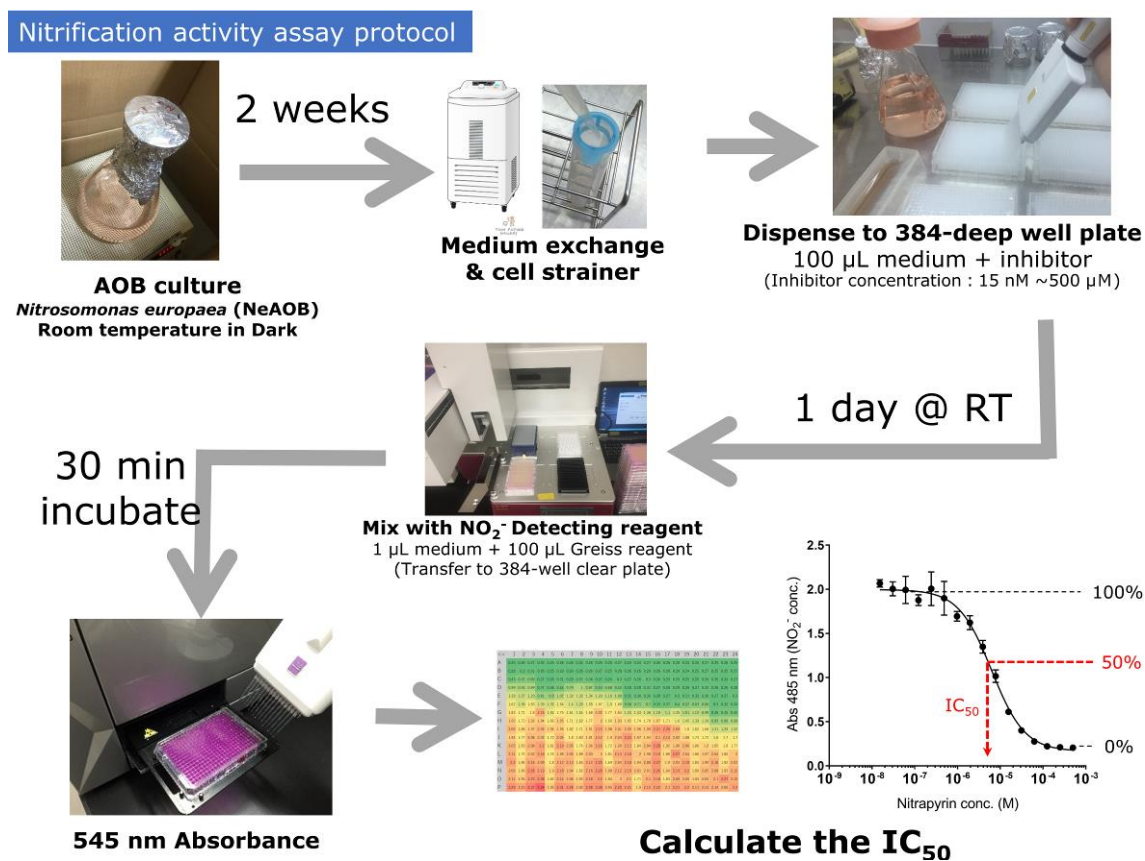
Figure 19. Nitrification activity assay procedure.

The most effective inhibitors in all and in commercially available nitrification inhibitors are allylthiourea (IC_{50} = 0.4 µM) and thiourea (IC_{50} = 0.5 µM), respectively. However, allylthiourea has not been registered as a commercially available nitrification inhibitor due to the toxicity. Furthermore, thiourea has not been used in farm-land today due to the toxicity, as far as I know. Top four effective inhibitors are highly toxic compounds including thiourea analogs or a mercury compound (**Figure 21**). The most popular commercially available nitrification inhibitors of nitrapyrin, DMPP, and dicyandiamide showed IC_{50} of 1.8 µM, 4.1 µM, and about 400 µM, respectively. Therefore, the first target value of inhibitory-activity for the newly developed nitrification inhibitor has been set at IC_{50} = 1.8 µM as same as that of nitrapyrin.

This re-profiling research also revealed the "weak effects" character for all of the assayed nitrification inhibitors. The most effective known nitrification inhibitor, allylthiourea, showed inhibitory-activity of IC_{50} = 0.4 μM only (**Figure 20** compound No.23). Compared with an average IC_{50} value of 10 nM for commercially available medicines, the allylthiourea is 60 fold weaker than the average value of medicine. Additionally, it was revealed that nitrapyrin (**Figure 20** compound No.3: developed by Dow agro), used in the United States mainly, and DMPP (**Figure 20** compound No.1: developed by BASF), used in Europe, are not strongest inhibitors, and dicyandiamide (**Figure 20** compound No.2: commonly used generic agrochemical[2]), used in the Japan and other country, showed slight inhibition activity.

These results are suggestive for the strategy and purpose for developing next generation nitrification inhibitors. Firstly, adaptation of medicinal drug discovery technique to nitrification inhibitor development will lead to production of new inhibitors which have medicine level inhibitory-activity (IC_{50} ~10 nM). Secondary, structure development for which thiourea moieties used as seeds will lead to more effective nitrification inhibitor; in this case, of course, it is necessary to consider reducing toxicity.

---

[2] Generic agrochemical: Patent expired agrochemical.

#	Name	IC$_{50}$ (μM)
1 ●	3,4-dimethylpyrazole phosphate (DMPP/Entec®)	4.1
2 ● J	Dicyandiamide (DCD)	~400
3 ●	Nitrapyrin	1.8
4 ● J	2-mercaptobenzothiazole (MBT)	3.9
5 ● J	2-sulfanilamido thiazole (ST)	>500
6 ● J	Thiourea	0.5
7 ● J	2-amino-4-chloro-6-methyl-pyrimidine	130
8 ●	Etridiazole	5
9 ● J	Guanylthiourea	4.1
10 ●	Metalaxyl	>500
11 ● J	3-mercapto-1,2,4-triazole	3.4
12 ● J	4-amino-1,2,4-triazole	~1800
13 ●	N-(n-Butyl) thiophosphoric triamide	>500
14 ●	Potassium azide	>500
15	trans-Ferulic acid	>500
16	Phenylmercuric acetate	1.1
17	p-Coumaric acid	>500
18	Gallic Acid Hydrate	>500
19	Potassium Amylxanthate	58.8
20	2-Chloroacetamide	>500
21	Caffeic acid	>500
22	Pottassium Ethylxanthate	38
23	1-Allyl-2-thiourea	0.44
24	N-Methylhydroxylamine Hydrochloride	241
25	2-Ethynylpyridine	4.0
26	Chlorogenic acid	>500
27	1-Hydroxypyrazole	>500
28	Potassium isopropylxanthate	26
29	Ammonium dithiocarbamate	>500
30	2-Butanone Oxime (MEKO)	57
31	Sodium diethyldithiocarbamate trihydrate	30
32	Trichloroethylene	>500
33	1-Phenyl-2-thiourea	0.59
34	carbofuran	>500
35	Carbon bisulfide	>500
36	Phenyl phospho rodiamidate	1102
37	Cyclohexanone oxime	>500
38	Acetaldoxime	>500

● : Registered
J : Registered in Japan

Figure 20. Re-profiling for 38 known nitrification inhibitors.
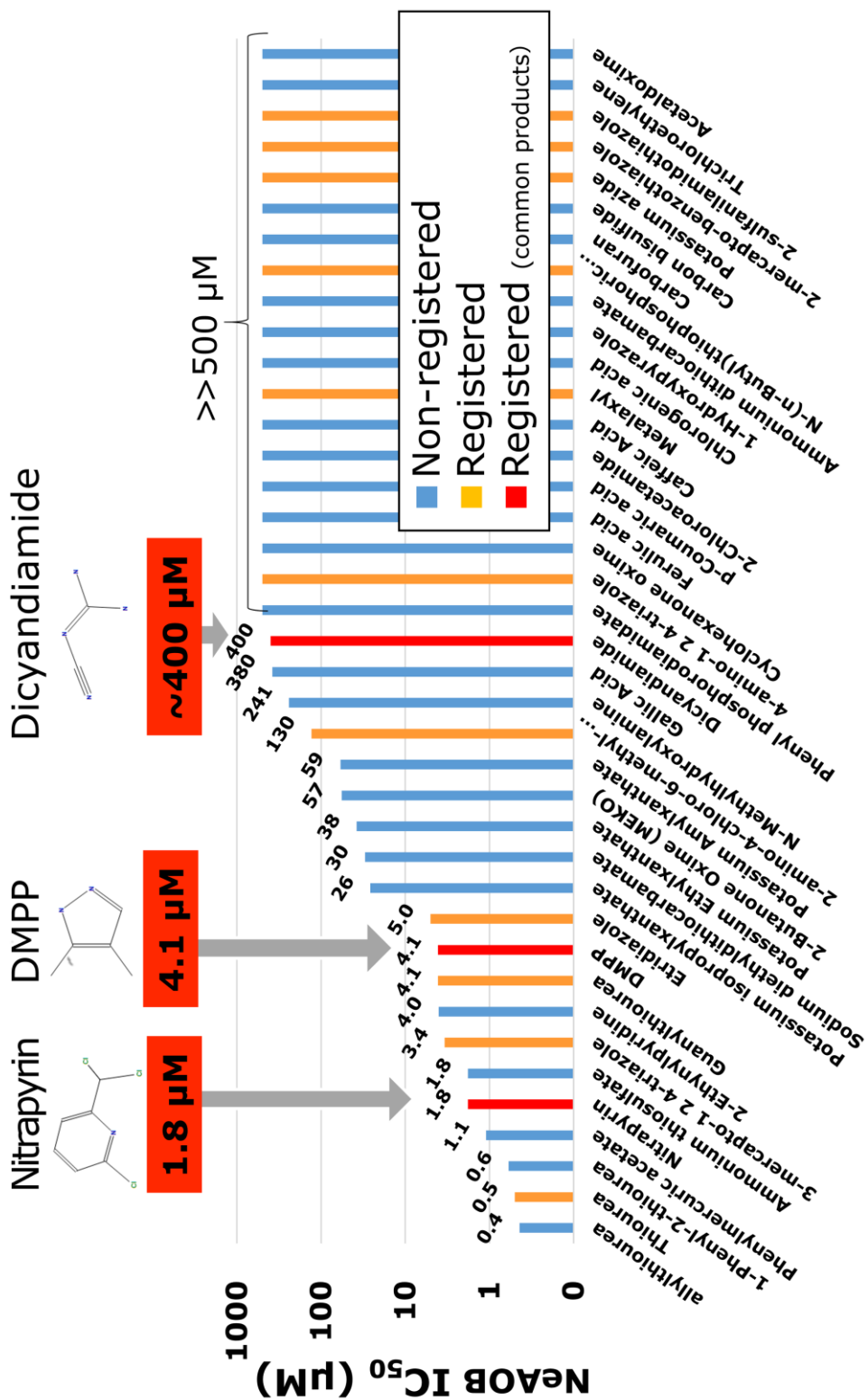
Figure 21. Sorted graph for IC$_{50}$ of known nitrification inhibitors.

Chapter 3
Comparative analysis of inhibitor response and crystal structure for HAO

Abstract

I have observed distinct inhibitory responses of HAOs from beta-proteobacterial AOB (βAOB) *Nitrosomonas europaea* (NeHAO) and gamma-proteobacterial AOB (γAOB) *Nitrosococcus oceani* (NoHAO) against phenylhydrazine, a well-known suicide inhibitor for NeHAO. Consistently, the live cells of *N. europaea*, *Nitrosomonas* sp. JPCCT2 and *Nitrosospira multiformis* of βAOB displayed higher responses to phenylhydrazine than those of γAOB *N. oceani*. My crystal structure analysis and homology modeling studies suggest that different inhibitory responses of βAOB and γAOB are originated from different local environments around the substrate-binding sites of HAOs in these two classes of bacteria due to substitutions of two residues. The results reported herein strongly recommend inhibitor screenings against both NeHAO of βAOB and NoHAO of γAOB to develop HAO-targeting nitrification inhibitors with wide anti-AOB spectra.

Introduction

For developing nitrification inhibitors that possess wide anti-AOB spectra against a variety of uncultured soil AOB, proper model AOB strains must be selected. Okano *et al*. [14] showed that *N. europaea* is adequate to screening of nitrification inhibitors by using common nitrification inhibitors, including AMO-targeting inhibitor nitrapyrin, and βAOB strains. However, γAOB, which was

believed to inhabit only the sea and salt lake, has been detected in soil by metagenomic analysis, recently [60]. I thus need to determine which AOB strains are adequate to screening of HAO-targeting nitrification inhibitors. In addition, a simple but effective protein purification system and high-throughput inhibitor screening/evaluation assay methods are also required to assess inhibitor response of HAO.

Here, I show different inhibitor responses of HAOs from βAOB and γAOB by using optimized inhibitor evaluation systems including simplified HAO purification procedure and high-throughput HAO activity assay. This results will assist developing effective nitrification inhibitors with wide anti-AOB spectra.

Materials and methods

Determine IC$_{50}$ for nitrification activity of AOB cell

Nitrification inhibition assays to determine IC$_{50}$ of inhibitors were described in in **Chapter 1**.

Determine IC$_{50}$ for HAO inhibitor

HAO inhibition assays to determine IC$_{50}$ of inhibitors were used HAO colorimetric assay described in **Chapter 1**.

Structure analysis for complexes of NoHAO-acetaldoxime and NoHAO-phenylhydrazine

Crystallization, data collection and structure analysis for NoHAO were described in **Chapter 1**. Crystals of NoHAO in complex with acetaldoxime or phenylhydrazine were obtained by soaking the apo-enzyme crystals to reservoir solution including 1 M acetaldoxime or 10 mM phenylhydrazine within 1 min, and were performed data collection immediately. Successively, the NoHAO-acetaldoxime and NoHAO-phenylhydrazine complex structures were solved by the molecular

replacement method using the resultant apo-enzyme form structure as the starting model.

Homology modeling

Homology modeling of βAOB *Nitrosospira multiformis* HAO (NmHAO) was performed using Molecular Operating Environment (MOE) software (version 2015.1001, Chemical Computing Group) with the following parameters: amino acid sequences of NmHAO (Uniprot: Q2YA36), template crystal structure of NeHAO (PDB:4n4n), induced fit includes hemes and a water molecule on the iron in heme P460, forcefield of Amber10:EHT. The graphical representations were prepared by PyMOL (version 1.7.0.1, Schrodinger, LLC.).

Results

Comparison of inhibitory response between NeHAO of βAOB and NoHAO of γAOB

NeHAO of βAOB and NoHAO of γAOB are characteristically different from each other in several points of views. NeHAO was purified as a complex with its partner protein NE1300 while NoHAO was purified as an isolated protein without any associate proteins (**Figure 22A**). As shown in **Figure 22B**, the dithionite-reduced UV–vis spectra measured under the same conditions showed a marked difference of the heme P460 absorption peak positions between NeHAO (461.2 nm) and NoHAO (466.2 nm), suggesting different local environment around the substrate-binding sites of these two proteins as expected by my structure analysis study that showed different arrangements of the pocket-forming residues between the βAOB HAO and γAOB HAO.

These results suggested that HAO inhibitor responses are similar in the classes, but are different between the two classes. To verify this statement, I compared inhibitory responses of NeHAO and NoHAO, as representatives of βAOB and γAOB, to phenylhydrazine, a well-known NeHAO inhibitor (**Figure 23A**). Phenylhydrazine inhibited about 60% of the NeHAO activity at 10 µM while the

NoHAO activity was scarcely inhibited at the same concentration (**Figure 23B**). Consistently, the live

cell assay showed higher phenylhydrazine response for βAOB, *N. europaea*, *N.* sp. JPCCT2 and *N.*

multiformis, (IC_{50} = 0.9−1.2 μM) than γAOB *N. oceani* (2.9 μM) (**Figure 23C**). This difference is

possibly caused by the difference of HAO structure between βAOB and γAOB.
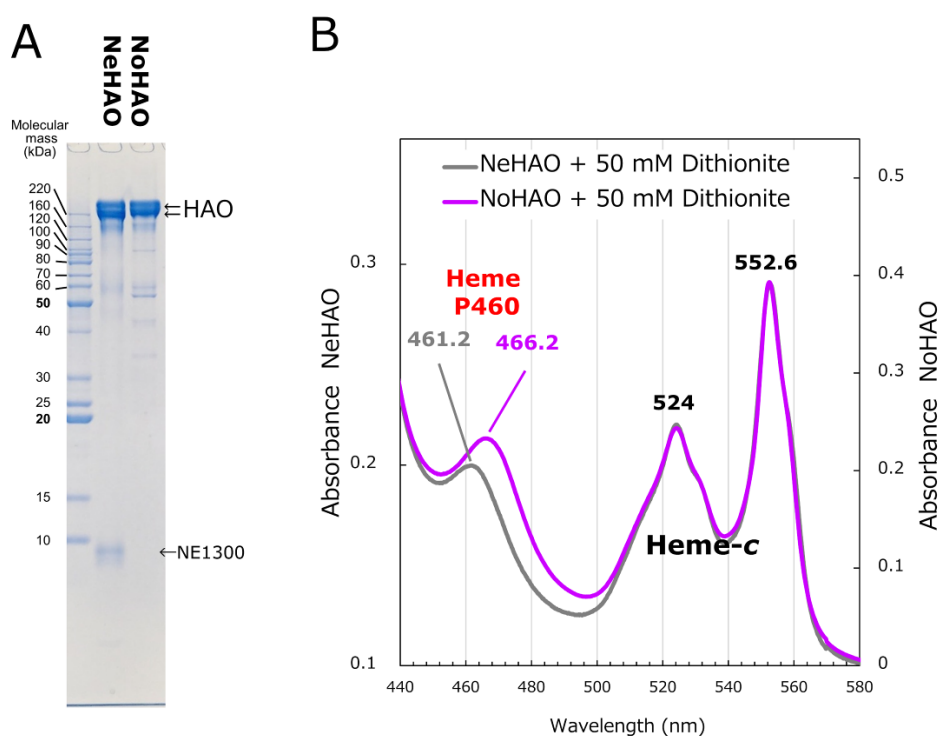
Figure 22. Comparison for SDS-PAGE and Uv−vis spectra of purified NeHAO and NoHAO.

(A) SDS-PAGE analysis for concentrated NeHAO/NE1300 complex and NoHAO (each ~2 μg). (B) Comparison of UV−vis spectra around the heme P460 in NeHAO and NoHAO. The spectral data are the same as those of **Figure 6D** and **Figure 7D** heme-*c* peaks of the two proteins.
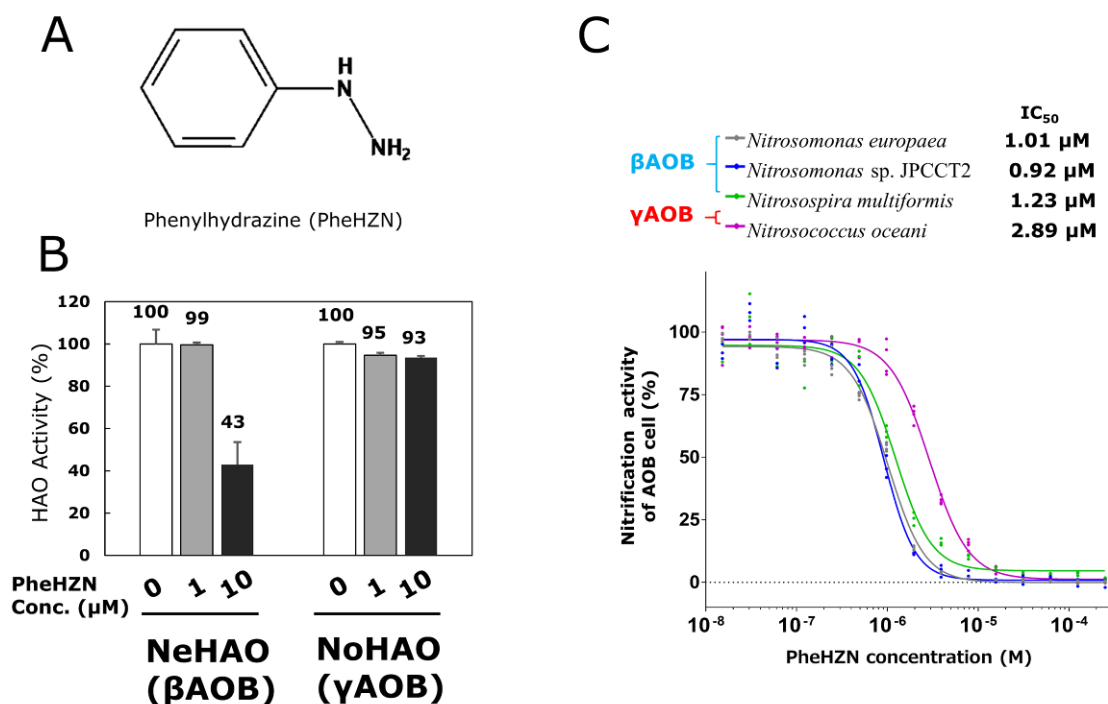
Figure 23. Difference of inhibitory responses of HAOs for phenylhydrazine.

(A) Phenylhydrazine (PheHZN), an HAO specific inhibitor. (B) Determination of the half maximal inhibition centration (IC$_{50}$) of phenylhydrazine against nitrification activity of live cells of three βAOB spices, *Nitrosomonas europaea* (NeAOB), *Nitrosomonas* sp. JPCCT2, *Nitrosospira multiformis* (NmAOB), and a γAOB spices, *Nitrosococcus oceani* (NoAOB). (C) Inhibition effects of phenylhydrazine against purified NeHAO from NeAOB (model of γAOB) and NoHAO from NoAOB (model of γAOB).

Comparison of crystal structures of NeHAO and NoHAO

The structures of NoHAO and NeHAO monomers could be superimposed to a rmsd of 0.79 Å for 499

Cα-carbons (**Figure 24C and D**). This conservation is also applied to the homotrimeric structure and

thus the positions of the 24 heme moieties arranged in a ring. In the previously reported crystal

structures of the βAOB NeHAO, a physiological HAO partner protein NE1300 with unknown function

is present on the NeHAO molecular surface [33,34]. In contrast, no additional electron density for such associated protein(s) was observed for the γAOB NoHAO crystal (**Chapter 1**). It is noteworthy that NE1300 homologous genes are not found in the genome of *N. oceani* strain ATCC19707 used in this study.

NoHAO has a γAOB HAO specific nine-amino-acid-long fragment, Thr220-Asp228, which is absent in the βAOB HAOs (**Figure 27**). This fragment is located at the edge of the substrate access channel on the molecular surface which is corresponding to the NE1300-binding site of the βAOB NeHAO (**Figure 25**). In fact, the γAOB HAO specific fragment of NoHAO occupies the same space as the NE1300 molecule in the NeHAO crystal structure when the HAO molecules are superimposed (**Figure 24C**). This observation suggests that the γAOB HAO specific fragment mimics a structural role of NE1300 in *N. europaea* to compensate the lack of the HAO partner protein. A similar structural role is also expected for the N1 domain (Gly38-Thr71, **Figure 27**) of the anammox HAO protein kustc1061 from *Kuenenia Stuttgartiensis* for which NE1300 homologous genes are not found in the genome. The N1 domain is apart from the enzyme core domain but occupies almost the same space as the γAOB HAO specific fragment of NoHAO and the NE1300 molecule in the NeHAO crystal (**Figure 25**). This difference between βAOB and γAOB may effect to the active center structure and its function.
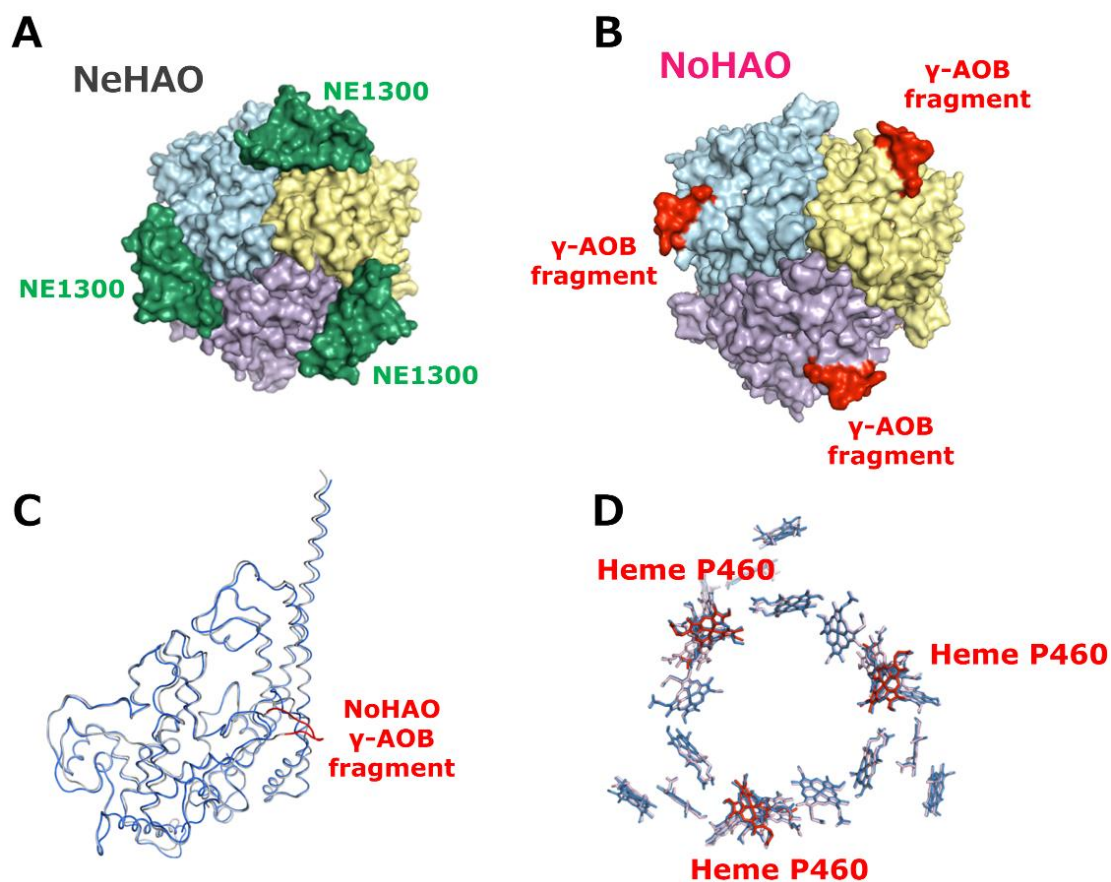
Figure 24. Comparison of NeHAO and NoHAO.

(A–B) Surface representation of NeHAO (PDB:4n4n, A) and NoHAO (B). (C) A superimposed main chain structures of NeHAO (blue) and NoHAO (grey) based on Cα-carbons. The γAOB fragment (T220–D228) of the NoHAO are shown in red. The superimpose calculation was performed by MOE. (D) A ring-like arrangements of hemes in trimeric structures of NoHAO (red: heme P460 and pink: heme-*c*) and NeHAO (blue). These hemes were superimposed by pair fitting on irons in each 24 hemes that the average rmsd value of the irons is 0.279 Å. The superimpose, pair fitting and figure preparations were performed by PyMOL.
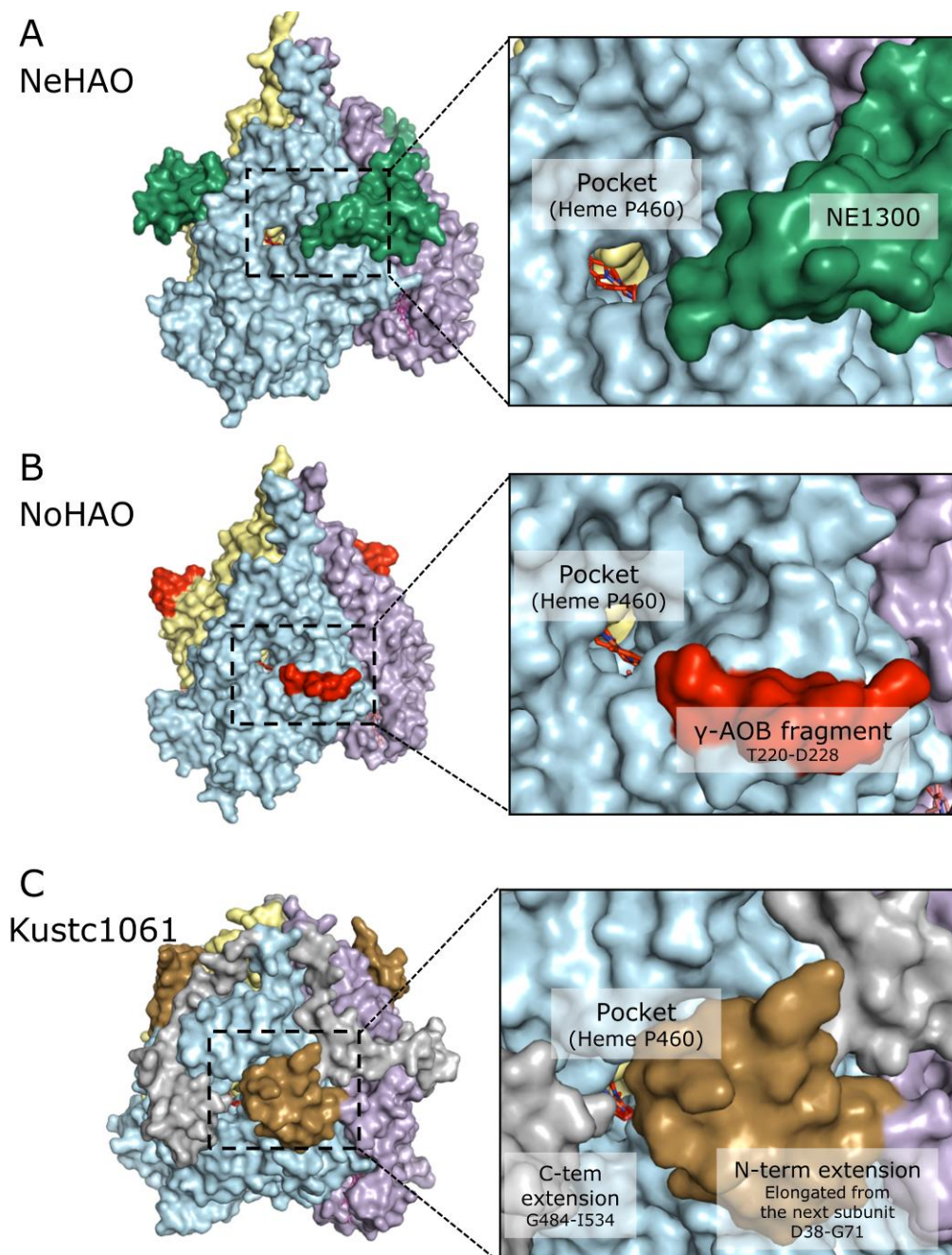
Figure 25. Relative arrangement of entrance side of the ligand binding pocket on the NeHAO, NoHAO and Kustc1061.

Surface representations of NeHAO with NE1300 (A), NoHAO (B) and Kustc1061 (C) are shown as side view (left) and clipped view around ligand binding pocket (right). (A) On NeHAO, small protein NE1300 (green) is located to an entrance side of the ligand binding pocket. (B) On NoHAO, γAOB fragment (red) is located to the pocket side instead of the NE1300. (C) On Kustc1061, the N-terminal extension (brown)

elongated from the next subunit is located to the pocket side instead of the NE1300 or the γAOB fragment. Furthermore, pocket entrance on the Kustc1061 is very narrow due to the overhanging of the N-terminal extension (brown) and the C-terminal extension (grey). The figures were prepared PyMOL.

Comparison of active center of HAOs

A lot of uncultured ammonia-oxidizing bacteria (AOB) live in soil, and nitrification inhibitors should be effective to all of these AOB. Identity tree of HAO in isolated AOB (A) reflects classification of AOB, which are divided into two classes of beta-proteobacterial AOB (βAOB) and gamma-proteobacterial AOB (γAOB), and βAOB are further divided into two families, *Nitrosomonas* and *Nitrosospira*, and γAOB includes one family, *Nitrosococcus*. We compared amino acid residues around the substrate binding pocket of HAO between βAOB and γAOB (**Figure 26**). Six residues arranged around the pocket on the catalytic heme P460 in the NeHAO crystal structure (**Figure 26C**) are completely conserved among three βAOB species (**Figure 26B**). **Figure 26D** shows that all of these six residues in the NmHAO model structure is nearly superimposable to those in the NeHAO crystal structure. On the other hand, sequence alignment and crystal structure revealed that two residues in γAOB (Phe[367]–Asn[368] in NoHAO) are varied from βAOB (Asn[357]–Tyr[358] in NeHAO). These results concluded that HAO inhibitor responses are similar in the classes, but are different between the two classes.
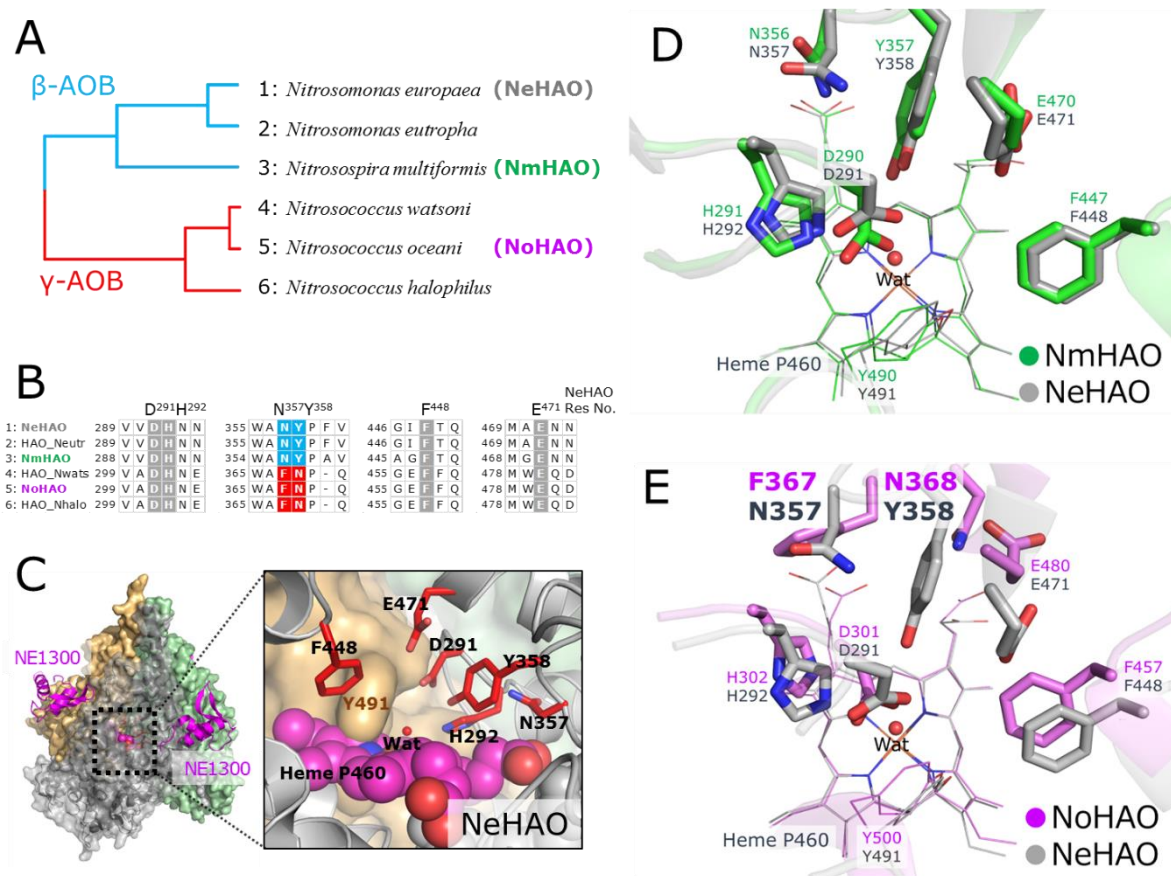
Figure 26. Comparison for active centers of NeHAO with other HAOs.

(A) Identity tree for HAO from AOB species. (B) Multiple alignment for active-site residues in HAOs. Full-length sequence alignment is represented in **Figure 27**. (C) Overall structure and close-up view of the around active site of NeHAO (PDB:4n4n). Comparison of active-site residues in the NeHAO crystal structure with those in NmHAO modeled structure (D) and NoHAO crystal structure (E). "Wat" represents a water molecule that binds on the iron in heme P460. The identity tree was calculated by average distance clustering algorithm using identity of the full-length HAO alignment by using MOE software version 2015.1001 (Chemical Computing Group Inc.).

Discussion

In this chapter, I revealed the difference of inhibitory response between βAOB and γAOB by using inhibition assay for both of purified HAO and live AOB cell and structure analysis for NeHAO, NoHAO, and NmHAO. My studies clearly showed that βAOB are more sensitive to inhibition by phenylhydrazine than γAOB due to different local environments around the substrate-binding sites of HAOs in these two classes of bacteria. Different inhibitory responses between βAOB and γAOB may be emerged not only by phenylhydrazine but also by other inhibitors that bind to the active center in HAO. Even small difference in inhibitor sensitivity increases a risk for appearance of drug-resistant bacteria. The findings reported herein indicate that effects of inhibitors should be examined for at least two types of HAOs purified from βAOB and γAOB. Selection of NeHAO and NoHAO is the best choice for discovery of novel nitrification inhibitors targeting HAO with wide anti-AOB spectra due to the established purification and high-throughput screening methods and the long phylogenetically distance between *N. europaea* (NeAOB) of βAOB and *N. oceani* (NoAOB) of γAOB.

A

Multiple alignment of HAOs

		UniProtKB Entry	PDB id
HAO_Nmult	HAO from β-AOB *Nitrosospira multiformis* (strain ATCC 25196ᵀ)	(Q2YA36_NITMU)	
HAO_Ncryo	HAO from β-AOB *Nitrosomonas cryotolerans* (strain ATCC 49181ᵀ)	(M5DDF6_9PROT)	
NeHAO	HAO from β-AOB *Nitrosomonas europaea* (strain ATCC 19718)	(HAO_NITEU)	(4n4n)
HAO_Neutr	HAO from β-AOB *Nitrosomonas eutropha* (strain C91)	(Q0AFG9_NITEC)	
HAO_Nnfc	HAO from comammox bacterium "*Ca.* Nitrospira nitrificans"	(CUS32689.1 (GenBank accession))	
HAO_Nntrs	HAO from comammox bacterium "*Ca.* Nitrospira nitrosa"	(CUS31385.1 (GenBank accession))	
HAO_Ninop	HAO from comammox bacterium "*Ca.* Nitrospira inopinata"	(CUQ65042.1 (GenBank accession))	
HAO_Nwats	HAO from γ-AOB *Nitrosococcus watsoni* (strain C-113)	(D8KBV1_NITWC)	
NoHAO	HAO from γ-AOB *Nitrosococcus oceani* (ATCC 19707ᵀ)	(Q3JCP2_NITOC)	(-------)
HAO_Nhalo	HAO from γ-AOB *Nitrosococcus halophilus* (strain Nc4)	(D5BZ44_NITHN)	
Kustc1061	HAO from anammox bacterium *Kuenenia stuttgartiensis*	(Q1PX48_9BACT)	(4n4k)
HAO_KSU-1	HAO from anammox bacterium "*Ca.* Jettenia caeni" (strain KSU-1)	(A9ZRZ6_9BACT)	

Kustc1061 N-term extension (D38-T71)

```
                                                                    Heme1
HAO_Nmult    1 ----------MLMKPWLRLV--TLACGVLFAGATWANFPSVPKETYKALKLEQS-ASPKELHS-ALVKRY
HAO_Ncryo    1 ----------MVAKSWLKIV--SLVCSGLLVAAAHASIPSVPDETYEALKLDRNTVTPKQMHE-ALVKRY
NeHAO        1 -----------MRIGEWMRGL-LLCAGLMMCGVVHADISTVPDETYDALKLDRGKATPKETYE-ALVKRY
HAO_Neutr    1 ----------MRLGEYLKGM--LLCAGLLLIGPVQADISTVPDETYEALKLDRSKATPKETYD-ALVKRY
HAO_Nntrs    1 ----------MTVKHLVKYA--LVVCGVLAAVQAQASFPTVPKETYEALKIDRS-ASPKELYE-ALLKRY
HAO_Nnfc     1 --MVWTQSMWTMSVNLMRVCALLVVCGVVLAAQAQADFPTVPKETYEALKIDRS-ASPKELYE-ALVKRY
HAO_Nino     1 ----------MSSKFAQKFV--MLVCGVLLAAPAQADFPTVPKETYEALKIDRS-ASPKELYE-ALVKRY
HAO_Nwats    1 ----------MSDSIIKRLLRAIAAVFSVSLLFVGNASADIPDELYEALGVDKYKASPKELYE-AITERY
NoHAO        1 ----------MSDSIIKRLLRAIATVFSVSLLFVGNASADIPDELYEALGVDKYKASPKELYE-AITERY
HAO_Nhalo    1 ----------MSDSIIGRLLRATATVASVSLLFVGSANAEIPNELYEALGVDKYEASPKELYE-AVTERY
KustC1061    1 MFEIFKKPLSRIVGATFAFAGVTLLACAMENGVAMAEGPTFQDVASQVFGQPVGPDNDGTLYIFGLTAKY
HAO_KSU-1    1 MLETLKKPLSRVAGLALAVAGVTFLTCTVGNGIARAEGPTFQDVASQVFGQPVGPDNDGTLYIFGLTAKY
consensus    1                 ..     ....  ... ...  .  .  .................  ........ .....*
```

```
                                                                 Heme1
HAO_Nmult   57 KDPA-QGAGRGTLAKYWEPIPMSMYFDPASYYKPPTSMKEVAAREECVKCHTDESPVWVSAWKRSTHANL
HAO_Ncryo   58 KDPA-QGAGRGTMAEYWEPIPYGIYLDPATFYTPPSSMKEVAGRSECVECHTDESPVWVQAWKRSTHANL
NeHAO       58 KDPA-HGAGKGTMGDYWEPIAISIYMDPNTFYKPPVSPKEVAERKDCVECHSDETPVWVRAWKRSTHANL
HAO_Neutr   58 KDPA-HGAGKGTMGDYWEPIALSIYMDPNTFYKPPVSPKEIAERKDCVECHSDETPVWVRAWKRSTHANL
HAO_Nntrs   57 LDPV-QGVGKGKYGDYWQPVSFSRYFDPHTFYKPPQAVKEVASREQCVKCHTDESPGWVAAWKKSTHANL
HAO_Nnfc    67 MDPAQQGVGKGKYGDYWQPVSFSKYFDPHTFYKPPQAVKEVASREQCVKCHTDESPGWVAAWKKSTHANL
HAO_Nino    57 LDP-EQGAGKGIYGQYWEPVTFSKYFDPTTFYKPPQAVKEVASREQCVKCHTDESPGWVAAWKRSTHANL
HAO_Nwats   60 YDPA-QGHGEGKYAEYWEPLPFSQYLDPYTYYSPPAQPAKVATREECIECHEDETRGWVHAWRKSVHANL
NoHAO       60 YDPA-QGHGEGKYAEYWEPLPFSQYLDPYTYYSPPAQPAKVATREECIECHEDETRGWVHAWRKSVHANL
HAO_Nhalo   60 YDPA-QGHGEGKYAEYWEPIPFSQYMDPYTYYKPPSSPAKVATREECVECHEDETRGWVHAWKKSVHANL
KustC1061   71 TEPE-YVDGRGPYKSFLKMLPSIRWYDPEHYWTNGSQTEGVFKNEECVLCHTVQTPTIVNDWKQSSHGSK
HAO_KSU-1   71 TQPE-YVEGRGPYKSFLKFLPSIRWYDPEHYWTPGSQNEGVFKNEECVLCHTVQTPTIVKDWKKSAHGNL
consensus   71  .*. .. *.* ........... . ** ......   .......*..**......*...*..*....
```

```
                                                              Heme2
HAO_Nmult  126 DKIRNLKPEDPTYYKKAKLEDVEKNLRSMGKLGANDKLKEVGCIDCHVDINKKDKADHMKDLRMPTADVC
HAO_Ncryo  127 DKIRDLKPSDPTYYKKAKLEGVEKNLRSMGKLGEKENLKEVGCIDCHVDINAKKKADHSKDLIMPTADVC
NeHAO      127 DKIRNLKSDDPLYYKKGKLEEVENNLRSMGKLGEKETLKEVGCIDCHVDVNKKDKADHTKDIRMPTADTC
HAO_Neutr  127 DKIRNLKPEDPLFYKKGKLEEVENNLRSMGKLGEKEVLKEVGCIDCHVDINAKKKADHTKDVRMPTADVC
HAO_Nntrs  126 DKIRKLTPKDDTFYKKAKLEAVEENLRSLGKLGKGEKLKEVGCIDCHFDINTKNKADHRKDIKIATADTC
HAO_Nnfc   137 DKIRKLTPKDETFYKKAKLEAVEANLRSIGKLGKGENLKEVGCIDCHFDINTKNKADHRKDIKLATADTC
HAO_Nino   126 DKIRKLTPKDETYYKKAKLEQIEENLRSMGKLGKGEQLKEVGCIDCHFEINAKGKADHRKDIKLATANTC
HAO_Nwats  129 DEIRNLPKDDSRYYKKKLIKEVEDNLRSMGKLEKNENLKEVSCIDCHVGVGA-EKGHHNQDLRLPDAAVC
NoHAO      129 DEIRDLPKDDSRYYKKKLIKEVEKNLRSMGKLEKNENLKEVSCIDCHVGVGA-EKGHHNQDLRLPDAAVC
HAO_Nhalo  129 DEIRNLPKDDSRYYKKRLIKEVEDNLRSLGKLGEDEELKEVACIDCHVGIGA-EKGHHKEDLRIPDAATC
KustC1061  140 DIRRGI------------------GIKKDGK--PVEDL--VGCADCH-------GNNHQKLEMPTYKLC
HAO_KSU-1  140 EMRRGLGIK------------------GKDGKPVE-GAVGCDVCH-------GNDHQKLFMPTYKHC
consensus  141 ...*  .  ...   ........... .....**...  . ...*.*..**...... ...........*
```

```
                γ-AOB fragment                                          Heme4
        Heme3        Loop        (No:T220-D228)                        (Heme P460)
HAO_Nmult  196 GTCHLQEFAERESERDTLVWPN---------KQWPQGRPSHSLDW-KANVEVAVFASMPQREIAEGCSMC
HAO_Ncryo  197 GVCHLQEFAERESERDTLIWPH---------DQWPAGRPSHALDY-KANVETTVWAAMPQREVAEGCSMC
NeHAO      197 GTCHLREFAERESERDTMVWPN---------GQWPAGRPSHALDY-TANIETTVWAAMPQREVAEGCTMC
HAO_Neutr  197 GTCHLREFAERESERDTMIWPN---------GQWPDGRPSHALDY-TANIETTVWAAMPQREVAEGCTMC
HAO_Nntrs  196 GACHLQEFAERFSERDTITWPK---------DQWPKGRPSHALDY-KANVEVEVYAGMPQREIADGCTGC
HAO_Nnfc   207 GTCHLQEFAERESERDTITWPK---------DQWPKGRPSHALDY-RANVEVEVYAGMPQREIADGCTGC
HAO_Nino   196 GTCHLQEFAERESERDTIIWPK---------DQWPKGRPSHALDY-KANVEVDVYAGMPQREIADGCTGC
HAO_Nwats  198 GTCHLQQFAERESERDTIVWPDTDVKGNKIEPVWPPGRPSHALDY-QANVDLATWAAMEDREVADGCTMC
NoHAO      198 GICHLQQFAERESERDTLTWPDTDVKGNKIEVWPPGRPSHALDY-QANVDLATWAAMEDREVADGCTMC
HAO_Nhalo  198 GACHLKEFAERESERDTLTWPTTDVKGNKIEPVWPPGRPSHALDY-QANVELATWAAMEDREVAEGCTMC
KustC1061  180 NDCHPKETAEHRAG--------------------GLGSHTHAYTVNVLEFSWHVGKPAEEVT-GCAHC
HAO_KSU-1  181 GECHPKETSEHRSG--------------------GLGSHTHAFTVNVLEFSWHVGKPAEEVA-GCAEC
consensus  211 ..**.....*..........             ... *..**...  ..... .........*...**..*
```

Figure 27 continues on next pages.

Figure 27 continued from previous page.

```
                    Heme5                 Heme6 (Ne:D291, No:D301, Ku:D262)
HAO_Nmult  256  H-TNQNKCDSCHTRHEFSAAESRHPEACATCHSGVDHNNWEAYSMSKHGKTVAIMGDKWNWNAPLKDAYT
HAO_Ncryo  257  H-TNQNKCDSCHTRHEFSAAESRKPEACATCHSGVDHNNWEAYSMSKHGKMVSMLGNKWNWDVQLKDAYA
NeHAO      257  H-TNQNKCDNCHTRHEFSAAESRKPEACATCHSGVDHNNWEAYTMSKHGKLAEMNRDKWNWEVRLKDAFS
HAO_Neutr  257  H-TNQNKCDNCHTRHEFSAAESRKPEACATCHSGVDHNNYEAYIMSKHGKLAEMNRGNWNWNVRLKDAFS
HAO_Nntrs  256  H-VNQNKCDTCHARHDFNVAESRKPEVCAQCHSGADHNNWEAYSLSKHGLKYQRDKDKWNFNVPIKEAMA
HAO_Nnfc   267  H-VNQNKCDTCHARHEFSVAESRKPEVCAQCHSGADHNNWEAYSLSKHGLKYQRAKDHWNFNIPIKEAIA
HAO_Nino   256  H-VNQNKCDTCHSRHEFSVAESRKPENCAQCHSGADHNNWEAYSLSKHGLKYQRDKDKWNFNIPIKEAIA
HAO_Nwats  267  H-INQNRCDTCHTRHQFSAVEARKPDACGNCHNGADHNEYENYLMSKHGTTYLMLGDTWDWEVPLKDAIA
NoHAO      267  H-INQNRCDTCHTRHQFSAVEARKPDACGNCHNGADHNEYENYLMSKHGTTYLMLGDTWDWEVPLKDAIA
HAO_Nhalo  267  H-INQNRCDTCHTRHQFSTVEARKPDACGYCHNGADHNEYENYLFSKHGAIYLMLGDEWDWEMPLRDAIG
KustC1061  227  HAIAENRCSGCHTRHKFDPAEARKPTACRVCHMGIDHDEWAMYNTSIHGALYEAESARMDWGKKLK----
HAO_KSU-1  228  HAIAENRCDGCHTRHVFSPAEARKPTACRFCHMGIDHDEWAMYNTSIHGCLYEAESATMDWSKPSK----
consensus  281  * ...*.*..**.**.*...*.*.*..*. **.*.**.....*..*.** ... .  ..... ........

                                   (Ne:Y358, No:F367, Ku:M327)
                    Heme7                Heme5 Active-center wall (No: D213-A239 (whole), W365-E379 (core))      Heme8
HAO_Nmult  325  KGGQTAPTCAGCHFEYEGKYSHNVVRKIR-WANYPAVPGIAENINSEWSEARLDSWVKTCTSCHSERFAR
HAO_Ncryo  326  KGGQNAPTCAGCHMEYEGEYTHNMVRKIR-WANYPFVPGIAENITSEWSEGRLDSWVVTCTQCHSERLAR
NeHAO      326  KGGQNAPTCAACHMEYEGEYTHNITRKTR-WANYPFVPGIAENITSEWSEARLDSWVLTCTQCHSERFAR
HAO_Neutr  326  KGGQTAPTCAACHMEYEGEYTHNITRKTR-WANYPFVPGIAENITSDWSEARLDSWVVTCTQCHSERFAR
HAO_Nntrs  325  KGAETAPTCQYCHMEYQGKIAHNIVRKVR-WANYPFVPGIRENIKTIWAEKRNDAWVKTCTNCHSETYAR
HAO_Nnfc   336  KGAETAPTCQYCHMEYQGKIAHNIVRKVR-WANYPFVPGIRENIKTEWADKRNDAWVKTCTQCHSETYAR
HAO_Nino   325  KGGLSAPTCQFCHMEYQGKITHNVVRKVR-WANYPFVPGIRENISTIWSEKRLDAWVKTCTNCHSESYAR
HAO_Nwats  336  ENEQTAPTCAFCHMEYKGRFGHNVVRKVR-WAFNPQ-EKIANNLEHEWYEKRNEAWIETCTNCHSATFAE
NoHAO      336  ENGQTAPTCAFCHMEYKGRFGHNVVRKVR-WAFNPQ-EKIANNLEHEWYEYRNEAWIETCTNCHSATFAE
HAO_Nhalo  336  RNGQTAPTCAFCHFEYKGRFGHNVVRKVR-WAFNPQ-EKIANNLEHEWYEDRKDAWVETCNNCHSPTFAE
KustC1061  293  KGNYRVPTCAYCHMQ---NGDHNPQRFGTIYSDMGMFQ---VDRGAHKHKAKRDSWIKECQDCHSPRFAA
HAO_KSU-1  294  KGNYRVPTCAYCHMQ---DGNHNPQQFGTIYSDMGM---FQVDRGAHRHKAKRDAWIKKCQDCHSPRFAA
consensus  351  ......***..**... ... **...... ............. ... ... ..*....*..***...*.

HAO_Nmult  394  SYLEFMDKGTLHGIAKYKEAHAVAEKLYKEGLLTGQKTNRPTPLPPDKEMFAGFTQL--YWSKDNNPAAI
HAO_Ncryo  395  SYLELMDKGTLQGLAKYQEAHEIVETLYNDGLLTGQKTNRPAPPAPEKPGFAQFSQL--FWSKGNNPASL
NeHAO      395  SYLDLMDKGTLEGLAKYQEANAIVHKMYEDGTLTGQKTNRPNPPEPEKPGFGIFTQL--FWSKGNNPASL
HAO_Neutr  395  SYLDLMDKGTLEGLAKYQEANAIVHKMYEDGTLTGQKTNRPNPPEPEKPGFGIFTQL--FWSKGNNPASL
HAO_Nntrs  394  AWMEFMDNGTFSGLEKYDEAHHVVEEQYKAGLLTGQKTNRPAPPAPETDGFEKFFQI--YWSKGNNPAAN
HAO_Nnfc   405  AWLEFMDNGTFSGIDKYDEAHHVVEEQYKSGLLTGQKTNRPAPPAPETDGFEKFFQI--YWSKGNNPAAN
HAO_Nino   394  AWMEFMDKGTYSGLDKYDEAHHVVEEQYKAGLLTGQKTNRPAPPPPVKDGFEQFFQI--YWSKGNNPAAN
HAO_Nwats  404  SYLEFVDNGIISGLKKQLEAKQIVEALYEDGLLPGQKTNRPAPPKPEHDAPGEFFQL--FIAKGNNPTTV
NoHAO      404  SYLEFVDNGIISGLKKQLEAKQIVEALYEDGLLPGQKTNRPAPPKPEHDAPGEFFQL--FIAKGNNPTAV
HAO_Nhalo  404  AYLEFIDNGIISGLKKQIEAKHIIEGLYEDGLLPGQKTNRPAPPKPEHDAPGEFFQL--FIAKDNNPTAV
KustC1061  357  DKLKEMDAGVNLSFTKWREAAAVIVGCYLDGVVDPM----PEGSAPDWYGHYTFSLLPGGDPRFYATSNL
HAO_KSU-1  358  DKLKEMDAGVNLSFTKWREAAAVIVGCFLDGVVDPM----PEGSPPDWYGHYTFSLLPGGDPRFYATSNL
consensus  421  ......* *..... *. **. ... .. .*.........*... *....... *...  ...........

                              Heme P460 linking Tyr
                (Ne:E471, No:E480, Ku:C431) (Ne:491,No:500, Ku:451)
HAO_Nmult  462  ELKVLEMGENNLPKLHVGLAHVNPGGWTYT-EGWGPMNRDYVEVMDENTKIREMAALQAKVAKLEAK-RK
HAO_Ncryo  463  ELKILEMGENQLAKMHVGLAHVNPGGWTYT-EGWGPMNRSYVEIQDENTKFREMMALQERVQKLESK-R-
NeHAO      463  ELKVLEMAFNNLAKMHVGLAHVNPGGWTYT-EGWGPMNRAYVEIQDEYTKMQELSALQARVNKLEGK-Q-
HAO_Neutr  463  ELKVLEMAFNNLAKMHVGLAHVNPGGWTYT-EGWGPMNRAYVEIQDEYTKMQEMTALQARVNKLEGK-K-
HAO_Nntrs  462  ELRLFEMAEDHLVQLHVSLAH-QYWGYTYT-VGWAAMNRAYVEIMDDDTRLKEKLDLQARVAKLEGH-MK
HAO_Nnfc   473  ELKLFEMAEDHLVQLHVSLAH-QYWGYTYT-VGWAAMNRAYVEIMDDDTRLKEKLDLQARVAKLEGQ-MK
HAO_Nino   462  ELKLFEMAEDHLVQLHVSLAH-QYWGYTYT-VGWAAMNRAYVEIMDDDTRLKETQKLLARVDKLESE-RK
HAO_Nwats  472  ELQYSKMWEQDLLKHYKALAHVNPGFWTYT-EGWGPLLERYTNIQDANTQLRAFAKLKSQVAMLEGDIKA
NoHAO      472  ELQYAKMWEQDLLKHYKALAHVNPGFWTYT-EGWGPLLERYTNIQDANTQLRAFAKLKAQVATLEGDVKA
HAO_Nhalo  472  ELQYAKMWEQDLLKHYKALAHANPGFWTYT-EGWGPLLERYTNIQDANTQLREFAKLKTKVAMMEGDIKA
KustC1061  423  ERLGLEMICYLTGNVYKAYAHMSMYNQTYGNGSAFEQDRKLVEIKTEAAKLRRFAAIEKKIG-LEH--KS
HAO_KSU-1  424  ERLGLEMICYLTGNVYKAYAHMSMYNQTYGNGSAFEQDRKLIEIKTEAAKLRRFAAIEKKIG-LEH--KS
consensus  491  *.....*... ........**......**. ........ ....... ..... ...........*.  .

HAO_Nmult  530  ASLFDLDSS-EKLSLGGLGGGMLLAGTLALAGWRRREKSERQ-----
HAO_Ncryo  530  TSLLDLDSTAEKISLGGLGGGMLLAGTLALAGWRKRKKIEG------
NeHAO      530  TSLLDLKGTGEKISLGGLGGGMLLAGALALIGWRKRKQTRA------
HAO_Neutr  530  TSLLDLKGAGEKISLGGLGGGMLLAGAIALIGWRKRKQTQA------
HAO_Nntrs  529  SSLLDLDSETGKISLGGIGGGMMLAGTLALAGWRRNKK---------
HAO_Nnfc   540  HSLLDLDTFTGKISLGGIGGGMMLAGTLALAGWRRHKK---------
HAO_Nino   529  HSLLDLDGPGGKLSIGGLGGGMMLAGTLAIAGWRRRERKDR------
HAO_Nwats  541  AKLLNLDSQVERAVVGGLGGGMVLAG-VGLVAWRRKQKTEG------
NoHAO      541  AKLLDLDSQVERAVVGGLGGGMVLAG-VGLVAWRRKQKTEG------
HAO_Nhalo  541  AGILDLDNQVERAVVGGLGGGMVLAG-VGLVAWRRKQQSEG------
KustC1061  490  ADFWKHGEYLDLLPGWKRKPGDVDVEWFKRTDIPHRANADAGVETHH
HAO_KSU-1  491  EAFWQHGEYLDLLPGWKRKPGDVDVEWFKRTDIPHRANADAGVEVHH
consensus  561  . ........ ................. ......... ....
```

Figure 27 continues on next page.

Figure 27 continued from previous page.

Figure 27. Structure-guided multiple protein alignment of HAOs from AOB, comammox and anammox.

(A) Structure-guided multiple alignment of HAOs from several βAOB, γAOB, comammox and anammox bacteria. The alignment was performed by the two step approach. First, structure-based sequence alignment was performed for three proteins whose structures were solved; NeHAO (PDB: 4n4n), NoHAO (resolved by this study, PDB: not available), Kustc1061 (PDB: 4n4k). Second, sequence-only alignment was performed for all 12 proteins with constraints for the result of structure-based alignment.

Protein identifiers and abbreviations represent on ahead of alignment. 'T' on strain names, such as ATCC 19707[T], shows type strains. The protein names belonged to βAOB, γAOB, comammox and anammox bacteria are printed in blue, green, red and brown, respectively. The protein names printed in bold are used for the structure-based alignment.

The amino acid sequence printed in grey are N-terminal signal and C-terminal residues that disordered/calved in the crystal structures. The heme binding motif (CxxCH) for heme-*c* (heme 1–3 and 5–8) and heme P460 (heme4) are printed in red. Activating residues on heme P460 defined by crystal structure are printed in green (the abbreviations of the residue number, Ne:NeHAO, No:NoHAO, Ku:Kustc1061). Inserted γAOB specific fragments are shown in red box. HAO loops includes the inserted fragments are shown in red dotted box. Active site walls are shown in blue dotted box.

Figure 27 (legend) continues on next page.

Figure 27 (legend) continued from previous page.

Note that the side chain aromatic ring of the two residues (NeHAO: Y358, NoHAO: F367) are occupied roughly same spaces in the crystal structures, in spite of the position of the Cα-carbon and the alignment were shifted one residue.

The alignment calculations were performed by MOE. Pretty printing of the alignment was performed by BOXSHADE 3.21 server (http://www.ch.embnet.org/software/BOX_form.html).

(B) Sequence identity tree. The tree was calculated by average distance clustering algorithm using identity of the protein sequences. The calculation and graphical representation were performed by MOE version 2015.1001.

(C) All-against-all pairwise identity matrix. The matrix values show identity percentages that were calculated by the following method; number of matched residues between sequences in row and column are divided by the length of sequence in the column. The calculation and graphical representation were performed by MOE.

Chapter 4
HAO inhibitor screening

Introduction

In this chapter, I performed HAO inhibitor screening and structure development. It is very difficult to design inhibitors from scratch by using only a structure of an apo-enzyme of HAO. I first searched seed inhibitors which have low inhibition activity but bind to HAO active center by using soaking of HAO crystals. Then, I developed lead inhibitor candidates by using fragment-based drug (FBDD) design approach combined with large scale *in-silico* screening.

Materials and methods

Analysis for HAO-inhibitor complex structure

Crystallization of NeHAO and NoHAO were described in **Chapter 1.** Data collection and structure analysis were described in **Chapter 1**.

Docking model of HAO-benzaldoxime

Docking model of HAO-benzaldoxime was prepared by energy minimization of molecular mechanism (MM) calculation using MOE 2014.10 software (Chemical Computer Group Inc.). The structure file of benzaldoxime was fetched from PubChem CID:5324611). For initial structure, benzaldoxime was arranged to NoHAO-acetaldoxime complex structure to overlap the hydroxylamine moiety (-N-OH) of each compounds. Then, energy minimization was performed for the initial structure using constraints with HAO and hydroxylamine moiety on the benzaldoxime.

In-silico screening

In-silico screening operations (conformation import and pharmacophore search) were performed using

Molecular Operating Environment (MOE) software (version 2015.1001, Chemical Computing Group) with the following parameters: database of Namiki shoji's 5.6 million commercial compound catalog, pocket shape filter with NeHAO and NoHAO (PDB:4n4n), ligand temperate of pharmacophore feature of phenylhydrazine and acetaldoxime.

Nitrification activity assay

Nitrification activity assay including cell culture and calculation of IC_{50} was used the methods described in **Chapter 1**.

Structure analysis for complex of NoHAO-benzaldoxime

Crystallization, data collection and structure analysis for NoHAO were described in **Chapter 1**. Crystals of NoHAO in complex with benzaldoxime was obtained by soaking the apo-enzyme crystals to reservoir solution including 10 mM benzaldoxime within 1 min, and were performed data collection immediately. Successively, the NoHAO-benzaldoxime complex structure was solved by the molecular replacement method using the resultant apo-enzyme form structure as the starting model.

Results and discussion

Screening seed compounds by using crystal soaking and structure analysis

I first screened seed compounds from 7 compounds including substrate mimics and known HAO inhibitors by using crystal soaking and structure analysis (**Figure 28**). Then, the two HAO-inhibitor complex structures were successfully solved for acetaldoxime, a non-commercial very weak nitrification inhibitor(CH_3-CH_2-O-NH) [61], and phenylhydrazine, a known HAO inhibitor (Phenyl-NH_2-NH_3) [31] (**Figure 29**).
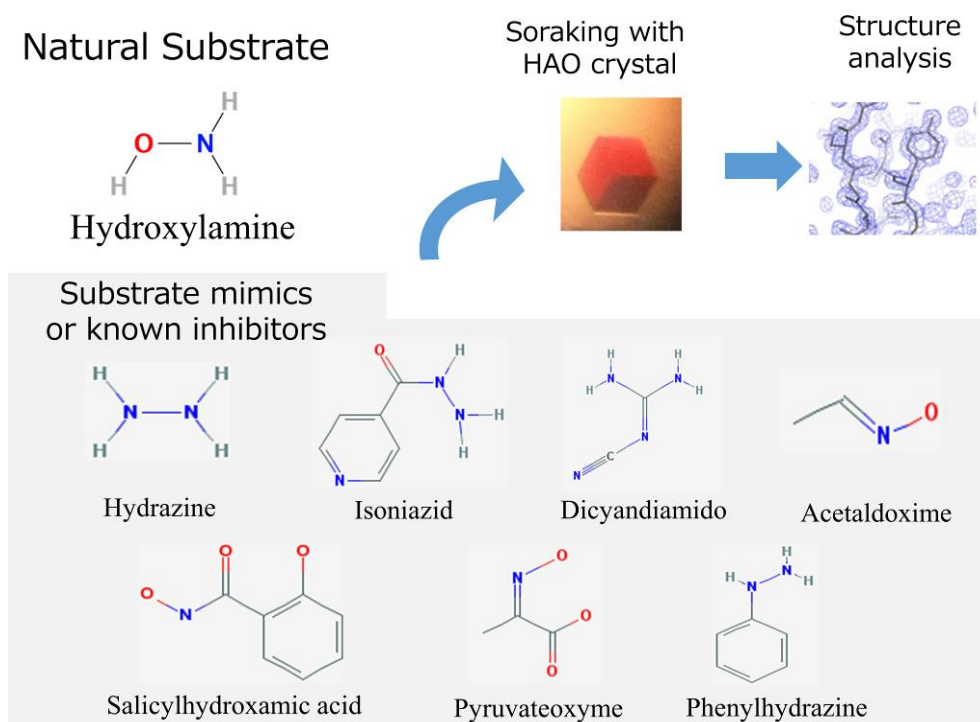
Figure 28. Screening procedure for HAO inhibitor by crystal soaking and structure analysis.

Acetaldoxime and phenylhydrazine were located in a slightly different position on the heme P460, the active center in ligand bind pocket of NoHAO, in each crystal structures (**Figure 29 A, B and C**). The acetaldoxime binds to the Fe on the heme P460, and interacts to the conserved residues of Asp-301 and His-302 with mimicking substrate manner (**Figure 29A and B**). The phenylhydrazine binds to the entrance of the ligand binding pocket of NoHAO; the phenyl group of phenylhydrazine fits well into the hydrophobic patch on around the entrance (**Figure 29C**).
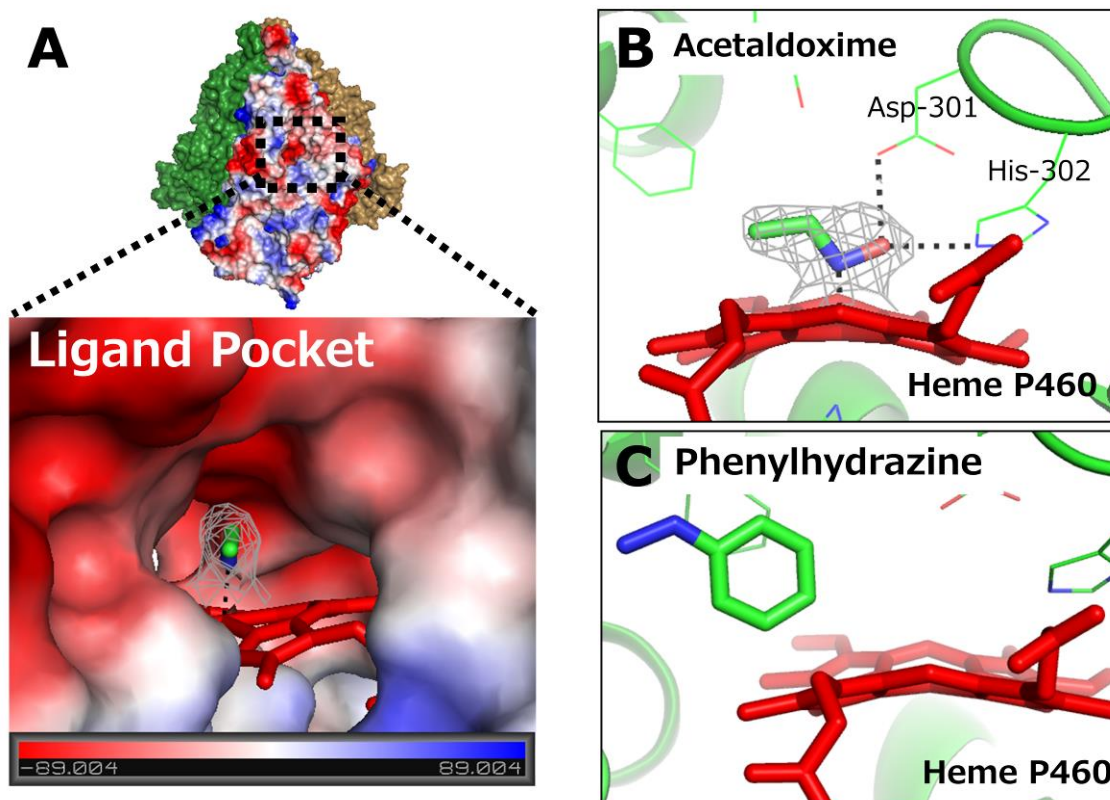
Figure 29. NoHAO-substrate mimic complex structures.

Ligand binding pocket of NoHAO to which inhibitors bind (A). Close-up views of around heme P460 in ligand binding pocket of HAO-acetaldoxime (B) and HAO-phenylhydrazine (C) complex structures.

Designing chimera compound by linking of two inhibitors by using fragment based drug design (FBDD) approach

The two compounds, acetaldoxime and phenylhydrazine, were located in a slightly different position on the heme P460. Taking advantage of this feature, I applied a linking strategy of fragment-based drug design (FBDD) approach to design more potent compounds. This strategy allows me to design benzaldoxime which has the structure linking acetaldoxime with phenylhydrazine (**Figure 30A**). By the docking simulation of benzaldoxime to NeHAO, benzaldoxime potentially binds on the heme P460 in the active-center pocket of NeHAO. Fortunately, benzaldoxime was listed in the Namiki shoji's

in-stock catalog library. To verify the utility of the FBDD approach, I purchased benzaldoxime and

performed an HAO-benzaldoxime complex structure analysis. The NeHAO-benzaldoxime complex

crystal structure was successfully solved (**Figure 30B**). The binding mode of benzaldoxime revealed

by the experimental structure was very similar with that of the predicted docking model (**Figure 30A**

and **B**). These results showed efficacy of the FBDD approach to develop inhibitors by using

phenylhydrazine and acetaldoxime bound HAO structures as seeds information. Therefore, I have

carried out designing new compounds using the FBDD approach combined with large scale *in-silico*

screening techniques.
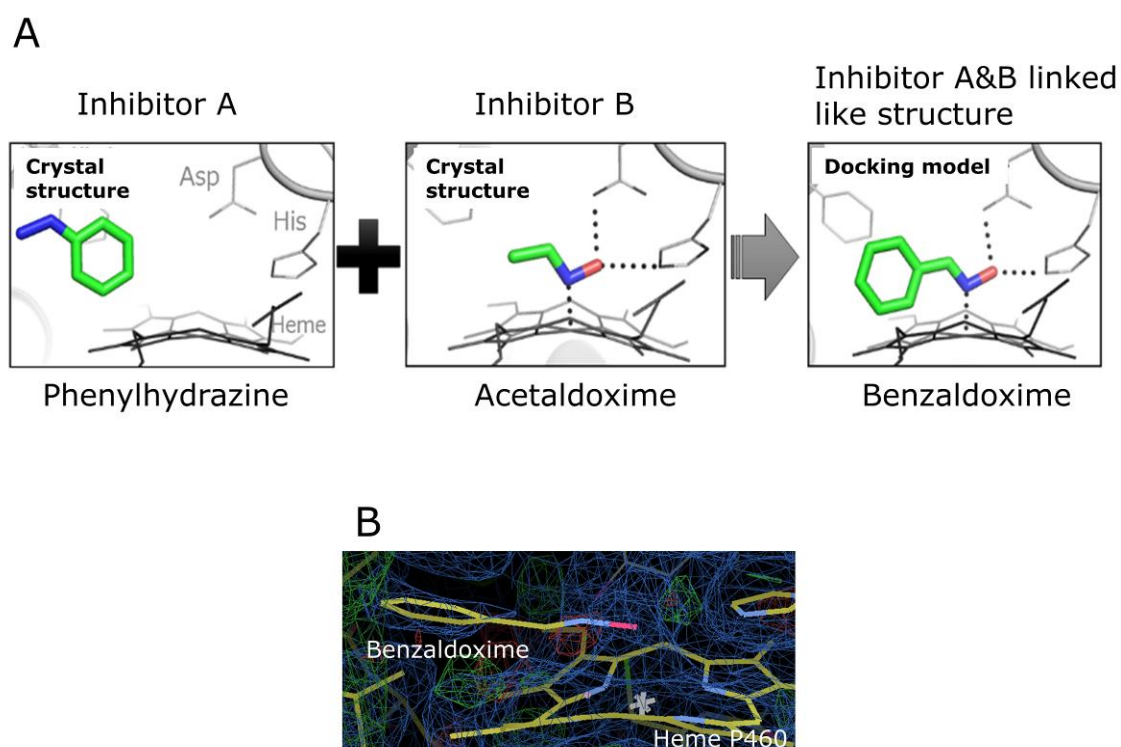
Figure 30. Benzaldoxime designed by fragment-based drug design (FBDD) approach.

(A) Benzaldoxime was designed by linking of two fragments (phenylhydrazine and acetaldoxime). (B) Crystal structure of NeHAO-benzaldoxime complex.

FBDD approach combined with *in-silico* screening

I carried out designing more effective inhibitors using FBDD approach combined with large-scale *in-silico* screening method featuring pharmacophore search.

For preparation of the pharmacophore search, I have curated the commercial compound database catalog (3D structure of 5.3 million compounds) for drug screening provided by reagent vender of Namiki shoji (Tokyo, Japan). The library was washed ("Wash" is a MOE software command that executes ionizing and deleting salts), filtered (MOE command that selects drug-like compounds by using Lipinski's rule of fives [62]), and executed conformation analysis (MOE command that search low energy conformations of the compounds) which are required for pharmacophore search.

Pharmacophore search was performed for the drug-like focused library with conformational analysis. Firstly, the overlapped image of the two inhibitors are prepared on the MOE software 2015.1001 (**Figure 31B**: superpose). Secondary, I set pharmacophore feature of aromatic ring (orange ball) on the phenyl ring of phenylhydrazine, hydrogen-bond donor (blue ball) on the oxygen, and hydrogen-bond donor/acceptor (pink ball) on the nitrogen of acetaldoxime (**Figure 31B**: Set pharmacophore). The pharmacophore represents steric and electronic features that is necessary to bind receptor. Thirdly, I set the pocket shape filter with NeHAO and NoHAO structure. This filters eliminated compounds that were larger than the pocket. Fourthly, I performed a search with the settings against commercially available 4.7 million compounds (**Figure 31B**: Search). In the results, I got 989 hit compounds that had same pharmacophore features with combination of phenylhydrazine and acetaldoxime (**Figure 31B**: Hit 989 compounds). In other words, these hit compounds were predicted to bind HAO by same binding mode as the acetaldoxime and phenylhydrazine.

Because the 989 compounds are too many perform assay, I selected 98 compounds from the 989 compounds by using clustering of similar compound (by using MOE software 2015.1001) and manual

selection to select wide variety of compounds. Finally, I purchased 77 compounds which is in-stock compounds out of the 98 compounds. In the next chapter, I assayed these hit compounds by using high-throughput assay methods that I have developed.
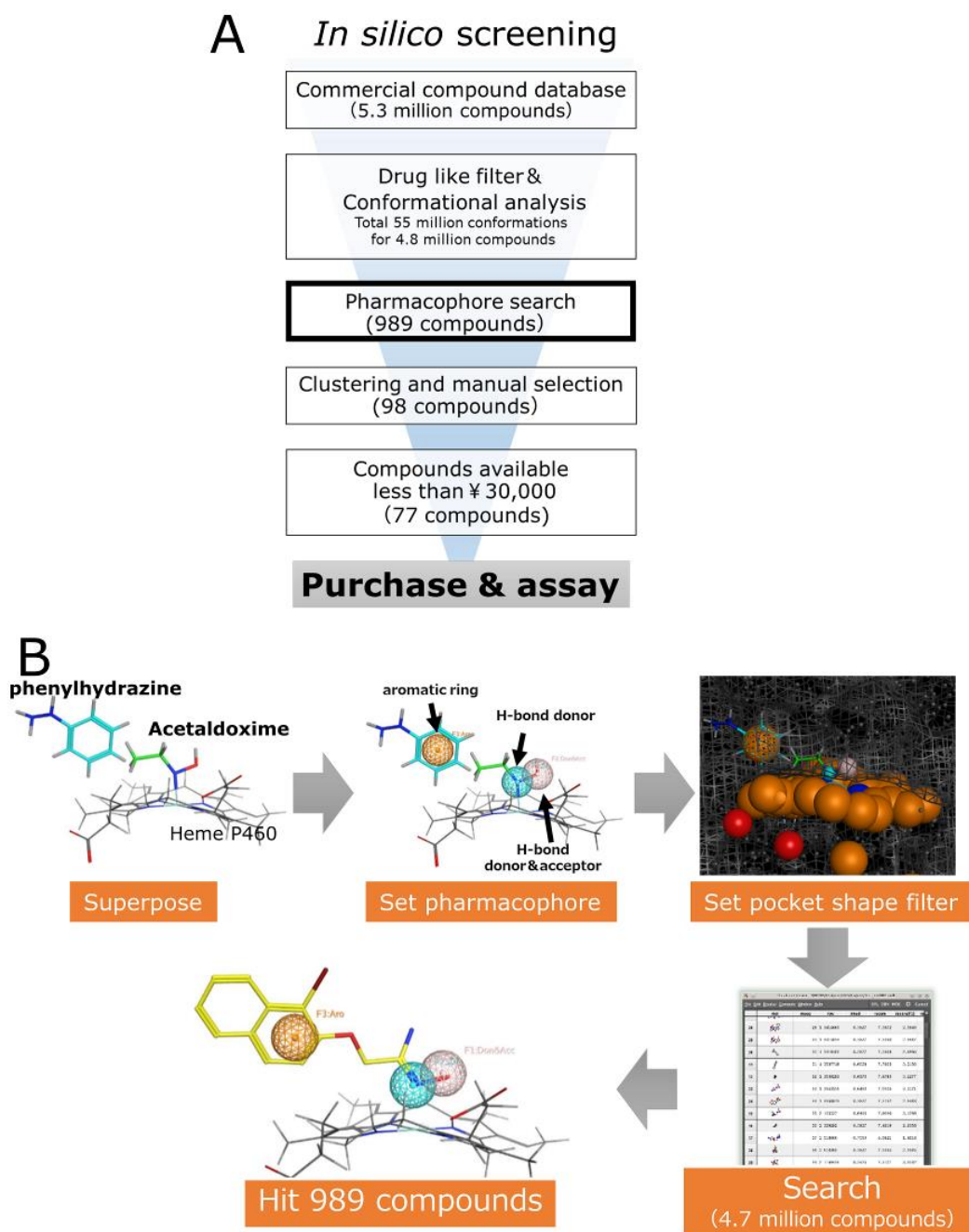
Figure 31. Scheme for *in-silico* screening combined with FBDD.
(A) Whole scheme for *in-silico* screening. (B) Scheme focused on pharmacophore search.

Appendix
Method development for future works

Appendix

Integrated method for purification of *Nitrosomonas europaea* cytochrome c_{554}, another potential target of nitrification inhibitor

Abstract

Cytochrome c_{554} is an electron transport protein involved in the nitrification pathway of *Nitrosomonas europaea*. A simplified production system for cytochrome c_{554} is required to reveal the functions of cytochrome c_{554}, aiding efforts to control nitrification. Here, I described a novel purification method for *N. europaea* cytochrome c_{554} by utilizing a combination of HiTrap Q, HiTrap SP, Superdex 200, and Mono S columns. My method does not require the cumbersome and time-consuming steps associated with conventional purification methods, such as ammonia-sulfate fractionation and dialysis. This purification method allowed us to obtain highly pure cytochrome c_{554} in 2 days. This method is also adaptable for scale-up and/or automated purification to produce a large amount of protein. Therefore, my study provides an improved method for the purification of *N. europaea* cytochrome c_{554} for applications that require a large amount of protein, such as crystal structure analysis and inhibitor screening.

Introduction

Cytochrome c_{554} from *Nitrosomonas europaea* (NeCyt c_{554}) is a tetra-heme protein involved in its bacterial nitrification. NeCyt c_{554} is believed to act as a functional electron acceptor for NeHAO

[66] (**Figure 3**, **Figure 40**) and an electron donor for cytochromes c_{552} and c_{M552} [25,67]. Furthermore,

NeCyt c_{554} may be directly involved in the emission of nitrous oxide (N_2O), a powerful greenhouse

gas. In low-oxygen conditions, cytochrome c_{554} may produce N_2O by reducing NO generated from

hydroxylamine by HAO [68,69] (**Figure 40**). However, the mechanism of this NeCyt c_{554} action is not

fully understood.
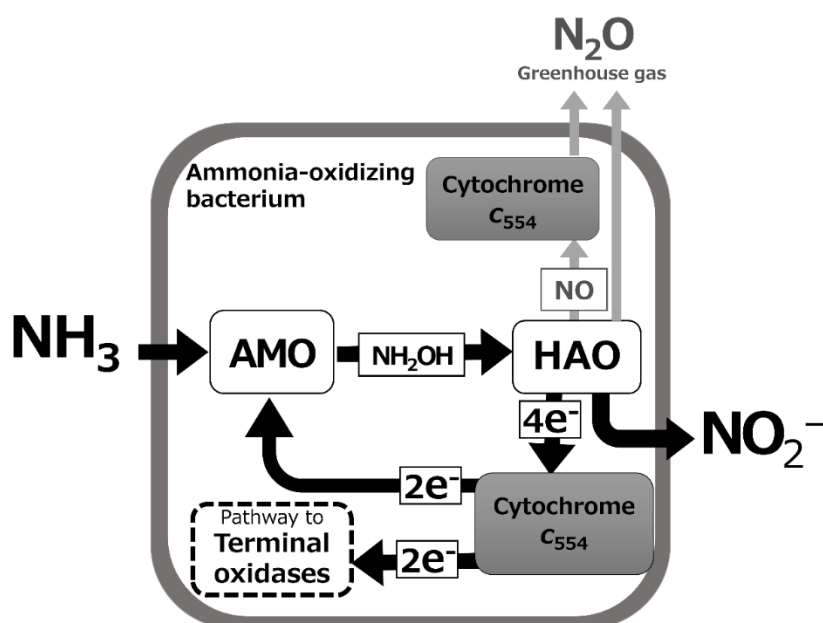
Figure 40. A simplified model of the nitrification pathway in *Nitrosomonas europaea* related with cytochrome c_{554}.

Ammonia monooxygenase (AMO) oxidizes ammonia (NH_3) to hydroxylamine (NH_2OH) using two electrons (e^-). In the common pathway (black arrows), the hydroxylamine oxidoreductase (HAO) subsequently releases four electrons from one hydroxylamine coupled with the oxidization of hydroxylamine to nitrite (NO_2^-). The released electrons are then transferred to cytochrome c_{554}. Half of the electrons are returned to AMO, and the remaining electrons are ultimately transferred to the terminal oxidases. In low-oxygen condition, a nitrous oxide (N_2O)-forming pathway may be taken (grey arrows). Here, HAO generates nitric oxide (NO) from hydroxylamine, which is then converted to nitrous oxide (N_2O) possibly by cytochrome c_{554}. The N_2O

pathway has not been fully characterized and alternative routes are believed to exist [27]. Some elements of the electron transfer pathway, such as the cytochrome c_{552} and cytochrome c_{M552}, are not present in this model (for a detailed pathway, see Whittaker *et al.* [25]).

The key components of the nitrification pathway are potential targets of nitrification inhibitors (See General introduction). AMO is the target of common commercial nitrification inhibitors such as nitrapyrin [28], and HAO has emerged as a new target for nitrification inhibitors [30,31]. Therefore, NeCyt c_{554} may also serve as a potential target in the development of novel nitrification inhibitors.

NeCyt c_{554} is a 26-kDa protein that covalently interacts with four c-type hemes. Functional analysis and crystal structure studies of NeCyt c_{554} have been performed [70,71] using NeCyt c_{554} purified by methods described by Yamanaka *et al.* [67] and Arciero *et al.* [72]. Development of inhibitors that target NeCyt c_{554} has not been reported. To develop NeCyt c_{554}-specific inhibitors, a large amount of protein is needed for studies such as inhibitor screening or crystal structure analysis of the protein-inhibitor complex. Because a recombinant system for NeCyt c_{554} production has yet to be established, purification of native protein from AOB cells is required to produce NeCyt c_{554}. However, current purification methods are associated with several cumbersome and time-consuming procedures, such as ammonia-sulfate fractionation and dialysis.

In this study, I demonstrated a novel procedure for the purification of native cytochrome c_{554} from *N. europaea* (NeAOB) strain NBRC 14298. The procedure encompassed optimized column types and conditions to obtain high purity product in a short period. This new procedure may be used to produce sufficient amounts of NeCyt c_{554} to accelerate its functional studies and the development of new nitrification inhibitors.

Materials and methods

Purification of cytochrome c_{554} from NeAOB

Cell line and cell culture method were described in **Chapter 1**. Frozen NeAOB cell pellet (1.5 g) was suspended in 40 mL buffer A (pH 7.5, 50 mM Tris-HCl) and sonicated. The suspension was then centrifuged at 40 000 × g for 40 min at 4 °C. Subsequently, the supernatant was applied to an anion-exchange column system composed of three tandemly connected HiTrap™ Q HP 5 mL columns (GE Healthcare, Buckinghamshire, England, UK), which were equilibrated with buffer A. A linear gradient of NaCl (illustrated in **Figure 41A**) was performed with 0–500 mM NaCl in 100 mL buffer A (this gradient elution step is not needed during a normal purification procedure). Post-elution cleaning was performed using 1 M NaCl. The flow-through fractions containing cytochrome c_{554} were then pooled and applied to a HiTrap™ SP HP 5 mL cation-exchange column (GE Healthcare) equilibrated with buffer A. Elution was performed by a linear NaCl gradient in buffer A (0–1 M, 100 mL). Following elution, cleaning was performed using 1 M NaCl. The eluted cytochrome c_{554} fractions were subsequently applied to a HiLoad™ 26/600 Superdex™ 200 pg gel-filtration column (GE Healthcare) equilibrated with buffer B (pH 7.5, 10 mM Tris–HCl, 150 mM NaCl). Thereafter, the eluted cytochrome c_{554} fractions were applied to a high-performance cation-exchange column Mono S® 10/100 GL (GE Healthcare). The elution was performed using a linear gradient of NaCl in buffer A (0–1 M, 100 mL). The eluted cytochrome c_{554} fractions were then stored at 4 °C until further experiments.

All chromatography procedures were performed using the *ÄKTAexplore* 100 system (GE Healthcare). All eluted fractions containing NeCyt c_{554} were detected by two methods: 1) wavelength monitoring by *ÄKTAexplore* (protein: 280 nm; c-type hemes in cytochrome c_{554}: 409 nm) and 2) SDS-PAGE analysis with Coomassie Brilliant Blue stain. The HiTrap Q column was regenerated by acid

acetone (80% acetone, 10% HCl, 10% water) to remove ingrained hemes after purification. The

concentration of NeCyt c_{554} was determined by absorbance in the reduced form with ϵ_{554} = 24.6 mM

$^{-1}$ cm^{-1} per heme [73].

Protein electrophoresis

Tris-Glycine-SDS-PAGE was performed as described as **Chapter 1**. The sample buffer was also

stocked in a −20 °C freezer in single-use volume because air oxidization of dithiothreitol led to

diffusion of the NeCyt c_{554} band, as same as HAO.

UV–vis spectroscopy

The UV–vis spectra were measured from 220 to 800 nm with 0.2 nm bandwidth and 0.1 nm s^{-1} scan

rate at 25 °C using Cary 400 Bio spectrophotometer (Varian, Zug, Switzerland). The measurement

buffers were 10 mM Tris-HCl (pH 7.5), 150 mM NaCl with or without 50 mM dithionite. The

dithionite was prepared as a 1 M solution, and was then added to the protein solution immediately

before measurement.

Mass spectrometry analysis

Identification of the NeCyt c_{554} was performed by peptide mass fingerprinting using matrix

assisted laser desorption/ionization time-of-flight mass spectrometry (MALDI-TOF/MS). The

purified cytochrome c_{554}, for which cysteine residues were not modified, was digested by L-

(tosylamido-2-phenyl) ethyl chloromethyl ketone (TPCK)-treated trypsin (Thermo Fisher Scientific)

for 18 hours at 37 °C in the Mono Q elution buffer condition. The digested peptide solution was mixed

with a matrix solution composed of saturated α-cyano-4-hydroxycinnamic acid (Bruker Daltonics,

Biellerica MA, USA) in 50:50:1 of water:acetonitrile:trifluoroacetic acid, spotted on a MALDI target

plate (MTP 384 massive; Bruker Daltonics), and dried at room temperature (25 °C). Acetonitrile and

trifluoroacetic acid were purchased from Wako Pure Chemical Industries and Sigma-Aldrich,

respectively. The mass spectrum was measured in a reflector-positive mode with a mass range of m/z

200 to 3000 using an autoflex™ III smartbeam MALDI-TOF/MS instrument (Bruker Daltonics).

Calibration was performed using the Peptide Calibration Standard (Bruker Daltonics). Data processing

and peak assignments were performed using the mMass software version 5.5.0 [74]. Peptide mass

fingerprinting search was performed by Mascot server (Matrix Science, Boston MA, USA) against the

Swiss-Prot database using the default parameter. The assignment results were verified using the

mMass software with the following parameters: the amino acid sequence of NeCyt c_{554} (UniprotKB

entry C554_NITEU), one missed-cleavage of trypsin digestion, and a peptide mass tolerance of ± 100

ppm.

Protein-Protein docking simulation

Protein-protein docking simulation for NeHAO and NeCyt c_{554} was performed by ZDOCK

server version 3.0.2 [75] with the crystal structure of NeHAO (PDB:4n4n) and NeCyt c_{554}

(PDB:1ft5). Graphical representations were performed by PyMOL 1.7.

Results

A new method for purifying native NeCyt c_{554}

In the present study, I reported an integrated purification method for native cytochrome c_{554} from *N.

europaea* strain NBRC 14298 (NeCyt c_{554}). My purification scheme (illustrated in **Figure 41A**) does

not involve inconvenient steps associated with conventional purification procedures, such as

ammonium-sulfate fractionation, dialysis, dilution, and concentration [67,72]. In the first

chromatography step, 40 mL of cell lysate containing NeCyt c_{554} was passed through a HiTrap Q

column system (**Figure 41B**). Because NeCyt c_{554} showed a high pI value of 10.7 [67], the NeCyt c_{554} was not adsorbed onto the anion-exchange column HiTrap Q. This step increased the purity of NeCyt c_{554} as assessed by SDS-PAGE (**Figure 41F**). In this study, I also demonstrated the effect of the HiTrap Q step through an additional NaCl-gradient elution. The elution profile clearly demonstrated that the HiTrap Q column was able to remove heme-containing proteins eluted at 115 mL (**Figure 41G**) and other non-heme contaminating proteins. This gradient elution is not necessary for normal NeCyt c_{554} purification. In the second chromatography step, a HiTrap SP column was used to separate the NeCyt c_{554} (eluted at approximately 120 mL) from eluted contaminants in the flow-through and peak fractions eluted at 85 mL (**Figure 41C**). This HiTrap SP step was important to concentrate the NeCyt c_{554} in solution to be applied into the next gel-filtration column (HiLoad 26/600 Superdex 200 pg column) which has a maximum load-volume of 13 mL. In the third chromatography step using the Superdex 200 column, NeCyt c_{554} was eluted at approximately 230–250 mL fractions and separated from contaminants and salt (**Figure 41D**). The gel-filtration column step was also important for the assessment and removal of aggregated proteins. Thus, no aggregated proteins were observed approximately the void-volume in this study. The final column step was performed using a high-performance cation-exchange column Mono S for further purification and protein concentration (**Figure 41E**). In Mono S chromatography, NeCyt c_{554} was eluted as a single peak at 160 mL and no other contamination peaks were observed. The peak fractions showed red coloring. The protein yield was 0.4 mg from 20 L of NeAOB culture.
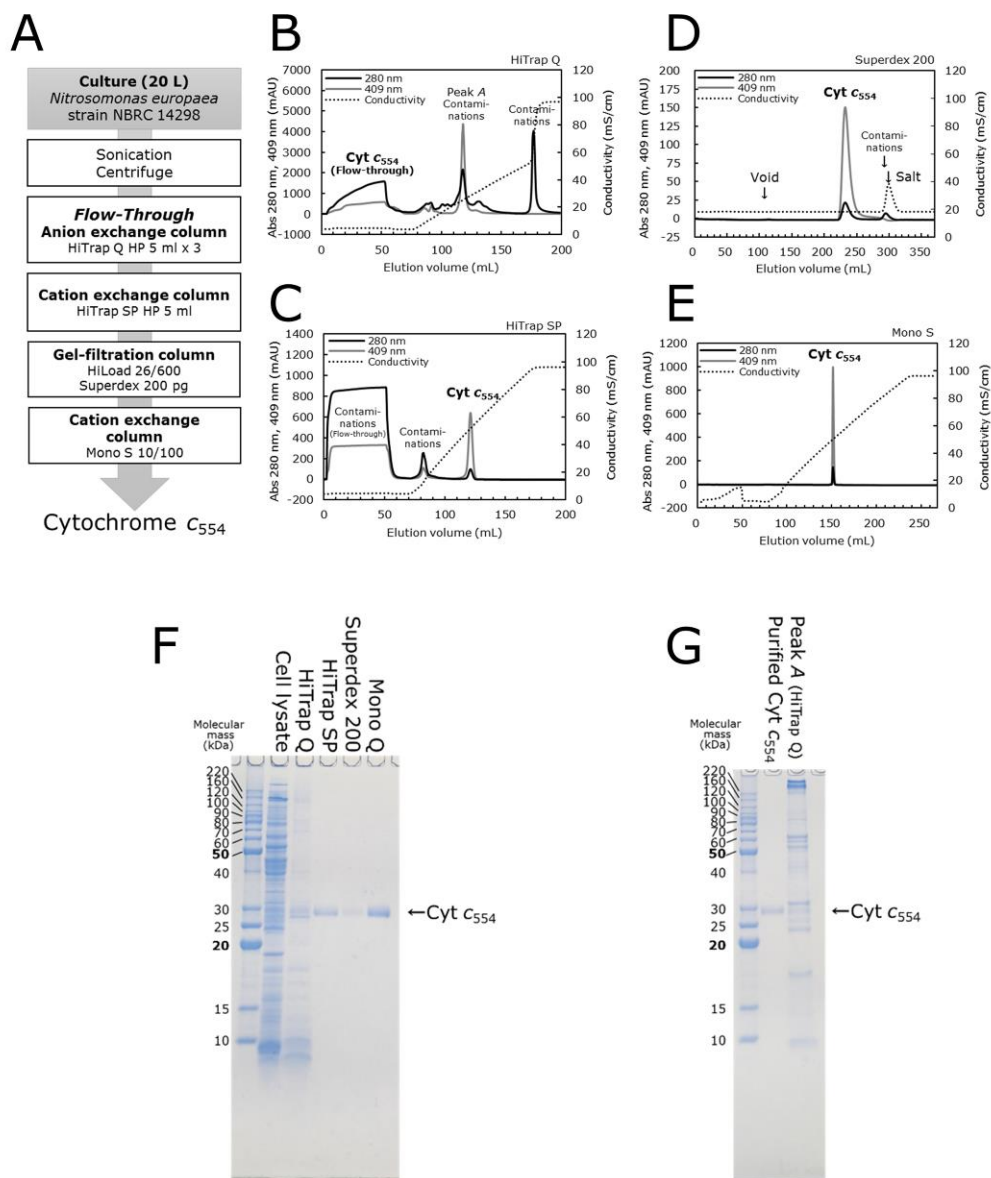
Figure 41. Purification scheme and elution profiles of chromatography for NeCyt c_{554}.

(A) Purification scheme for cytochrome c_{554} from NeAOB (NeCyt c_{554}).
(B) An anion-exchange chromatography using three tandemly connected HiTrap Q 5 ml columns. The flow-through fractions contained NeCyt c_{554}. Peak A is a contamination peak that includes heme proteins.
(C) A cation-exchange chromatography using a HiTrap SP 5 ml column. Elution was performed using 100 mL of NaCl linear gradient (0–1 M).
(D) A gel-filtration chromatography using a HiLoad 26/600 Superdex

94

200 pg column. (E) A high performance cation-exchange chromatography using a Mono S 10/100 column. Elution was performed with 100 mL of NaCl linear gradient (0–1 M). NeCyt c_{554}-containing fractions were detected by absorbance at 409 nm. (F) SDS-PAGE analysis of the NeCyt c_{554} during purification. The cell lysate and column elution fractions were analyzed by 15% SDS-PAGE. The cell lysate lane contained centrifuged supernatant fraction of sonicated cell lysates. Other lanes contained pooled fractions eluted from each column. Mono Q-eluted sample was concentrated and analyzed by SDS-PAGE in Fig 3A. (G) SDS-PAGE analysis of the heme-containing peak (peak *A*) fraction on HiTrapQ chart (B) was compared with purified cytochrome c_{554} (purified Cyt c_{554}). Cyt c_{554} may be found in the peak *A* fraction, but the amount was small.

Characterization of the purified NeCyt c_{554}

The purified protein was analyzed by SDS-PAGE and observed as a single band of approximately 27 kDa in size with high purity (**Figure 42A**). The apparent molecular mass was in agreement with the calculated molecular mass of 26.2 kDa for cytochrome c_{554} that includes four hemes. The purified protein was also identified as NeCyt c_{554} using a peptide mass fingerprinting through tryptic digestion and MALDI-TOF mass analysis (**Figure 42B and C**). Five peaks were assigned on the sequence of NeCyt c_{554}. The sequence coverage and Mascot Search Results score were 18% and 64, respectively. I also evaluated the *c*-type hemes in NeCyt c_{554} by measuring the UV–vis spectra of the air-oxidized and dithionite-reduced status (**Figure 42D**). The spectra showed an absorption peak at 406 nm in the oxidized form and peaks at 419, 523.6, and 553.4 nm in the reduced form. These were in agreement with the previously reported spectra of NeCyt c_{554} showing an absorption peak at 407 nm in the oxidized form and peaks at 421, 524, and 554 nm in the reduced form [67]. Additionally, 430 nm shoulder on the Soret peak, a characteristic feature of NeCyt c_{554}, was also observed in the spectrum of the oxidized form using the NeCyt c_{554} purified by my method. These spectral features demonstrated

that the purified protein was a mature NeCyt c_{554} containing c-type hemes. Purity of the protein was

also verified using the spectrum of oxidized NeCyt c_{554}. The absorbance ratio of 406 nm/280 nm

(A_{406}/A_{280}) was 6.5. Given that Arciero et $al.$ reported an A_{406}/A_{280} value of 6.6 for NeCyt c_{554} [72],

the cytochrome c_{554} purified using my method was highly pure and comparable to proteins prepared

using conventional purification methods. These results indicated that my purification method can

provide highly purified functional NeCyt c_{554} proteins using a much simpler procedure relative to the

conventional methods.
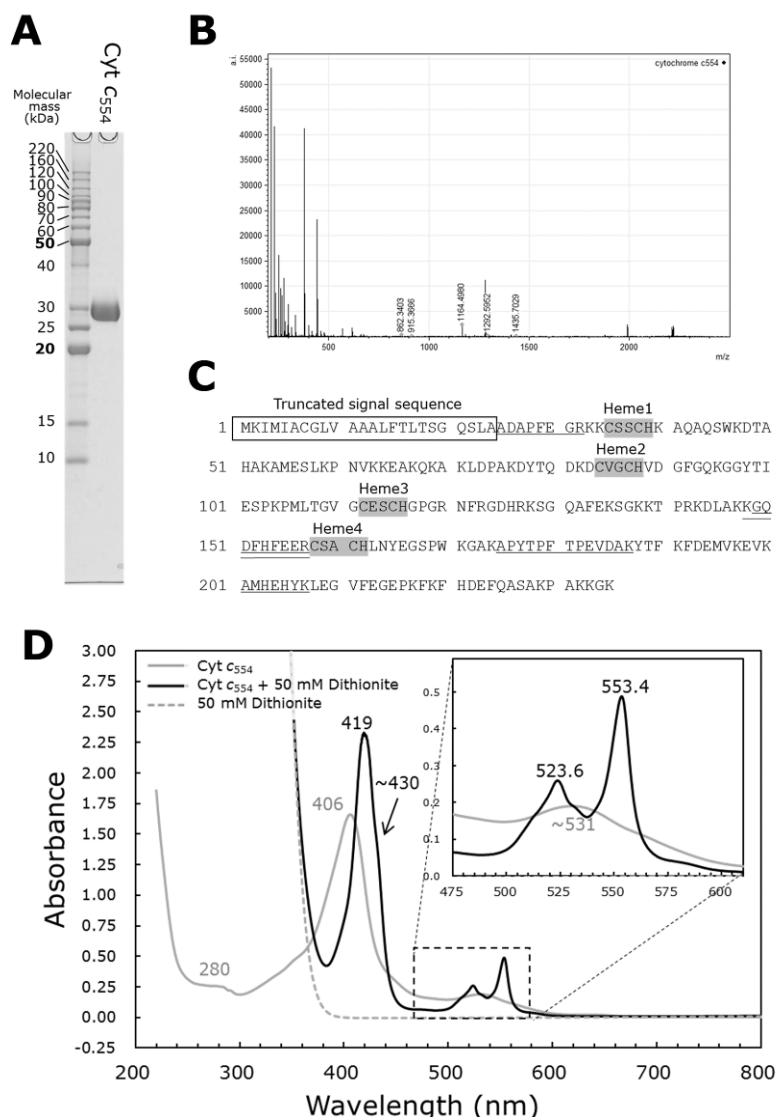
Figure 42. Identification of purified NeCyt c_{554} protein.

(A) Purified and concentrated cytochrome c_{554} was analyzed by 15% SDS-PAGE with Coomassie Brilliant Blue stain using 0.9 µg of protein. The purified NeCyt c_{554} was observed as a single band at approximately 27 kDa. (B) The MALDI-TOF mass spectrum of tryptic-digested purified NeCyt c_{554}. (C) Assignment for the mass spectrum peaks. The matched peptides are underlined, and the "K[148]GQDFHFEER" was assigned as a peptide with one miss-cleavage in the C-terminal of Lys[148]. The truncated export-signal sequence is boxed, and the heme binding motifs (-CxxCH-) are highlighted in grey. The sequence coverage was 18%. (D) Assessment of heme in the purified NeCyt c_{554} by a UV–vis spectrum analysis. Air-oxidized cytochrome c_{554} (grey line) and cytochrome c_{554}

reduced by 50 mM dithionite (black line) were represented in the spectra. The spectral scan was performed with a buffer composed of 10 mM Tris-HCl (pH 7.5) and 150 mM NaCl at 25 °C. The protein concentration was 5 µM. The values on peak tops are wavelengths (nm) which were determined by the highest absorbance of a simple 3-point moving average. The inset provides a detailed view of the area around Q-band of the NeCyt c_{554}.

Docking simulation for NeHAO and NeCyt c_{554}

Protein-protein docking simulation was performed for NeHAO and NeCyt c_{554} (**Figure 43**). The model structure of the result showed that the NeCyt c_{554} binds to a valley on the interface of subunits of the NeHAO. The heme-c in NeHAO which located on the NeCyt c_{554}-NeHAO binding surface is exposed to NeHAO surface. The heme-c in NeHAO is very close to a heme-c in NeCyt c_{554} (**Figure 43**). Edge-to-edge distance between the two hemes was 6.9 Å, which distance is capable for electron transfer from NeHAO to NeCyt c_{554} [76]. Therefore, the binding model is presented for the reliable prediction of interaction mode of NeCyt c_{554} with NeHAO. To design of protein-protein interaction inhibitors binding to the interaction surface will lead to new nitrification inhibitors which have novel mode of inhibitory-action.
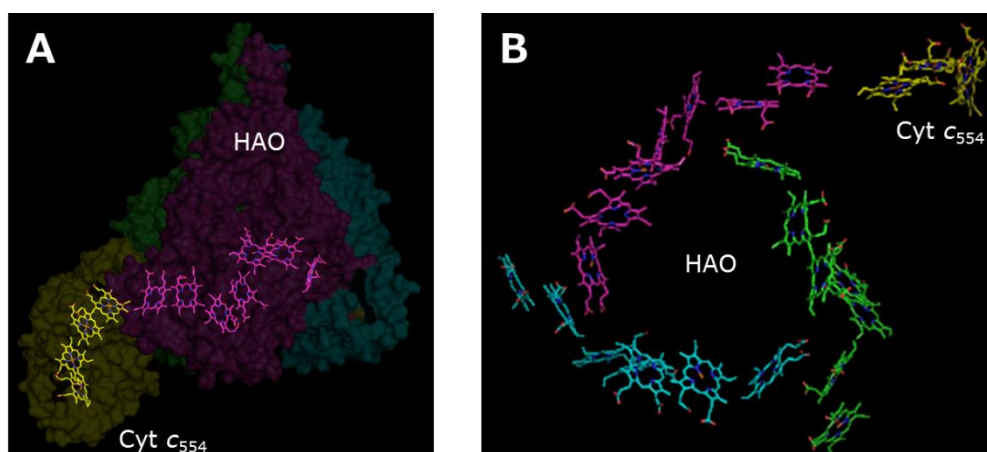
Figure 43. NeHAO-NeCyt c_{554} docking model.
(A) Over all structure of NeHAO (red, blue green) and Cyt c_{554} (yellow) with hemes (wire model). (B) Arrangement of hemes in the complex.

Discussion

Cytochrome c_{554} may directly be involved in the nitrification and N_2O emission of AOB. My purification method will accelerate the study of NeCyt c_{554} mechanism, leading to the discovery of nitrification and N_2O emission controlling technologies including nitrification inhibitors. Previously, a purification method for NeCyt c_{554} was described by Yamanaka, *et al.* [67] and its modification was described by Arciero, *et al.* [72], which were applied in several biochemical and structure analyses [54,70,71]. The method described by Arciero, *et al.* was simplified from the Yamanaka, *et al* method, yet it requires cumbersome procedures that involved the following steps: cell disruption by three freeze-thaw cycle, 80–90% ammonia-sulfate fractionation, hydrophobic interaction chromatography using Octyl-Sepharose, dialysis for desalting, cation-exchange chromatography using Amberlite CG-50, and gel-filtration chromatography using Sephadex-G1000. These steps require a considerable amount of time, especially the ammonia-sulfate fractionation and dialysis steps, which take more than 2 days and a day to complete, respectively. My method is simpler than these conventional methods. One major improvement was the removal of the ammonia-sulfate fractionation and dialysis steps. The column-operation procedure was also redesigned to take advantage of the pI value of 10.7 featured in NeCyt c_{554} [67]. In my method, a combination of flow-through into anion-exchange column and adsorption onto cation-exchange columns were utilized. Therefore, my method allowed for a complete purification within 2 days, including buffer preparation and column cleaning steps.

Additionally, my purification method is readily applicable for scale-up and/or automated purification. Purified NeCyt c_{554} has been used not only for crystal structure and functional mechanism analyses [70,71], but also for colorimetric probe to measure the HAO activity [54]. Inconvenient purification method was a bottleneck for these studies that require a large amount of purified NeCyt c_{554}. My purification method involved column operations only and no concentration, buffer exchange, and desalting steps were required. These features have allowed us to utilize a pilot-scale

chromatography system and/or an automated multistep chromatography system such as the ÄKTAxpress (GE Healthcare). Preparation of a large amount of NeCyt c_{554} enables us to perform inhibitor screening for NeCyt c_{554} and NeHAO binding inhibitors which bind to the protein-protein interaction surface. It will lead new paradigm of designing nitrification inhibitor.

Acknowledgements

Finally, I would like to thank my family for their continuous support throughout my student life.

Declaration of financial interests

Yuki Nishigaya are an inventor in patent pending application JP-A-2016-010983 (patent applicant:

NARO), which includes HAO purification and fluorescence assay methods described in this paper.

There are no other conflicts of interest to declare.

References

[1]   D.L. Dinnes, D.L. Karlen, D.B. Jaynes, T.C. Kaspar, J.L. Hatfield, T.S. Colvin, et al., Nitrogen Management Strategies to Reduce Nitrate Leaching in Tile-Drained Midwestern Soils, Agron. J. 94 (2002) 153–171. doi:10.2134/AGRONJ2002.1530.

[2]   J. Liu, L. You, M. Amini, M. Obersteiner, M. Herrero, A.J.B. Zehnder, et al., A high-resolution assessment on global nitrogen flows in cropland., Proc. Natl. Acad. Sci. U. S. A. 107 (2010) 8035–40. doi:10.1073/pnas.0913658107.

[3]   G.V. Subbarao, O. Ito, K.L. Sahrawat, W.L. Berry, K. Nakahara, T. Ishikawa, et al., Scope and Strategies for Regulation of Nitrification in Agricultural Systems—Challenges and Opportunities, CRC. Crit. Rev. Plant Sci. 25 (2006) 303–335. doi:10.1080/07352680600794232.

[4]   R.J. Haynes, K.M. Goh, Ammonium and nitrate nutrition of plants, Biol. Rev. 53 (1978) 465–510. doi:10.1111/j.1469-185X.1978.tb00862.x.

[5]   B.G. Forde, D.T. Clarkson, Nitrate and Ammonium Nutrition of Plants: Physiological and Molecular Perspectives, Adv. Bot. Res. 30 (1999) 1–90. doi:10.1016/S0065-2296(08)60226-8.

[6]   S.C. Jarvis, Future trends in nitrogen research, Plant Soil. 181 (1996) 47–56. doi:10.1007/BF00011291.

[7]   K.L. Sahrawat, Nitrification in some tropical soils, Plant Soil. 65 (1982) 281–286. doi:10.1007/BF02374659.

[8]   S.D. Donner, C.J. Kucharik, Corn-based ethanol production compromises goal of reducing nitrogen export by the Mississippi River., Proc. Natl. Acad. Sci. U. S. A. 105 (2008) 4513–8. doi:10.1073/pnas.0708300105.

[9]   H.I. Shuval, N. Gruener, Epidemiological and toxicological aspects of nitrates and nitrites in the environment., Am. J. Public Health. 62 (1972) 1045–52.

[10]   J.M. Bremner, J.C. Yeomans, Effects of nitrification inhibitors on denitrification of nitrate in soil, Biol. Fertil. Soils. 2 (1986). doi:10.1007/BF00260840.

[11]   H. Nimenya, A. Delaunois, D. La Duong, S. Bloden, J. Defour, B. Nicks, et al., Short-term Toxicity of Various Pharmacological Agents on the In Vitro Nitrification Process in a Simple Closed Aquatic System., Altern. Lab. Anim. 27 (1999) 121–35.

References

[12]   B. Alpaslan Kocamemi, F. Ceçen, Kinetic analysis of the inhibitory effect of trichloroethylene (TCE) on nitrification in cometabolic degradation., Biodegradation. 18 (2007) 71–81. doi:10.1007/s10532-005-9037-3.

[13]   A.J. Sipos, H. Urakawa, Differential responses of nitrifying archaea and bacteria to methylene blue toxicity., Lett. Appl. Microbiol. (2015). doi:10.1111/lam.12534.

[14]   R. Okano, H. Takazaki, D. Matsuba, T. Tokuyama, Y. Sato, K. Wakabayashi, *Nitrosomonas europaea* ATCC25978 is the right ammonia-oxidizing bacterium for screening nitrification inhibitors, J. Pestic. Sci. 29 (2004) 50–52.

[15]   D. Matsuba, H. Takazaki, Y. Sato, R. Takahashi, T. Tokuyama, K. Wakabayashi, Susceptibility of ammonia-oxidizing bacteria to nitrification inhibitors., Z. Naturforsch. C. 58 (2003) 282–7.

[16]   G.V. Subbarao, T. Ishikawa, O. Ito, K. Nakahara, H.Y. Wang, W.L. Berry, A bioluminescence assay to detect nitrification inhibitors released from plant roots: a case study with Brachiaria humidicola, Plant Soil. 288 (2006) 101–112. doi:10.1007/s11104-006-9094-3.

[17]   G. V Subbarao, K. Nakahara, M.P. Hurtado, H. Ono, D.E. Moreta, A.F. Salcedo, et al., Evidence for biological nitrification inhibition in Brachiaria pastures., Proc. Natl. Acad. Sci. U. S. A. 106 (2009) 17302–7. doi:10.1073/pnas.0903694106.

[18]   H. Akiyama, X. Yan, K. Yagi, Evaluation of effectiveness of enhanced-efficiency fertilizers as mitigation options for N_2O and NO emissions from agricultural soils: meta-analysis, Glob. Chang. Biol. 16 (2010) 1837–1846. doi:10.1111/j.1365-2486.2009.02031.x.

[19]   H.J. Di, K.C. Cameron, Nitrate leaching losses and pasture yields as affected by different rates of animal urine nitrogen returns and application of a nitrification inhibitor—a lysimeter study, Nutr. Cycl. Agroecosystems. 79 (2007) 281–290. doi:10.1007/s10705-007-9115-5.

[20]   D.E. Canfield, A.N. Glazer, P.G. Falkowski, The evolution and future of Earth's nitrogen cycle., Science. 330 (2010) 192–6. doi:10.1126/science.1186120.

[21]   K.M.J. Merz, D. Ringe, H.C. Reynolds, Drug Design -Pharmacology and Drug Discovery-, Cambridge University Press, 2010. http://www.cambridge.org/fr/academic/subjects/life-sciences/pharmacology-and-drug-discovery/drug-design-structure-and-ligand-based-approaches?format=HB.

[22]   L.G. Ferreira, R.N. Dos Santos, G. Oliva, A.D. Andricopulo, Molecular docking and

References

structure-based drug design strategies., Molecules. 20 (2015) 13384–421. doi:10.3390/molecules200713384.

[23]   L.B. Salum, I. Polikarpov, A.D. Andricopulo, Structure-based approach for the study of estrogen receptor binding affinity and subtype selectivity., J. Chem. Inf. Model. 48 (2008) 2243–53. doi:10.1021/ci8002182.

[24]   B. Kuhn, W. Guba, J. Hert, D.W. Banner, C. Bissantz, S.M. Ceccarelli, et al., A Real-World Perspective on Molecular Design., J. Med. Chem. (2016). doi:10.1021/acs.jmedchem.5b01875.

[25]   M. Whittaker, D. Bergmann, D. Arciero, A.B. Hooper, Electron transfer during the oxidation of ammonia by the chemolithotrophic bacterium *Nitrosomonas europaea*., Biochim. Biophys. Acta. 1459 (2000) 346–55. http://www.ncbi.nlm.nih.gov/pubmed/11004450 (accessed January 12, 2015).

[26]   T.C. Hollocher, S. Kumar, D.J.D. Nicholas, Respiration-dependent proton translocation in *Nitrosomonas europaea* and its apparent absence in *Nitrobacter agilis* during inorganic oxidations., J. Bacteriol. 149 (1982) 1013–20.

[27]   J.A. Kozlowski, J. Price, L.Y. Stein, Revision of N_2O-producing pathways in the ammonia-oxidizing bacterium *Nitrosomonas europaea* ATCC 19718., Appl. Environ. Microbiol. 80 (2014) 4930–5. doi:10.1128/AEM.01061-14.

[28]   S.J. Powell, J.I. Prosser, Effect of copper on inhibition by nitrapyrin of growth of *Nitrosomonas europaea*, Curr. Microbiol. 14 (1986) 177–179. doi:10.1007/BF01568371.

[29]   A. Roy, A. Kucukural, Y. Zhang, I-TASSER: a unified platform for automated protein structure and function prediction., Nat. Protoc. 5 (2010) 725–38. doi:10.1038/nprot.2010.5.

[30]   Y. Wu, Y. Guo, X. Lin, W. Zhong, Z. Jia, Inhibition of bacterial ammonia oxidation by organohydrazines in soil microcosms, Front. Microbiol. 3 (2012) 1–8. doi:10.3389/fmicb.2012.00010.

[31]   M.S. Logan, A.B. Hooper, Suicide inactivation of hydroxylamine oxidoreductase of *Nitrosomonas europaea* by organohydrazines., Biochemistry. 34 (1995) 9257–64.

[32]   N. Igarashi, H. Moriyama, T. Fujiwara, Y. Fukumori, N. Tanaka, The 2.8 Å structure of hydroxylamine oxidoreductase from a nitrifying chemoautotrophic bacterium, *Nitrosomonas europaea*, Nat. Struct. Biol. 4 (1997) 276–284. doi:10.1038/nsb0497-276.

[33]   P. Cedervall, A.B. Hooper, C.M. Wilmot, Structural studies of hydroxylamine

References

oxidoreductase reveal a unique heme cofactor and a previously unidentified interaction partner, Biochemistry. 52 (2013) 6211–8. doi:10.1021/bi400960w.

[34]   W.J. Maalcke, A. Dietl, S.J. Marritt, J.N. Butt, M.S.M. Jetten, J.T. Keltjens, et al., Structural Basis of Biological NO Generation by Octaheme Oxidoreductases., J. Biol. Chem. 289 (2014) 1228–42. doi:10.1074/jbc.M113.525147.

[35]   NBRC, NBRC Medium No.829, http://www.nbrc.nite.go.jp/NBRC2/NBRCMediumDetailServlet?NO=829.

[36]   H. Urakawa, J.C. Garcia, J.L. Nielsen, V.Q. Le, J.A. Kozlowski, L.Y. Stein, et al., Nitrosospira lacus sp. nov., a psychrotolerant ammonia-oxidizing bacterium from sandy lake sediment., Int. J. Syst. Evol. Microbiol. 65 (2015). doi:10.1099/ijs.0.070789-0.

[37]   T. Hozuki, T. Ohtsuka, K. Arai, K. Yoshimatsu, S. Tanaka, T. Fujiwara, Effect of Salinity on Hydroxylamine Oxidation in a Marine Ammonia-Oxidizing Gammaproteobacterium, *Nitrosococcus oceani* strain NS58: Molecular and Catalytic Properties of Tetraheme Cytochrome *c*-554, Microbes Environ. 25 (2010) 95–102. doi:10.1264/jsme2.ME09154.

[38]   D. Giustarini, R. Rossi, A. Milzani, I. Dalle-Donne, Nitrite and nitrate measurement by Griess reagent in human plasma: evaluation of interferences and standardization, Methods Enzymol. 440 (2008) 361–80. doi:10.1016/S0076-6879(07)00823-3.

[39]   M.S. Logan, C. Balny, A.B. Hooper, Reaction with cyanide of hydroxylamine oxidoreductase of Nitrosomonas europaea., Biochemistry. 34 (1995) 9028–37.

[40]   P.E. Cedervall, A.B. Hooper, C.M. Wilmot, Crystallization and preliminary X-ray crystallographic analysis of a new crystal form of hydroxylamine oxidoreductase from *Nitrosomonas europaea*, Acta Crystallogr. Sect. F. Struct. Biol. Cryst. Commun. 65 (2009) 1296–8. doi:10.1107/S1744309109046119.

[41]   L.M.G. Chavas, N. Matsugaki, Y. Yamada, M. Hiraki, N. Igarashi, M. Suzuki, et al., Beamline AR-NW12A: high-throughput beamline for macromolecular crystallography at the Photon Factory., J. Synchrotron Radiat. 19 (2012) 450–4. doi:10.1107/S0909049512009727.

[42]   Z. Otwinowski, W. Minor, Macromolecular Crystallography Part A, Methods Enzymol. 276 (1997) 307–326. doi:10.1016/S0076-6879(97)76066-X.

[43]   A. Vagin, A. Teplyakov, Molecular replacement with MOLREP., Acta Crystallogr. D. Biol. Crystallogr. 66 (2010) 22–5. doi:10.1107/S0907444909042589.

[44]   P. Emsley, K. Cowtan, Coot: model-building tools for molecular graphics., Acta Crystallogr.

References

D. Biol. Crystallogr. 60 (2004) 2126–32. doi:10.1107/S0907444904019158.

[45]   M.D. Winn, *et al.* Overview of the CCP4 suite and current developments. Acta Crystallogr. D. Biol. Crystallogr. 67, (2011) 235–42.

[46]   G.N. Murshudov, A.A. Vagin, E.J. Dodson, Refinement of macromolecular structures by the maximum-likelihood method., Acta Crystallogr. D. Biol. Crystallogr. 53 (1997) 240–55. doi:10.1107/S0907444996012255.

[47]   G.N. Murshudov, P. Skubák, A.A. Lebedev, N.S. Pannu, R.A. Steiner, R.A. Nicholls, et al., REFMAC5 for the refinement of macromolecular crystal structures., Acta Crystallogr. D. Biol. Crystallogr. 67 (2011) 355–67. doi:10.1107/S0907444911001314.

[48]   S.C. Lovell, I.W. Davis, W.B. Arendall, P.I.W. de Bakker, J.M. Word, M.G. Prisant, et al., Structure validation by Calpha geometry: phi,psi and Cbeta deviation., Proteins. 50 (2003) 437–50. doi:10.1002/prot.10286.

[49]   E.F. Pettersen, T.D. Goddard, C.C. Huang, G.S. Couch, D.M. Greenblatt, E.C. Meng, et al., UCSF Chimera--a visualization system for exploratory research and analysis., J. Comput. Chem. 25 (2004) 1605–12. doi:10.1002/jcc.20084.

[50]   Molecular Operating Environment (MOE), 2014.09; Chemical Computing Group Inc., 1010 Sherbooke St. West, Suite #910, Montreal, QC, Canada, H3A 2R7, 2014.

[51]   POV-ray: Persistence of Vision Pty. Ltd. (2004). Persistence of Vision (TM) Raytracer. Persistence of Vision Pty. Ltd., Williamstown, Victoria, Australia. http://www.povray.org/.

[52]   J.C. Garcia, H. Urakawa, V.Q. Le, L.Y. Stein, M.G. Klotz, J.L. Nielsen, Draft Genome Sequence of *Nitrosospira* sp. Strain APG3, a Psychrotolerant Ammonia-Oxidizing Bacterium Isolated from Sandy Lake Sediment., Genome Announc. 1 (2013). doi:10.1128/genomeA.00930-13.

[53]   J. Zhang, T. Chung, K. Oldenburg, A Simple Statistical Parameter for Use in Evaluation and Validation of High Throughput Screening Assays., J. Biomol. Screen. 4 (1999) 67–73.

[54]   D.M. Arciero, C. Balny, A.B. Hooper, Spectroscopic and rapid kinetic studies of reduction of cytochrome *c*554 by hydroxylamine oxidoreductase from *Nitrosomonas europaea*, Biochemistry. 30 (1991) 11466–72.

[55]   A.B. Hooper, A. Nason, Characterization of hydroxylamine-cytochrome c reductase from the chemoautotrophs *Nitrosomonas europaea* and *Nitrosocystis oceanus*., J. Biol. Chem. 240 (1965) 4044–57.

References

[56]   L. Pohjala, P. Tammela, Aggregating behavior of phenolic compounds--a source of false bioassay results?, Molecules. 17 (2012) 10774–90. doi:10.3390/molecules170910774.

[57]   T. Hino, Y. Matsumoto, S. Nagano, H. Sugimoto, Y. Fukumori, T. Murata, et al., Structural basis of biological N_2O generation by bacterial nitric oxide reductase., Science. 330 (2010) 1666–70. doi:10.1126/science.1195591.

[58]   J. Langedijk, A.K. Mantel-Teeuwisse, D.S. Slijkerman, M.-H.D.B. Schutjens, Drug repositioning and repurposing: terminology and definitions in literature., Drug Discov. Today. 20 (2015) 1027–34. doi:10.1016/j.drudis.2015.05.001.

[59]   T.T. Ashburn, K.B. Thor, Drug repositioning: identifying and developing new uses for existing drugs., Nat. Rev. Drug Discov. 3 (2004) 673–683. doi:10.1038/nrd1468.

[60]   N.L. Olivera, L. Prieto, M.B. Bertiller, M.A. Ferrero, Sheep grazing and soil bacterial diversity in shrublands of the Patagonian Monte, Argentina, J. Arid Environ. 125 (2016) 16–20. doi:10.1016/j.jaridenv.2015.09.012.

[61]   N.G. Love, R.J. Smith, K.R. Gilmore, C.W. Randall, Oxime Inhibition of Nitrification during Treatment of an Ammonia-Containing Industrial Wastewater on JSTOR, Water Environ. Res. 71 (1999) 418–426.

[62]   C.A. Lipinski, Drug-like properties and the causes of poor solubility and poor permeability., J. Pharmacol. Toxicol. Methods. 44 235–49.

[63]   G.M. King, C.F. Weber, Distribution, diversity and ecology of aerobic CO-oxidizing bacteria., Nat. Rev. Microbiol. 5 (2007) 107–18. doi:10.1038/nrmicro1595.

[64]   C. Abad-Zapatero, J.T. Metz, Ligand efficiency indices as guideposts for drug discovery, Drug Discov. Today. 10 (2005) 464–469. doi:10.1016/S1359-6446(05)03386-6.

[65]   J.J. Irwin, B.K. Shoichet, ZINC--a free database of commercially available compounds for virtual screening., J Chem Inf Model. 45 (2005) 177–182. doi:10.1021/ci049714+.

[66]   D.C.Y. Tsang, I. Suzuki, Cytochrome *c*554 as a possible electron donor in the hydroxylation of ammonia and carbon monoxide in *Nitrosomonas europaea*., Can. J. Biochem. 60 (1982) 1018–24. doi:10.1139/o82-131.

[67]   T. Yamanaka, M. Shinra, Cytochrome *c*-552 and cytochrome *c*-554 derived from *Nitrosomonas europaea*. Purification, properties, and their function in hydroxylamine oxidation., J. Biochem. 75 (1974) 1265–73.

References

[68]   A.K. Upadhyay, A.B. Hooper, M.P. Hendrich, NO reductase activity of the tetraheme cytochrome *c*554 of *Nitrosomonas europaea.*, J. Am. Chem. Soc. 128 (2006) 4330–7. doi:10.1021/ja055183+.

[69]   L.Y. Stein, Surveying N_2O-producing pathways in bacteria., Methods Enzymol. 486 (2011) 131–52. doi:10.1016/B978-0-12-381294-0.00006-7.

[70]   T.M. Iverson, D.M. Arciero, B.T. Hsu, M.S.P. Logan, A.B. Hooper, D.C. Rees, Heme packing motifs revealed by the crystal structure of the tetra-heme cytochrome *c*554 from *Nitrosomonas europaea.*, Nat. Struct. Biol. 5 (1998) 1005–12. doi:10.1038/2975.

[71]   T.M. Iverson, D.M. Arciero, A.B. Hooper, D.C. Rees, High-resolution structures of the oxidized and reduced states of cytochrome *c*554 from *Nitrosomonas europaea.*, J. Biol. Inorg. Chem. 6 (2001) 390–7.

[72]   D.M. Arciero, M.J. Collins, J. Haladjian, P. Bianco, A.B. Hooper, Resolution of the four hemes of cytochrome *c*554 from *Nitrosomonas europaea* by redox potentiometry and optical spectroscopy., Biochemistry. 30 (1991) 11459–65.

[73]   K.K. Andersson, J.D. Lipscomb, M. Valentine, E. Münck, A.B. Hooper, Tetraheme cytochrome *c*-554 from *Nitrosomonas europaea*. Heme-heme interactions and ligand binding, J. Biol. Chem. 261 (1986) 1126–1138.

[74]   M. Strohalm, D. Kavan, P. Novák, M. Volný, V. Havlícek, mMass 3: a cross-platform software environment for precise analysis of mass spectrometric data., Anal. Chem. 82 (2010) 4648–51. doi:10.1021/ac100818g.

[75]   B.G. Pierce, K. Wiehe, H. Hwang, B.-H. Kim, T. Vreven, Z. Weng, ZDOCK server: interactive docking prediction of protein-protein complexes and symmetric multimers., Bioinformatics. 30 (2014) 1771–3. doi:10.1093/bioinformatics/btu097.

[76]   S.L. Mayo, W.R. Ellis, R.J. Crutchley, H.B. Gray, Long-range electron transfer in heme proteins., Science. 233 (1986) 948–52.

[77]   D.C.N. Prof. Dr. Detlev Ganten, Prof. em. Dr. Klaus Ruckpaul, Prof. Dr. Walter Birchmeier, Prof. Dr. Jörg T. Epplen, Prof. Dr. Klaus Genser, Dr. Manfred Gossen, Dr. Birgit Kersten, Prof. Dr. Hans Lehrach, Prof. Dr. Hartmut Oschkinat, Prof. Dr. Patrizia Ruiz, Dr., Homogeneous Assay, in: Encycl. Ref. Genomics Proteomics Mol. Med., Springer Berlin Heidelberg, Berlin, Heidelberg, 2006: p. 814. doi:10.1007/3-540-29623-9_7359.